UNIVERSITÀ
DI PAVIA

Dipartimento di Biologia e Biotecnologie "L. Spallanzani"

Cell stress and ageing affect nucleolus and heterochromatin organization in mouse hepatocytes

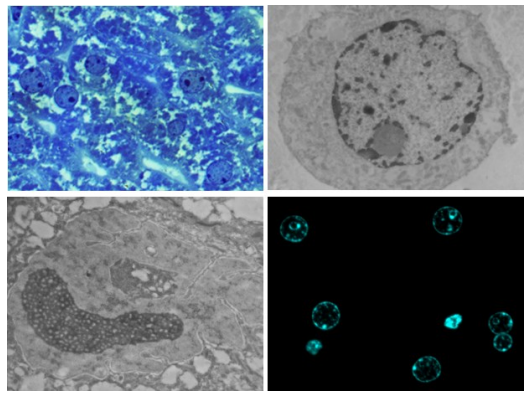

Lorena Zannino

Dottorato di Ricerca in
Genetica, Biologia Molecolare e Cellulare
Ciclo XXXIV – A.A. 2018-2021

TABLE OF CONTENTS

ABSTRACT

Ageing is characterized by progressive physiological decline of tissues functions and performances, which ultimately lead to death. It is a multi-factorial process, influenced by various environmental, genetic and epigenetic factors, in which the organism continuously adapts the progressive accumulation of damages to the system maintenance over time. This prompted researchers to find possible strategies to delay ageing in order to extend lifespan and improve human's quality of life.

Liver, the largest gland in our body, carries out many different metabolic processes that are fundamental for our organism and is, therefore, a vitally important organ. Liver is a stable tissue; the low rate of cell renewal and the high metabolism of hepatocytes probably makes them particularly prone to the effects of ageing. Additionally, the involvement in such different metabolic processes and the frequent exposure to different exogenous molecules due to their prominent role in detoxification, make hepatocyte ageing complex to analyze and subjected to great variations depending on individual lifestyle.

In this study, we investigated the effects of ageing and of various stressful conditions that could affect ageing process by accelerating or slowing it down in hepatocytes, on the murine model, both on mouse hepatic tissue and the mouse hepatocyte cell line AML12. We focused on the nucleus and specifically on the changes induced in the heterochromatin organization and the nucleolar activity. More in detail, we compared liver tissue from young (3 months old) and old (24 months old) mice. Moreover, we analyzed the effects of exposure to the toxic agent mercury chloride, because of the primary liver involvement in xenobiotics detoxification; the depletion of serum to mimic the reduction of calorie intake, given the critical role of the liver in sugars and fats metabolism and being this a strategy known to slow down ageing. We investigated whether the use of a high dose of dexamethasone, a corticosteroid with anti-inflammatory properties, could exert a protective effect and finally, we analyzed senescent hepatocytes as a model of precocious ageing.

Studying the effect of ageing in liver tissue on mouse model in a controlled environment did not highlight major variations in the heterochromatin organization and more generally in the nuclear architecture. We only detected changes in some histone post-translational modifications associated to heterochromatin.

Concerning the hepatocytes cell model of senescence instead, as generally happens, they have larger dimensions, consequently, the nuclei were also

enlarged compared to control hepatocytes. Heterochromatin domains increased their extension and in many cases occupies the largest part of the nucleoplasm. The nucleoli were very large with many fibrillar centers.

Mercury Chloride treatment induced changes in morphology and activity of the nucleoli making them similar to that observed in senescent cells. However, this treatment, differently from senescence, causes extensive heterochromatin decondensation.

Serum-depleted cells show a similar degree of chromatin condensation as in control cells grown in complete medium, although the total amount of heterochromatin resulted higher, while nucleoli have a reduced size and activity compared to the control.

Finally, Dexamethasone treatment seemed to induce changes that are different from the other cell stress analyzed and opposite to those observed in senescent cells, as chromatin decondensation, but at the same time a reduction of the activity and size of the nucleolus.

Based on these results we could uncover a trend according to which smaller and less active nucleoli slow down the ageing process. Conversely, a general correlation between the organization of heterochromatin and ageing or the effects of cell stress was more difficult to establish, probably because of the subtle dynamics that come into play in the different conditions that are hardly attributable to a single trend at the level of the total fraction of repressed chromatin and not of the specific gene locus.

ABBREVIATIONS

1mA: N1-methyladenine

3C: chromosome conformation capture

4C: circularized 3C

5C: 3C carbon copy

5caC: 5-carboxylcytosine

5fC: 5-formylcytosine

5hmC: 5-hydroxymethylcytosine

5mC: 5-methylcytosine

6fA: 6-formyladenine

6hmA: 6-hydroxymethyladenine

6mA: N6-methyladenine

ADP: adenosine diphosphate

AGEs: advanced glycation end products

ANOVA test: analysis of variance test

ARF: ADP ribosylation factor

ATAC-seq: assay for transposase-accessible chromatin using sequencing

ATP: adenosine triphosphate

ATSDR: Agency for toxic substance and disease registry

B2m: beta-2-microglobuline

BALM: binding activatable localization microscopy

BAZ2A: bromodomain adjacent to zinc finger domain 2A

BCL-2: B cell lymphoma

BCL-xL: B cell lymphoma extra large

BER: base excision repair

C: carboxyl

CBX: chromo box protein

CDKi: cyclin-dependent kinase inhibitor

cDNA: complementary DNA

ChIP: chromatin immunoprecipitation

CLSM: confocal laser scanning microscopy

CNV: copy-number variation

COVID-19: coronavirus disease 2019

CR: calorie restriction

CRISPR: clustered regularly interspaced short palindromic repeats

Ct: threshold cycle number

CTCF: CCC3C-binding factor

CTRL: control

DamID: DNA adenine methyltransferase identification

DAMT-1: DNA N6-adenine methyltransferases

DDR: DNA damage response

DEX: dexamethasone

DFC: dense fibrillar component

dH_2O: distilled water

DMEM: Dulbecco's modified Eagle's Medium

DNA: deoxyribonucleic acid

DNase-seq: DNAseI hypersensitive sites sequencing

DNMT: DNA methyltransferase

EDTA: ethylendiaminotetracetyc acid

EED: embryonic ectoderm development

ER: endoplasmic reticulum

ESCs: embryonic stem cells

EXOSC: Exosome component

EZH2: enhancer of zeste homolog 2

FAIRE-seq: formaldehyde-assisted isolation of regulatory elements sequencing

FBS: fetal bovine serum

FC: fibrillar center

FISH: fluorescent in situ hybridization

GC: granular component

GSH: glutathione

GTP: guanosine triphosphate

H2K119Ub: ubiquitination of lysine 119 on histone H2

H3K27me2: dimethylation of lysine 27 on histone H3

H3K27me3: trimethylation of lysine 27 on histone H3

H3K36me2: dimethylation of lysine 36 on histone H3

H3K36me3: trimethylation of lysine 36 on histone H3

H3K4me3: trimethylation of lysine 4 on histone H3

H3K79: lysine 79 on histone H3

H3K9me2: dimethylation of lysine 9 on histone H3

H3K9me3: trimethylation of lysine 9 on histone H3

H4K20me1: monomethylation of lysine 20 on histone H4

H4K20me2: dimethylation of lysine 20 on histone H4

H4K20me3: trimethylation of lysine 20 on histone H4

HDAC3: histone deacetylase 3

HGPS: Hutchinson–Gilford progeria syndrome

HOX: homeobox

HP1α: heterochromatin protein 1

HPTM: histone post-translational modification

Hst: Hybrid sterility

IDR: intrinsically disordered region

IGF-1: insulin growth factor 1

IGS: intergenic sequence

IIS: insulin-IGF1 signaling

ITS: insulin transferrin selenium

KMT5B : lysine methyltransferase 5B (also known as SUV420H1)

KMT5C : lysine methyltransferase 5C (also known as SUV420H2)

LADs: lamin associated domains

LLPS: liquid-liquid phase separation

MAPK: mitogen-activated protein kinase

MNase-seq: micrococcal nuclease digestion with deep sequencing

mRNA: messenger RNA

mtDNA: mitochondrial DNA

mTOR: mechanistic target of rapamycin

N: amino

NADs: nucleolus associated domains

ncRNA: non coding RNA

NF-kB: nuclear factor kappa-B

NIH: National Institute of Health

NMR: nuclear magnetic resonance

NOG: nogging

NoRC: nucleolar remodelling complex

NORs: nucleolus organizer regions

NSUN5: NOP2-Sun RNA methyltransferase 5

PALM: photoactivated localization microscopy

PBS: phosphate saline buffer

PCR: polymerase chain reaction

PFA: paraformaldehyde

PIC: preinitiation complex

PRC1: polycomb repressive complex 1

PRC2: polycomb repressive complex 2

R.T.: room temperature

rDNA: ribosomal DNA

RNA pol I: RNA polymerase I

RNA Pol II: RNA polymerase II

RNA Pol III: RNA polymerase III

RNA: ribonucleic acid

RNAi: RNA interference

ROS: reactive oxygen species

RP: ribosomal protein

rRNA: ribosomal ribonucleic acid

RRP9: ribosomal RNA processing 9

RT-qPCR: real time quantitative PCR

SAM: s-adenosyl methionine

SD: standard deviation

SEM: standard error of the mine

SINEs: short interspersed nuclear elements

SIRT: sirtuin

SL1: promoter selectivity factor

SPRITE: split-pull recognition of interactions by tag extension

STORM: stochastic optical reconstruction microscopy

SUV39H1: suppressor of variegation 3-9 histone-lysine N-methyltransferase H1

SUV39H2: suppressor of variegation 3-9 histone-lysine N-methyltransferase H2

TADs: topologically associated domains

TAFs: TBP associated factor

TBP: TATA-box binding protein

TEM: transmission electron microscopy

TET: ten-eleven translocation

TIF: translation initiation factor

TN5: transposase 5

TNF-α: tumor necrosis factor α

tp53: tumor protein 53

tRNAs: transfer ribonucleic acids

UBTF: upstream binding transcription factor

UCE: upstream control element

1. INTRODUCTION

1.1 The nucleus

The nucleus is a rounded cellular organelle delimited by an envelope, the nuclear envelope, consisting of flattened cisternae separated by the nuclear pores. From an ultrastructural point of view, nuclear pores appear as discoidal structures with an outer diameter of 130 nm and an inner pore with an effective diameter for diffusion of 9 nm. The nuclear pore complex has an octagonal symmetry and is formed by the assembly of more than 50 proteins, the nucleoporins. Nuclear pores are freely permeable to small molecules, ions and proteins up to 17 kDa (Lin et al., 2016). Molecules and particles of higher molecular weight cannot pass through the pores by simple diffusion, but must be selectively transported. This occurs thanks to a “signal sequence” that is recognized by one or more receptors of the nuclear pore complex. Following recognition, transport occurs thanks to energy consumption (Peters, 2006). Therefore, nuclear pores allow communication between cytoplasm and nucleoplasm and are traversed by many molecules in both directions. Mainly the enzymes necessary for the various activities that take place in the nucleus are imported. While exports largely concern messenger RNAs (mRNAs) and the ribosomal subunits necessary for their translation into proteins in the cytoplasm (Peters, 2006).

The outer surface of the envelope is in continuity with the endoplasmic reticulum and, like the latter, is covered with ribosomes that actively synthesize proteins.

The nucleus is configured as a cellular compartment within which the genetic information is contained and spatially organized. The need for compartmentalization appears mainly in eukaryotes with few exceptions and seems to derive as the result of possible selective pressures. In fact, according to some hypotheses, the nucleus may be a means of protection for DNA from biological agents, since it could reduce opportunities for integration of foreign DNA, thus acting as a possible barrier to infection or invasion of exogenous genetic elements (Labrie et al., 2010; Koonin et al., 2017). Moreover, it has been proposed that nuclear compartmentalization may avoid some unintended interactions between molecules. For example, it could be relevant to prevent ribosomal readthrough into introns (Lopez-Garcia and Moreira, 2006; Martin and Koonin, 2006). According to this model, interactions must occur in a specific order, from this comes the necessity of physical separation of transcription and translation thus providing a temporal means for splicing to complete before translation begins, therefore preventing

the formation of aberrant proteins via translational readthrough into unspliced introns, which may have toxic effects.

The compartmentalization generally allows a greater order and protection of the genetic material and consequently ensures greater efficiency in carrying out molecular processes also thanks to a lower dispersivity and greater physical proximity. This last parameter plays a very important role, in addition to the chemical affinity between molecules, in determining the probability and frequency of occurrence of a specific chemical reaction. For this same reason, the DNA and the other nuclear molecules are contained within the nucleus in a specific arrangement such that their 3D organization reflects specific functional needs. The specific nuclear localization of a genomic sequence seems in fact to be important in influencing its access to distinct enzymatic complexes with specialized functions such as transcription and splicing machinery, allowing the realization of specific transcriptional programs (Cremer and Cremer, 2001).

1.2 Chromatin organization within the nucleus

Several models have been proposed for the spatial organization of DNA in the nucleus, sometimes even discordant. However, a universally accepted basic point is the association of DNA with various nuclear proteins, that allow and influence its spatial organization and function, to form chromatin (Wu et al., 2007).

Human DNA, if arranged linearly, would cover a length of about 2 meters. It must therefore be tightly packed and folded to be contained within the cell nucleus. This is achieved thanks to the formation of chromatin structures of increasing complexity (Cremer and Cremer, 2001). A first degree of compaction can be achieved thanks to the wrapping of DNA around the nucleosomes: protein complexes formed by eight histone proteins. The DNA between one nucleosome and another is called the linker DNA (Wu et al., 2007). Specific DNA regions at different times may or may not be associated with nucleosomes. When these latter are free from nucleosomes, they are more accessible to nuclear enzymes and therefore could be actively transcribed or involved in replication or recombination. Histones are the most abundant proteins associated with eukaryotic DNA. Histone proteins are rich in basic amino acids, thanks to which they bind negatively charged DNA. The interactions between the histone core and the DNA are mediated by many sequence-independent contacts, mainly through hydrogen bonds between the proteins and the oxygen atoms of the phosphodiester bonds near the minor groove of the DNA (Wu et al., 2007). Once the nucleosomes have

formed, a higher level of packing can be achieved thanks to the binding of histone H1. Histone H1 binds to both the DNA linker and the median part of the DNA sequence associated with the histone core, thus inducing greater DNA packaging around the histones. The bond of H1 stabilizes a chromatin fiber with a cross-section of 30nm (Wu et al., 2007). Two models have been proposed to explain the formation of the 30 nm chromatin fiber: the solenoid model in which DNA is organized forming a superhelix containing approximately six nucleosomes per revolution; an alternative model in which the 30 nm fiber is a compact structure formed by nucleosomes arranged in a zig-zag pattern (Wu et al., 2007). The 30nm chromatin fibers existence is not certain; some studies suggest the formation of more flexible and dynamic chromatin structures (Nishino et al., 2012). However, numerous successive levels of folding are then required to explain the arrangement of DNA in the nucleus. Commonly accepted models affirm that the 30 nm fiber folds to form loops that constitute functionally and topologically defined domains, thanks to the interaction with protein complexes. These structures are not static and continuously present, but vary in shape and composition according to the cell cycle phase and more in general to the cell metabolic state (Cavalli and Misteli, 2013).

The organization of chromatin in complex molecular structures influences the gene function, determining the accessibility of specific genomic portions to specific molecular processes, without modifying the basic reading code of the genetic material, i.e. the nucleotide basic sequence. This is therefore defined as epigenetic regulation.

1.3 Epigenetics and nuclear architecture

Multicellular organisms originate from a single cell, the zygote. During development, this cell divides repeatedly to realize the complexity of the tissues and structures that characterize the individual. Although all the cells of the organism share a genome identical to that of the zygote, humans, for example, have about 200 different cell types, each of which performs specialized functions that correlate to a specific morphology, to the expression of specific sets of genes and to the mediation of specific communications and contacts with other cells and with the extracellular environment. The realization of this diversity is possible because an identical code, represented by the sequence of nucleotide bases, can be interpreted in different ways. The definition of Epigenetics includes any phenotypic or functional diversity that is not determined by changes in the DNA base sequence (Allis et al., 2013).

The term "epigenome" was subsequently coined, i.e. the set of epigenetic modifications affecting the entire genome. Epigenetic regulation occurs at different molecular levels of increasing complexity. A basic level of epigenetic regulation is DNA methylation. In mammalian cells, DNA methylation occurs mainly as the addition of a methyl group on the carbon 5 of the cytosine of the CpG dinucleotides which is catalyzed by a family of enzymes called DNMT (DNA-methyl-transferase) (Espada et al., 2010). The methylation of CpG sites is involved in important molecular processes, such as the regulation of gene expression, the inactivation of the X chromosome, the mechanisms of imprinting and the silencing of transposable elements. The methylation pattern is preserved during DNA replication, thanks to the DNMT1 enzyme, the most abundant DNA methyltransferase in somatic cells, which preferentially methylates the hemimethylated DNA (Poetker et al., 2010). DNMT3a and DNMT3b, on the other hand, are indicated as methyltransferases preferentially involved in de novo methylation (Ragoczy et al., 2014) However, several publications report that both DNMT1 and DNMT3 can perform both de novo and maintenance functions by cooperating in the creation of the global methylation pattern (Rhee et al., 2002; Kim et al., 2002).

Theoretically, each of the DNA bases can be modified, but 5mC is well known and the most studied. However, other modifications such as oxidation of 5mC to 5-hydroxymethylcytosine (5hmC), 5-formylcytosine (5fC), 5-carboxylcytosine (5caC), and the methylation of adenine to N6-methyladenine (6mA), are being identified as important epigenetic regulators so far (Klungland and Robertson, 2017).

Indeed, specific mechanisms are also needed to maintain specific regions free from methylation. Methylation level is dynamically controlled by DNA demethylation processes. DNA demethylation takes place by active and/or passive methods. During active DNA demethylation, 5mC is oxidized to 5-hmC, 5fC, and further to 5caC followed by base-excision repair (BER) mechanism. This enzymatic removal of 5mC is mediated by the ten-eleven translocation (TET) family proteins. These epigenetic marks have been reported to play an important role in the regulation of transcription process, chromatin remodeling, and recruitment of DNA repair-associated complexes in animals (Fong et al., 2013; Yue et al., 2016).

Adenine is methylated by DNA N6-adenine methyltransferases (DAMT-1) to produce N6-methyladenine (6mA) and may also be methylated to N1-methyladenine (1mA) by the endogenous or environmental alkylating agents (Sedgwick et al., 2007). Oxidation of the methyl group of 6mA by AlkB family of dioxygenases (e.g., 6mA demethylases) leads to the formation of N6-

hydroxymethyladenine (6hmA) and N6-formyladenine (6fA), which can restore the original base by releasing formaldehyde (Fu et al., 2013). While 5mC increases DNA helix stability, 6mA destabilizes the DNA helical structure. Therefore, 5mC is considered to be a repressor of transcription process when it occurs in the promoter region, while 6mA as an activator.

A second level of epigenetic regulation concerns histone variants. While the wrapping of DNA around the nucleosomes allows for the organization in a more compact structure, on the other, it limits access to transcription factors and RNA polymerase. Several mechanisms influence the dynamic competition between nucleosomes and other DNA-binding proteins: some chromatin remodeling enzymes can displace or alter the position of nucleosomes and replace canonical histones with other histone variants. Histone variants can affect both the properties and the dynamics of nucleosomes (Weber and Henikoff, 2014). This appears to be important, for example, in the regulation of transcription, where the different histone variants can influence the binding of different protein factors to support specific transcriptional programs. For example, the histone variants H2AZ and H3.3 have been found in association with various complexes of transcription factors at the level of active transcription initiation sites and enhancers where they seem to facilitate transcriptional activity. Other studies indicate a role of H3.3 during the development and maintenance of cell pluripotency (Maze et al., 2014). Still, other publications associate particular histone variants with aberrant transcriptional activity associated with oncogenesis (Vardabasso et al., 2014).

Canonical histones and histone variants possess protruding amino and carboxy-terminal domains that can undergo different post-translational modifications. In recent years, many histone-modifying enzymes have been identified: enzymes for acetylation, methylation, phosphorylation, ubiquitination, sumoylation, ADP-ribosylation, citrullination and proline-isomerization (Kouzarides, 2007). Most of these modifications are dynamic and the corresponding enzymes able to remove them have been identified. Methyltransferases and kinases are the enzymes that have the higher specificity; in other cases, the enzymatic specificity can be determined by the type of protein complex to which the enzyme can associate (Kouzarides, 2007).

Distinct sets of histone modifications have been associated with states of minor or major accessibility to chromatin. Post-translational modifications of histones can influence the formation of higher-order chromatin structures due to histone contacts in adjacent nucleosomes or long-range interactions. These contacts can be favored by proteins that are recruited at specific

histone modifications through specific domains. For example, methylation is recognized by protein possessing chromo-like domains (Tudor, MBT) and PHD domains, acetylation is recognized by bromodomain, while phosphorylation by domains owned by proteins 14-3-3 (Kouzarides, 2007). Furthermore, certain histone modifications can specifically prevent the binding of certain proteins to chromatin (Kouzarides, 2007). Several models have been proposed that predict the organization of chromatin in higher-order molecular structures, as a result of long-range interactions between distal segments of DNA. For example, it is known that enhancers can exert their regulatory action also on regions at different kilobases away along the linear arrangement of the DNA, thanks to the formation of loops that allow distant elements to be brought closer (Pombo and Dillo, 2015). These loops allow transcriptional factors associated with enhancers to contact a target promoter and influence the composition of the pre-initiation complex (Pombo and Dillo, 2015).

A subsequent structural organization level is represented by the so-called chromatin hubs, structures that are formed through direct contacts between many enhancers and the promoter of their target gene thanks to long-range contacts. The formation of a chromatin hub requires the recruitment of transcription factors that have specific affinities for each other and for the DNA sequence they bind, proximity and specificities determine which sequences and which promoters will form the chromatin hub and therefore which gene will be specifically expressed. Furthermore, according to some models, different transcriptional factors can also cluster to form distinct functional nuclear compartments. Examples of this type of organization include foci of DNA and RNA polymerase or of chromatin regulatory protein complexes, such as the Polycomb complex (Pombo and Dillo, 2015). DNA polymerase clusters are referred to as “replication factories”. According to this model, RNA polymerase is also organized in discrete domains called "transcription factories".

High-resolution chromatin interaction maps have been produced. This led to the formulation of a model of chromatin organization into distinct functional modules called physical domains or topologically associated domains (TADs). The genomic regions within each TADs form extensive interactions between them, while when crossing the boundaries between one TADs and the other, the interactions are drastically reduced (Dixon et al., 2012). This type of organization is extremely widespread in the organization of different cell types and is strongly conserved among the genomes of different species. The boundaries of TADs are abundantly bound by the CTCF protein, which acts as an insulator element and contains sequences encoding housekeeping genes, tRNAs and SINEs elements, indicating that these could play a role in

the formation of the topological domain structure of the genome (Dixon et al., 2012). The DNA folded through various mechanisms is finally organized into chromosomes that occupy discrete regions of the nucleus, the so-called "chromosomal territories" (Nemeth and Längst, 2011).

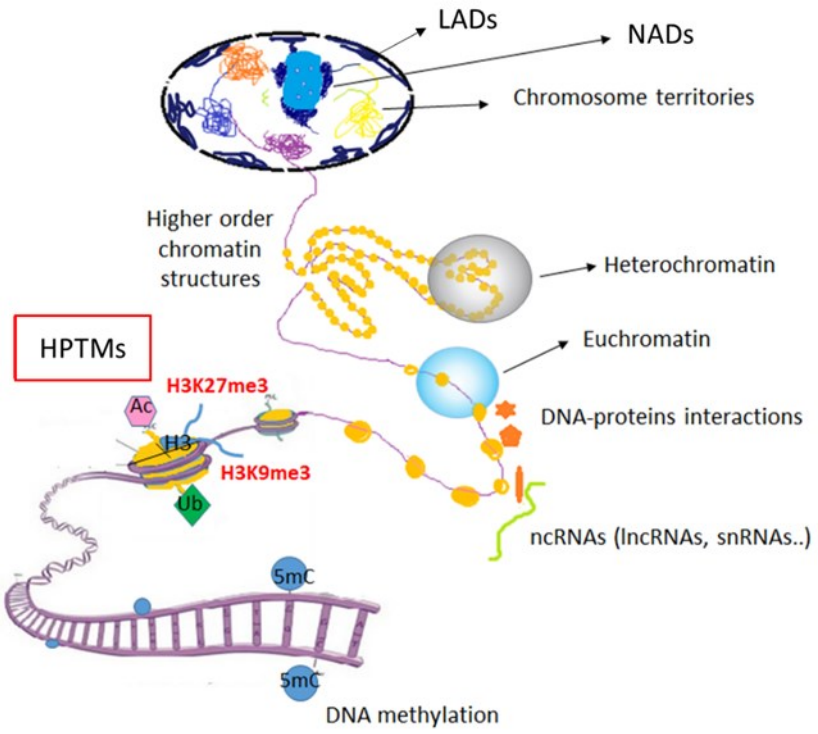

Figure 1.1: Epigenetic regulation occurs at different molecular levels of increasing complexity and influences chromatin 3D organization inside the nucleus.

1.4 Heterochromatin and Euchromatin

The name chromatin derives from the fact that this structure resulting from the association of DNA with proteins can be intensely stained and visualized under microscopy using different contrast techniques that will be discussed later. The portions of DNA that show less associated with proteins are less intensely stained. Indeed, roughly speaking, there are two different states of chromatin in the genome, heterochromatin characterized by a more compact structure and less accessible to transcription factors and euchromatin, more relaxed and permissive to transcription. The boundaries between the two different states are defined by some transcription factors, including CTCF, a protein capable of recruiting chromatin remodeling enzymes (Kouzarides,

2007). In mammals, heterochromatin is mainly characterized by low levels of acetylation and high levels of methylation in specific sites: lysine 9 and 27 on histone H3, lysine 20 on histone H4 (H3K9, H3K27, H4K20). Euchromatin, typically actively transcribed, shows instead a high rate of acetylation and trimethylation at the level of lysine 4, 36, 79 on histone H3 (H3K4, H3K36 and H3K79) (Dixon et al., 2012). Bivalent chromatin domains were also discovered characterized by both typical modifications of active and repressed chromatin. Usually, these domains are found in embryonic stem cells (ESCs) cells or in undifferentiated cells and this reflects the low level of expression of transcription factors related to differentiation. When these cells begin the path of differentiation, usually only one type of modification is preserved (Kouzarides, 2007).

1.5 The heterochromatin HPTMs: H3K9me3, H4K20me3 and H3K27me3

The post-translational modifications of histone tails by either histone modifying complexes or chromatin remodelling complexes lead to complex, combinatorial transcriptional outputs. The carboxyl (C) terminal end of the histones contributes to histone-histone interactions, as well as histone-DNA interactions, while the amino (N) terminal charged tails are sites of the post-translational modifications. Heterochromatin represents a major fraction of the higher eukaryotic genome and exerts pivotal functions of silencing repetitive elements, maintenance of genome stability and control of gene expression. Among the different HPTMs associated with heterochromatin, tri-methylation of H3K9 (H3K9me3) represents a molecular feature of constitutive heterochromatin in many eukaryotes. This HPTM is catalyzed by the suppressor of variegation 3-9 histone–lysine N-methyltransferase SUV39H1 and SUV39H2 in mammals. The H3K9me readers HP1α selectively bind methylated H3K9 through its chromodomains. H3K9me3 can be coupled with other repressive marks such as DNA 5mC (Allshire and Madhani, 2018). Suv39h methyltransferases direct H3K9me3 formation at pericentric heterochromatin, which is made up of major satellite repeats and accumulates at intergenic major satellite repeats (Bulut-Karslioglu et al., 2014). H3K9me3, although traditionally associated with the noncoding portions of the genome, has also emerged as a key player in repressing lineage-inappropriate genes. H3K9me3 can influence cell identity by preventing binding by diverse transcription factors, thus constituting a major barrier to cell reprogramming. Its deposition provides a restriction on developmental potency in the early embryo and promotes the stability of specific differentiated cell fates (Becker et al., 2016).

Considering the HPTMs on histone H4, in mammalian cells, the majority of methylation is detected in the N-terminal tail on lysine 20 (H4K20). This methylation mark is evolutionarily conserved from yeast to human (Schotta et Al., 2008) and exists as mono-, di- and trimethylation. Each of these states results in distinct biological outputs: Mono- (H4K20me1) and dimethylated H4K20 (H4K20me2) are involved in DNA replication and DNA damage repair, whereas trimethylated H4K20 (H4K20me3) is another hallmark of constitutive heterochromatic regions. In mammals, the different H4K20 methylation states are established by several methyltransferases of which KMT5B and KMT5C mediate the majority of tri-methylation. H4K20me3 is highly enriched at pericentric heterochromatin, telomeres, imprinted regions and repetitive elements, suggesting that this modification is involved in transcriptional silencing. H4K20me3 appears to be important for the silencing of repetitive DNA and transposons (Schotta et al., 2008). When it is present at promoters, it is associated with the repression of transcription (Wang et al., 2008).

H3K27me3 is another histone methylation occurring on the amino (N) terminal tail of the core histone H3. It is a hallmark of facultative heterochromatin in numerous organisms and is associated with the downregulation of nearby genes via the formation of heterochromatic regions. EZH2, a component of the PRC2 protein complex, catalyzes H3K27 di-methylation and tri-methylation (H3K27me2/3) in association with EED and SUZ12. H3K27me3 can be recognized by a chromodomain protein in the canonical Polycomb Repressive Complex 1 (PRC1) (Fischle et al., 2003; Min et al., 2003; Cao et al., 2002). PRC1 will bind to H3K27me3 and contribute to the compaction of the nearby chromatin by mediating the ubiquitination of histone H2 on lysine 119 (H2K119Ub) (Endoh et al., 2012). PcG proteins maintain gene silencing that is established during early development and is required for appropriate cell fate specification. The significance of H3K27me in maintaining appropriate long-term gene expression patterns is demonstrated by the range of mutations in PRC2 complex members, and its substrate (H3K27), in cancers. Both loss of function and change of function mutations in PRC2 have been reported in cancers, but a common outcome is an altered distribution of H3K27me, which perturbs differentiation (Nishino et al. 2012).

Actively transcribed regions of the genome marked by H3K4me3 and H3K36me2/3 are generally distinct from those marked by H3K27me3. H3K4me3 and H3K27me3 are mutually exclusive at HOX genes in Drosophila embryos (Papp and Müller, 2006) and differentiated mammalian cells, but these modifications can coexist in “bivalent” domains in ESCs (Bernstein et al., 2006).

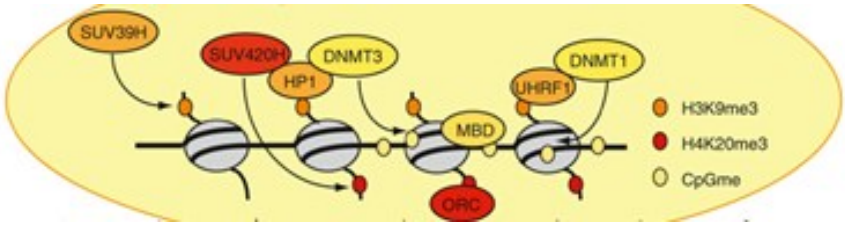

Figure 1.2: Constitutive heterochromatin formation in mammals. SUV39H establish H3K9me3, a histone mark recognized by HP1 proteins, which in turn recruits SUV420H and DNMTs, leading to H4K20me3 and DNA methylation, respectively. Adapted from Saksouk et al., 2015.

1.6 Nuclear crowding and phase separation are driving forces for nuclear compartmentalization and 3D nuclear architecture organization

The precise spatial organization of nuclear elements, suggests the existence of discrete functional sub-compartments. Among these two most prominent are heterochromatin and nucleoli. These functional domains are not delimited by lipid membranes as commonly observed for the other cell organelles; while it was hypothesized that they rather emerge as separated in the nucleoplasm, mainly thanks to two leading forces: macromolecular crowding and phase separation (Richter et al., 2007). They can be observed for long at light microscopy in living cells, but despite this long-term macroscopic stability, nuclear compartments are highly dynamic at the molecular level, as suggested by fluorescence redistribution after using photobleach/activation techniques (Lippincott-Schwartz et al., 2001; Patterson and Lippincott-Schwartz, 2002). To explain this, nuclear compartments have been proposed to self-organize cooperatively by a multitude of stereospecific short-lived interactions of their components (Misteli, 2005). The crowded nuclear environment favors biomolecules assembly (Hancock, 2004). In fact, crowding induces volume exclusion since the volume occupied by co-solutes is inaccessible to others. It also slows down diffusion up to several orders of magnitude as co-solutes act as obstacles (Saxton, 1993a; Saxton, 1993b). Finally, crowding shifts reactions towards bound states (Minton, 1995, 1998, 2006) because of the reduction of available volume. Therefore, the formation of these compartments is driven by molecular crowding due to an enhancement of molecular interactions by a self-governed biophysical process that is generic and independent of any specific biological function or structure of the interactors. It could therefore promote maintenance of

compartments at low cellular energy cost and without the need for membranes.

Crowding, causing volume exclusion, diffusive hindrance and enhanced affinity in dense nuclear compartments, dictating the behaviour of nuclear proteins, affecting chromatin compaction and several other nuclear processes (Hancock, 2004). For instance, transcription kinetics is influenced by the surrounding molecules that can deeply affect the thermodynamic equilibrium of this process (Richter et al., 2007). In fact, highly crowded nucleoplasm decreases nuclear molecules' diffusion rates, thus favouring interaction with DNA and promoters (Shim et al., 2020).

Moreover, recent studies have demonstrated that membrane-less organelles exhibit liquid-like properties that are thermodynamically reversible (Shin et al., 2017). These intracellular membrane-less compartments are formed by a liquid-liquid phase separation (LLPS, also known as condensation or coacervation) of DNA, RNA and protein mixtures which behave like liquid droplets (Nakashima et al., 2019). The liquid phase of molecules can vary their condensation resulting in a more dilute or concentrated droplet phase under certain conditions (Zhou et al., 2018).

LLPS could be related to nuclear crowding, since phase-separated compartments forms as a consequence of the interaction between nuclear molecules (Shin et al., 2017). An important driving force underlying liquid droplet formation and stability is multivalent protein-protein and nucleic acid-protein interactions (Jiang et al., 2015). The formation of the liquid droplet and its volume is determined by local changes in key constituents: DNAs, RNAs and proteins, due to changes in expression, localization, degradation and solubility. There is a molecular concentration required for the formation of a liquid droplet that occurs only when this overcomes a threshold (saturation concentration) (Banani et al., 2017). Above this threshold, dense liquid droplets separate from the diluted nucleoplasm phase through an LLPS (Aumiller and Keating, 2017). These compartments are “permeable” or allow the association of specific biomolecules while excluding others based on their shape and chemical features, hence determining a partition without the need for lipid layers (Su et al., 2016). The strength of interaction, inside each compartment, is predicted to be strong enough to allow association, but not so much to prevent the internal dynamicity typical of liquid state (Hyman et al., 2014). A recent model suggests that heterochromatin domains are organized via phase separation driven by specific proteins, such as the HP1α, through interactions with different binding partners (Strom et al., 2017). HP1α is able to drive LLPS because it possesses oligomerization domains, an intrinsically disordered region (IDR) and a substrate-binding domain. These features seem to be particularly important to drive the formation of

membrane-less domains, de-mixed from the surrounding solutions (Wang et al., 2019; Feng et al., 2019).

Other representative examples of membrane-less compartments are Cajal bodies, germline P granules (germ cell granules or nuages), histone locus bodies, nuclear speckles, nucleoli, processing bodies, promyelocytic leukemia nuclear bodies and stress granules (Uversky, 2017; Gibson et al., 2019; Shaw et al., 2008; Moser et al., 2010). High-resolution imaging has shown similarities in their morphology, conformation and dynamics, despite the differences in their composition, location and function (Banani et al., 2017). In particular, a growing number of studies have revealed that the nucleolus and its diverse dynamic functions can be explained assuming a liquid droplet-like nucleolus nature (Lafontaine et al., 2021). Nucleolus is denser than the surrounding nucleoplasm and provides an example of a liquid droplet that is formed from nucleolar RNA-binding proteins which exhibits a thermodynamic preference for RNA, ensuring that droplets preferentially grow at transcriptionally active rDNA loci accompanied by RNA polymerase I (RNA Pol I) (Berry et al., 2015).

1.7 The rRNA synthesis in eukaryotes

Ribosome synthesis is one of the most energetically demanding and complex cell processes (Fromont-Racine et al., 2003; Henras et al., 2008; Kressler et al., 2008). The 80S ribosome is a ribonucleoprotein complex that comprises a large 60S subunit containing the 28S, 5.8S and 5S rRNA, and 46 RPs and a small 40S subunit containing the 18S rRNA and 33 RPs (Fromont-Racine et al., 2003; Henras et al., 2008; Kressler et al., 2008). Ribosome biogenesis begins in the nucleolus, where the rRNA species 18S, 5.8S and 25S, are co-transcribed by RNA Pol I as a single polycistronic transcript.

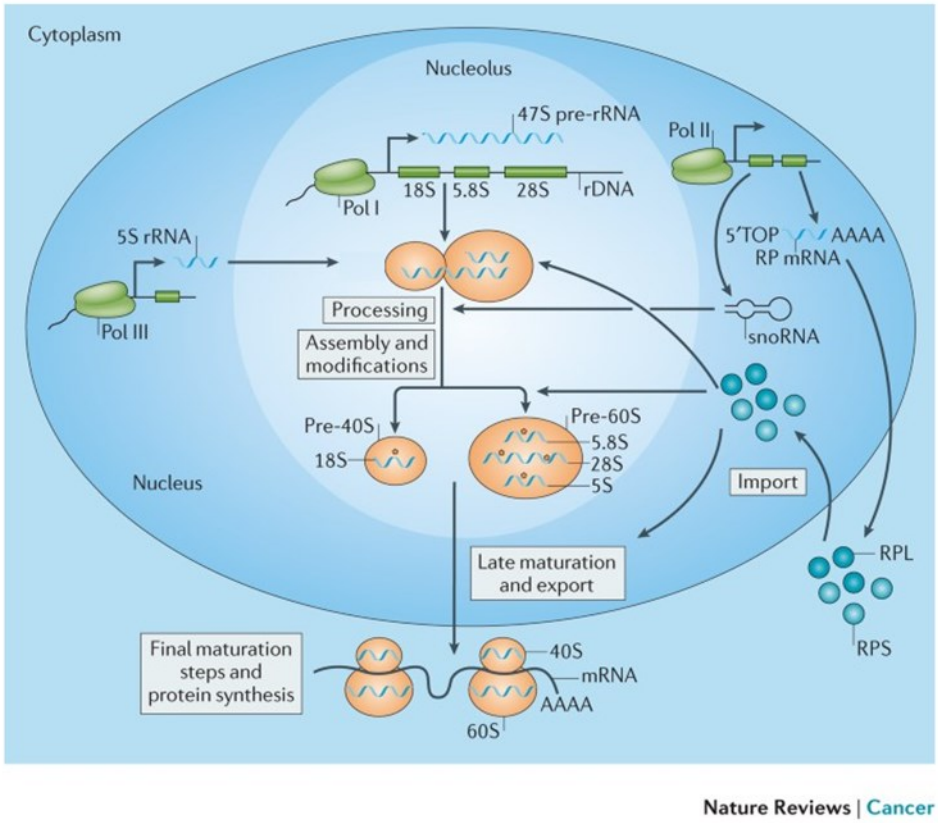

Figure 1.3: schematic overview of ribosome biogenesis in eukariotes. Modified from Pelletier et al., 2017.

In human cells, rDNA localizes on the p arms of the ten acrocentric chromosomes (Henderson et al., 1972) and is organized as clusters of repetitive sequences, called nucleolus organizer regions (NORs) (Sylvester et al., 1986). Each repeated unit is composed of rRNA genes separated by intergenic spacer sequences (IGS). rDNA is transcribed to produce the 47S nascent transcripts in human (45S in mouse) (Dundr and Olson, 1998), which consist of the 18S, 5.8S, and 28S rRNAs, 5′, 3′ external transcribed spacer sequences and of two internal transcribed spacers flanking 5.8S rRNA. External and internal transcribed spacer sequences are then excised through various steps that start co-transcriptionally by different endo- and exonucleases. The three mature rRNAs together with 5S rRNA constitute the functional core of the two ribosomal subunits. 5S rRNA is transcribed by Pol III outside nucleoli and is, subsequently, imported. The IGS sequences

contain enhancers and give rise to RNA molecules that recruit factors involved in transcriptional control (Schöfer and Weipoltshammer, 2018).

The nucleolus is the site of the highest RNA synthesis rate in cell nuclei producing more than 60% of the entire RNA pool. RNA pol I catalyzes rDNA transcription, binding directly to two regulatory sequences: the CORE, located between -45 to +20 and near the transcription start site, and the upstream control element (UCE), located between -200 and -107. Transcription requires the formation of a preinitiation complex (PIC) that is composed of RNA Pol I, UBTF and the promoter selectivity factor (SL1) or TIF-IB in mouse (Goodfellow and Zomerdijk, 2013). UCE and CORE come in contact thanks to the dimerization of UBTF that form loops, allowing the formation of the enhanceosome with the consequent binding of SL1 and the formation of a stable PIC. The two DNA binding regions within UBTF, if phosphorylated, lead to the unfold of the enhanceosome that results in transcription repression (Stefanovsky et al., 2006). UBTF is also involved in the regulation of transcription elongation (Stefanovsky and Moss, 2008). The recruitment of RNA Pol I to the rDNA promoter is mediated by TBP-associated factors (TAFs) that interact with UBTF and TIF-1A, a component of RNA Polymerase I (Goodfellow and Zomerdijk, 2013).

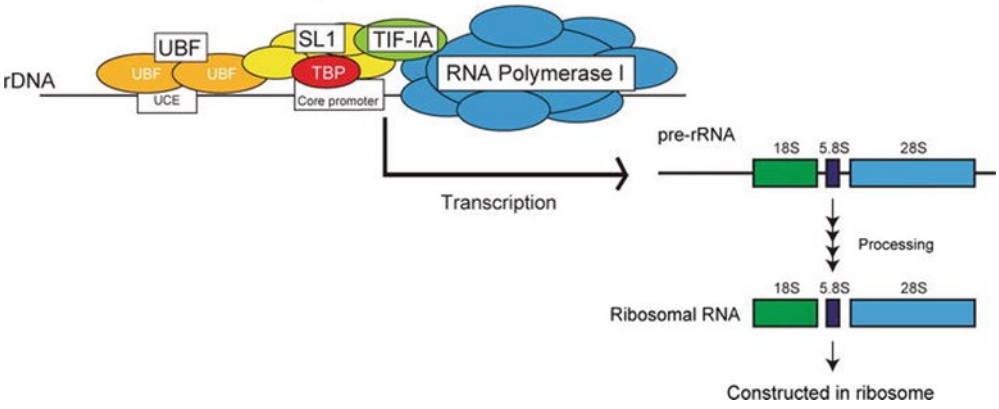

Figure 1.4: the basic composition of the PIC for RNA polymerase I. PIC is assembled on the rDNA promoter by synergistic action of UBTF (bound at the UCE), SL1 (bound to the core promoter) through TBP, TIF-IA and RNA Pol I. SL1 recruits RNA polymerase I through TIF-IA. Once PIC is formed, Pol I is released from the promoter and starts to transcribe pre-rRNA. Pre-rRNA is processed giving rise to 18S, 5.8S, and 28S rRNAs to construct ribosomes. Adapted from Tanaka and Tsuneoka, 2018.

Silencing of rRNA genes relies on epigenetic factors and is majorly mediated by the NoRC complex (Santoro and Grummt, 2002). Epigenetic regulation of rRNA transcription adapts the cytoplasmic ribosome availability for protein synthesis to different internal and environmental stimuli. Tumor cells, for instance, increase rRNA transcription to satisfy the increased demand for ribosomes useful to sustain malignant transformation (Drygin et al. 2011; van Sluis and McStay 2014).

The total number of rRNA genes per diploid human genome is approximately 400 copies (Gibbons et al. 2014; Schmickel 1973). However, the repetitive rDNA sequences are genomic hotspots for recombination events, determining great variations of the number and the distribution of genes over the ten NORs between individuals (Gibbons et al. 2014; Stults et al. 2008). The copy-number variation (CNV) of the rDNA arrays seems to be related to the copy number of the extra-nucleolar 5S rDNA (Gibbons et al. 2015), which range from 50 to 300 repeats (Stults et al. 2008). Only a fraction of rRNA genes are actively transcribed in a particular context, so that rRNA synthesis is regulated according to a broad range of metabolic demands. Moreover, the number of active genes is species- and tissue-specific; human fibroblasts, for instance, have about 115 actively transcribed genes per cell (Haaf et al. 1991). Inversions of arrays, palindromic structures, and the reversal of the head-to-tail orientation of ribosomal genes influence the number of potentially active rDNA genes (Caburet et al. 2005). rDNA instability is thought to be an important contributor of cellular ageing (Kobayashi, 2008).

In mammalian cells, the number of active genes is constant under stable metabolic conditions and during cell cycle (Conconi et al. 1989; Haaf et al. 1991). Under conditions of changing demand for ribosomes, new rRNA genes are recruited for transcription or, conversely, are silenced. They may be permanently silenced or converted into a poised state, which is competent of transcriptional activation. Differentiated cells have a higher amount of poised rRNA genes (Xie et al. 2012).

1.8 The nucleolus roles in nuclear architecture organization, NADs and LADs

The nucleolus is a membrane-less compartment composed of the fibrillar center (FC), the dense fibrillar component (DFC), and the granular component (GC). Transcription of rRNA is thought to occur at the boundary between FC and DFC, whereas processing of the pre-rRNA occurs in the DFC region and pre-ribosomal subunit assembly takes place in the GC region (Biggiogera et al., 2001). Recent results revealed that these nucleolar

subcompartments are organized in distinct liquid phases formed by phase separation which induces the formation of multilayered liquids. These physical properties seem to facilitate sequential RNA processing reactions in a variety of ribonucleoprotein bodies (Zhou et al., 2018).

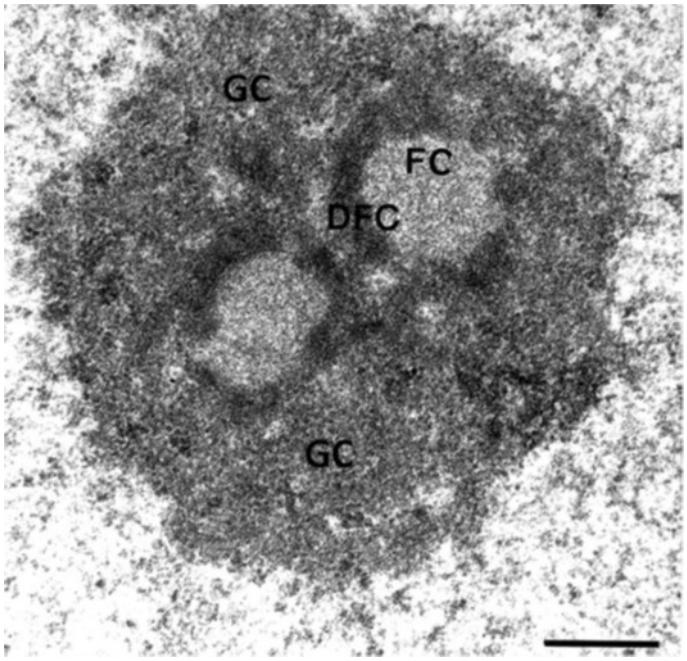

Figure 1.5: Nucleolus of a HELA cell at TEM. The sub-nucleolar compartments: granular component (GC), dense fibrillar component (DFC), fibrillar center (FC) are clearly visible. Bar, 0.5 μm. Adapted from Sirri et al., 2002.

The cell nucleus may contain many nucleoli. In each cell, the fraction of rRNA genes transcriptionally active localize within nucleoli while inactive rDNA repeats localized at the periphery of the nucleolus in a perinucleolar inactive chromatin compartment (Mathenson and Kaufam, 2016; Jakociunas et al. 2013, Zhou et al., 2002; Santoro and Grummt, 2005). Silencing of rDNA repeats is mediated by NoRC complex that recruits histone-modifying and DNA methylating enzymes (Santoro and Grummt, 2002; Guetg et al., 2010) The NoRC recruited to the perinucleolar region may also introduce heterochromatic marks such as 5mC, H3K9me3 and H4K20me3, into other chromatin regions in the vicinity of the nucleolus. For instance, centromeric heterochromatin is often located close to the nucleolus, and depletion of BAZ2A, a subunit of NoRC compromises both rDNA silencing and assembly of centromeric heterochromatin (van Koningsbruggen, 2010).

In the last decades, several results indicate that the role of nucleolus might go beyond the sole production of ribosomes and that it can play important roles in the organization of 3D genome architecture. Heterochromatin domains close to nucleoli are observed in all somatic cells.
Genomic segments located within the perinucleolar compartment are commonly referred to as nucleolus-associated chromatin domains (NADs).
Beyond silenced rDNAs NADs contain sequences located in the short arms of acrocentric chromosomes, centromeric and pericentromeric chromatin of most chromosomes and subtelomeric regions of some chromosomes. Moreover, NADs contain more than 1000 genes. Among these, there are those encoding for the T-cell receptors, olfactory receptors and two families of immunoglobulin genes. Many NAD-associated genes have similar features: they are tissue-specific and form large gene clusters (Guelen et al., 2008). The inactive X chromosome was also found to contact the perinucleolar compartment during the mid/late-S-phase and it was suggested that this location could be important for faithful duplication of silent chromatin (Zhang et al., 2007). Initial genome-wide studies identified NADs by biochemical purification of nucleoli, through sonication of nuclei, adjusting the power so that nucleoli remain intact because of their denser nature (Sullivan et al., 2001). NADs were found to correspond to regions of low gene densities, low transcriptional levels and repressive histone modifications: H4K20me3, H3K27me3, and H3K9me3. Interactions of genomic loci with nucleoli have also been identified by measuring the contacts between the rRNA genes and the rest of the genome using Hi-C (Lieberman-Aiden et al., 2009). These assays revealed that in lymphoblastoid (LCL) and erythroleukemia (K562) cells rRNA genes contacts segments of repressed, late replicating chromatin and CTCF binding sites (Yu et al., 2018; Rao et al., 2014). rRNA transcripts that correspond to DNA located around the nucleolus were also identified by split-pool recognition of interactions by tag extension (SPRITE) (Quinodoz et al., 2018), a method that can measure RNA and DNA interactions, allowed the identification of genomic regions contacting. This analysis revealed that regions that are linearly close to the centromere are closer to the nucleolus, consistently with the previous observations of centromeres co-localization with the nucleolar periphery; while actively transcribed regions were excluded from the nucleolar compartment even when they reside in linear proximity to a centromere. MiCEE, a multicomponent ribonucleoprotein complex containing factors of the exosome (C1D, EXOSC10 and EXOSC5), and PRC2 were found to tether loci of bidirectionally active genes to the perinucleolar region and induce ncRNA degradation and transcriptional silencing by heterochromatin formation (Singh et al., 2018). Therefore, nucleolus appears to act as an attractive compartment for repressed genomic portions and, together with the nuclear lamina, represents a hub for the

organization of the inactive heterochromatin (Padeken et al., 2014; Guetg et al., 2012; Peric-Hupkes et al., 2010).

The nuclear lamina forms a scaffold on the inner surface of the nuclear envelope, towards the nucleoplasm and is formed by a class of intermediate filaments called lamines. The lamine filaments cross at right angles to form an irregular anastomotic network that provides mechanical support to the envelope, determining the shape of the nucleus and providing the binding site for a variety of proteins that anchor chromatin (Gruenbaum, 2005).

In mammalian cells, large portions of the genome associate with the nuclear lamina at the periphery of the nucleus and are identified as lamina-associated domains (LADs). LADs are essentially composed of regions with silent chromatin molecular features (Peric-Hupkes et al., 2010).

Sequences belonging to LADs are detected in all chromosomes, usually as domains ranging from 100 kb to 10 mb. LADs are characterized by low gene density and replicate in late S phase (Luperchio et., 2018; Chen et al., 2018). Accordingly, LADs, like NADs are rich in di- and trimethylated H3K9 (H3K9me2 and H3K9me3) (Guelen et al., 2008; Lund et al., 2014). This repressed state is reached also through histone deacetylation, as demonstrated for instance by the interactions of LAP2β with HDAC3 (Somech et al., 2005) and of A-type lamins with the sirtuins SIRT1 and SIRT6 (Ghosh et al., 2015). Reporter genes inserted into LADs show lower expression than in inter-LAD regions, demonstrating again the role of nuclear lamina anchoring in gene silencing (Akhtar et al., 2013). Moreover, changes in gene expression depending on their association with the nuclear lamina have been observed during cell differentiation (Rønningen et al. 2015; Robson et al., 2016; Peric-Hupkes et al., 2010, Lund et al., 2013).

NADs and LADs share many molecular features of heterochromatin. This evidence led to the hypothesis that the nucleolus and nuclear lamina could serve as interchangeable scaffolds for the localization of heterochromatic domains that attracted portions of the genome to be silenced. Accordingly, some studies reported that LADs from the mother cell after mitosis division can be positioned to the nucleoli of the daughter cells (Kind et al., 2013; Ragoczy et al., 2014) and similarly that NADs can relocate from nucleoli nearby of the nuclear envelope (van Koningsbruggen et al., 2010).

However, some studies highlighted the differences between these domains. For instance, SPRITE analysis provided an important distinction between NADs and LADs by determining the presence of inter-chromosomal contacts at the same nucleolus, while lamina-associated interactions generally occur

between regions that are linearly close to each other (Quinodoz et al., 2018). Vertii and colleagues also found a subset of perinucleolar chromatin which is rarely distributed to the lamina. Specifically, through biochemical purification of nucleoli followed by deep sequencing, they found distinct classes of loci belonging to NADs and they proposed a software to analyze the sequencing data called “NADfinder” to individuate sequences specifically associated with NADs based on their molecular properties and some bioinformatics inferences (Vertii et al., 2019).

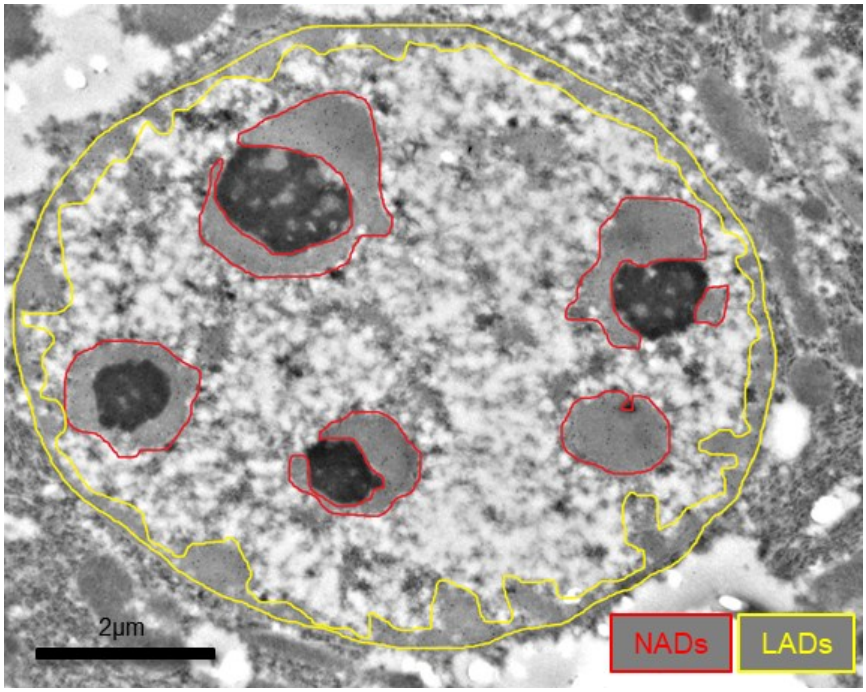

Figure 1.6: section of a mouse hepatocyte nucleus at TEM. NADs boundaries are indicated by red lines, while LADs boundaries by yellow lines.

1.9 Techniques to discriminate heterochromatin from euchromatin

1.9.1 Molecular approaches

Different molecular and microscopic approaches can be used to distinguish the more compact heterochromatin regions from euchromatin.

Molecular approaches are mainly based on the fact that the euchromatin regions show greater sensibility to enzymatic digestion than heterochromatin

due to the reduced association with proteins and major exposure of the naked DNA strand to enzymes. The first technique developed in this category was DNase-seq (DNase I hypersensitive sites sequencing) which is used to identify the location of regulatory regions, based on the genome-wide sequencing of regions sensitive to cleavage by DNase I (Boyle et al., 2008; Madrigal and Krajewski, 2012). A similar technique MNase-seq relies on the use of a non-specific endo-exonuclease, the micrococcal nuclease derived from Staphylococcus aureus, to bind and cleave protein-unbound regions of DNA (Schones et al., 2008, Klein and Hainer, 2019). While FAIRE-seq is based on the fact that the formaldehyde cross-linking is more efficient in nucleosome-bound DNA than it is in nucleosome-depleted regions of the genome. Then the selected non-cross-linked DNA in open chromatin is sequenced (Giresi et al., 2007). Later on, ATAC-seq was developed. It identifies accessible DNA regions by probing open chromatin with hyperactive mutant Tn5 Transposase that inserts sequencing adapters into open regions of the genome. In a process called "tagmentation", Tn5 transposase cleaves and tags double-stranded DNA with sequencing adaptors. The tagged DNA fragments are then purified, PCR-amplified, and sequenced using next-generation sequencing (Picelli et al., 2014). Sequencing reads can then be used to infer regions of euchromatin as well as to map regions of transcription factor binding sites and nucleosome positions. The number of reads for a region correlates with the degree of chromatin accessibility (Buenrostro et al., 2015).

1.9.2 Microscopy approaches

Imaging DNA is possible thanks to DNA specific labels such as intercalating dyes like SYBR Green, TOTO-1, YOYO-1, SYTO and the minor or major groove binding dyes like Hoechst and PicoGreen (Lakadamyali and Cosma, 2015).

Hoechst stains are a family of blue fluorescent dyes. These dyes bind to the minor groove of double-stranded DNA with a preference for sequences rich in adenine and thymine (AT-rich sequences) (Portugal J and Waring MJ, 1988).

DAPI is another fluorescent stain that binds strongly to AT-rich sequences and is used extensively in fluorescence microscopy (Kapuscinski, 1995).

Acridine orange is an organic compound that serves as a nucleic acid-selective fluorescent dye that interacts with DNA by intercalation and RNA via electrostatic attractions (Mirrett, 1982). When bound to DNA, acridine orange has a maximum excitation at 502nm and 525 nm (green); while when associates with RNA, it has a maximum excitation shift from 525 nm (green)

to 460 nm (blue). The shift in maximum excitation also produces a maximum emission of 650 nm (red) (Sharma et al., 2020).

In all these cases, the heterochromatin regions which locally contain a major quantity of DNA due to their more compact conformation, tend to be more intensely stained.

A more accurate method for imaging heterochromatin regions in sections of nuclei at transmission electron microscopy (TEM) is the EDTA regressive staining (Bernhard's technique) which exploits EDTA as a chelating agent to reveal with heavy contrast cell structures containing RNA, while deoxyribonucleoproteins and heterochromatin lose most of the stain, so they appear as bleached or lighter portion in the nucleoplasm, usually localized close to the nucleolus and in the inner part of the nuclear envelope. Specifically, this happens because this procedure is based on the proposition that after staining ultrathin sections with uranyl, the stain is preferentially removed from DNA rather than RNA by the action of the chelating agent EDTA (Bernhard, 1969).

Finally, the Feulgen reaction is a classic cytochemical method suitable to reveal DNA. Feulgen-positive sample sections exhibit a magenta (red-purple) color when observed at light microscopy or a red color under the fluorescence microscope. This technique was proposed by Robert Feulgen and Heinrich Rossenbeck in 1924 and nowadays is still used in cytogenetics, cell biology and cytopathology (Hardie et al., 2002, Biesterfeld et al., 2011, Nielsen et al., 2012). During the Feulgen reaction, a Schiff reagent binds to aldehyde groups in the DNA molecule, previously engendered by HCl acid hydrolysis and resumes a red fuchsia colour. All reagents, which react specifically with aldehyde groups in the presence of H_2SO_3, are defined Schiff-like reagents (Biggiogera et al., 1996). At the beginning of the seventies, Gautier et al. synthetized an inorganic ammine of osmium and used it in transmission electron microscopy for the specific detection of DNA (Olins et al., 1989). This staining technique is based on a Feulgen-type reaction, consisting of acid hydrolysis to obtain free aldehyde groups on DNA followed by their binding to osmium ammine. Since the DNA interaction with the osmium ammine is specific, the nuclear domains characterized by high DNA concentration, like heterochromatin, appear dark on a lighter background (Biggiogera et al., 1996).

1.10 Techniques to study 3D genome organization

Genome sequencing has opened the way to a deep knowledge of our genome and that of model organisms, allowing a much faster annotation of coding sequences and providing information on possible functional aspects of non-coding regions. This shed light on many molecular features of genetic diseases previously unknown. Furthermore, subsequent assays based on sequencing have allowed identifying the position of epigenetic modifications in the DNA nucleotide base sequence, such as Whole Genome Bisulfite Sequencing, a next-generation sequencing technology used to determine the DNA methylation status of single cytosines (Clark, 1994).

However, as previously described, the complex network of molecular processes that take place in the nucleus are profoundly influenced by the three-dimensional organization of chromatin.

We have described how the wrapping of DNA around nucleosomes constitutes a first level of regulation of gene expression and how specific histone modifications can influence the binding or dissociation of histones from DNA and favouring or inhibiting the binding of specific protein complexes. Different protein complexes, in turn, can catalyze different chemical reactions on specific DNA sequences or build supportive structures to bring distal segments of DNA close together. ChIP-seq assay (Johnson et al., 2007) or the alternate method DamID (van Steensel et al., 2000), allowing to identify the binding sites of specific proteins along the DNA sequence, have provided a lot of fundamental information to understand this level of epigenetic regulatory mechanisms. Another variant is ChIP-on-Chip which combines ChIP with DNA microarray and allow the identification of protein biding site on DNA on a genome-wide basis. This technique is usually applied to determine binding sites of transcription factors, replication-related proteins, histones and their variants (Aparicio, 2004).

An alternative microscopy approach to obtain information about the structure and dynamics of nucleic acids is Nucleic acid NMR spectroscopy. Parameters taken from the nucleic acids spectrum can provide information about their local structural features such as glycosidic bond angles, dihedral angles and sugar pucker conformations. This methodology has been used to probe the binding of nucleic acid molecules to other molecules, such as proteins or drugs. Moreover, for large-scale structures, NMR is useful for investigating bent helices, non-Watson–Crick base-pairing, coaxial stacking and the 3D conformation of RNA oligonucleotides (Bloomfield, 2000).

Over the years many microscopic and molecular biology techniques have been proposed to gain information about the three-dimensional conformation of chromatin and its chemical-physical properties in different cell types and under different physiological and pathological conditions.

A molecular technique widely used to investigate the contacts between distal sequences of DNA to form topologically defined three-dimensional domains is the Chromosome Conformation Capture (3C) and its subsequent implementations (4C, 5C and Hi-C). The original 3C methodology allows studying the frequency of interaction between two specific genomic regions in a cell population (Denker and de Laat, 2016). The cells initially subjected to formaldehyde treatment to form stable crosslinks between genomic sequences physically close in the 3D conformation are then lysed and the chromatin is fragmented through the use of restriction enzymes. Thereafter, a ligation reaction is carried out in conditions of strong dilution to favour the binding between contiguous sequences. Finally, the ligation product between the two interacting sequences is detected by PCR. Thanks to 4C (circularized 3C) is possible to determine the interactions established by a specific DNA sequence with the other genome sequences. While 5C assay (3C Carbon copy) revealed the contacts between many selected genomic regions. Finally, Hi-C offers the possibility of studying the interactions that occur genome-wide (Belton et al., 2012).

Microscopy studies were carried out in parallel with the molecular approaches. In fact, if the latter provides a type of high-throughput data on a large cell population, on the other hand, the microscopy techniques allow direct visualization of the dynamics of the DNA organization in the nucleus and the one can confirm the results obtained with the others and vice versa.

Concerning the microscopy techniques, the fluorescence in situ hybridization (FISH) and chromosome painting, from the 70s onwards, showed the localization of specific chromosome portions within the nucleus (Tucker, 2015). Thanks to implementations in fluorescence microscopy techniques, FISH assays have evolved to the 3D visualization of specific DNA regions or even RNA molecules within nuclear space. This methodology is called 3D FISH and is made possible thanks to a fixation strategy that preserve the nuclear structure as much as possible and CLSM (confocal laser scanning microscopy) microscopy which allows 3D reconstruction of the nucleus, through serial acquisition of optical sections. Moreover, thanks to specific adaptations is now possible the visualization of multiple target sequences, marked through the use of different fluorescent molecules (Walter et al., 2006).

However, optical microscopy has a resolution limited by the forced use of wavelengths in the visible range and by diffraction phenomena, so it is not suitable for resolving structures below 200-300nm. Lately, thanks to the advent of super-resolution microscopy techniques, the study of chromatin organization on a nanometer scale has begun to become possible (Lakadamyali and Cosma, 2015). Chromosome organization was observed dynamically in vivo thanks to super resolution microscopy techniques, such as the combination of PALM (photoactivated localization microscopy) and single-nucleosome tracking (Nozaki et al., 2017). In addition, the use of the CRISPR / Cas9 system applied to cell imaging allows following the dynamics of specific genomic loci with great precision in time-lapse in living cells (Bukhari and Müller, 2018).

1.11 Ageing

Ageing is an inevitable fate of life characterized by a progressive physiological decrease of tissues and organs functionality, which increases the risk of mortality for the organism. In fact, ageing is associated with higher susceptibility to cancer, neurodegeneration, cardiovascular diseases, and metabolic disorders (Brunet and Berger, 2014; Kennedy et al., 2014; Moskalev et al., 2014).

The ageing process is influenced by various environmental, genetic and epigenetic factors. For instance, in 1935, calorie restriction was found to greatly extend lifespan in rats (McCay et al., 1935) then many studies in different animal models confirm this trend (Fontana et al., 2010; Piper et al., 2011; Vermeij et al., 2016); while it is known that rare human mutations can cause accelerated ageing diseases (Coppedè, 2021). This evidence has drawn attention to investigating possible strategies to delay ageing and improve human quality of life.

Individuals of the same age may age at different rates. Quantitative biomarkers of aging can be a way to measure physiological age and potentially predict individual health span and life span (Kooman et al., 2019).

Establishing biological features of ageing is challenging. Criteria based on phenotype and some biomarkers have been proposed. Phenotypically ageing is characterized by frailty, reduced physical function, and cognitive dysfunction, but these are not definite criteria and given the complex nature of the ageing process, the biomarkers of ageing are multilayered and multifaceted (Kooman et al., 2019).

A decrease in telomere length is considered a marker of ageing. In particular, the length of telomeres in leukocytes has been associated with life span duration and age-related diseases, such as cardiovascular diseases (Rehkopf et al., 2016; Hammadah et al., 2017) cancer (Blackburn et al., 2015) and neurological disorders (Eitan et al., 2014). DNA damage and repair have also been implicated in ageing since cells accumulate genomic rearrangements over time. This was directly probed by the controlled induction of DNA double-strand breaks in mouse liver which caused the onset of ageing pathologies (White et al., 2015).

Ageing have been related to many changes in epigenetics features and patterns, among which variation in methylation profile have drawn the attention of many researchers and will be discussed more in details in the next section.

RNA sequencing (RNA-seq) has been very useful in determining changes in transcriptome during ageing and in defining molecular biomarkers of ageing. In particular, cell-to-cell expression variations have been highlighted by single-cell RNA-seq in blood cells and was associated with ageing and disease susceptibility (Lu et al., 2016).

It is quite likely that ageing process is related to changing in cellular and organism metabolism. In fact, as mentioned previously, dietary restriction is one of the most accepted strategy to extend life span and health span from yeast to mammals and different metabolic factors have been indicated as possible ageing biomarkers. The insulin/insulin-like growth factor 1 (IGF-1) signaling (IIS) pathway, which participates in glucose sensing, is the most known pathway to influence longevity. IGF-1 declines in mouse models of premature ageing, whereas decreasing IIS activity extends life span (Schumacher et al., 2008, Corpas et al., 1993, Crimmins et al., 2008). Another example is the target of rapamycin (mTOR) protein and its downstream target: the phosphorylated S6 ribosomal protein (p-S6RP Inhibition of mTOR). Their expression increases with age and therefore their inhibition was demonstrated to increase lifespan (Johnson et al., 2013; Dieterlen et al., 2012; Bajwa et al., 2016).

Oxidative stress has long been regarded as an ageing biomarker. It occurs due to an imbalance between the production and the accumulation of oxygen reactive species (ROS) in cells and tissues and the ability of a biological system to detoxify these reactive products. ROS include Superoxide radicals (O_2•−), hydrogen peroxide (H_2O_2), hydroxyl radicals (•OH), and singlet oxygen ($1O_2$); they are generated as metabolic by-products by biological systems (Sato et al., 2013; Navarro-Yepes et al., 2014). Processes, like

protein phosphorylation, activation of several transcriptional factors, apoptosis, immunity, and differentiation, generate ROS and their presence inside cells need to be kept at a low level (Kumar Rajendran et al., 2019). Increased ROS production has harmful effects on different cell components, affecting proteins, lipids and nucleic acids structures (Wu et al., 2013). The concentration of these biomarkers in body fluids can be detected via high-performance liquid chromatography and mass spectrometry. Oxidative stress can be responsible for the onset and/or progression of several diseases, such as cancer, diabetes, metabolic disorders, atherosclerosis, and cardiovascular diseases (Taniyama and Griendling, 2003).

One important source of oxidative stress are mitochondria. However, mitochondria dysfuctions have been implied in ageing process even independently of reactive oxygen species production. Mitochondrial dysfunction has an important role in the ageing process (Piko et al., 1988). Increasing age in mammals correlates with accumulation of somatic mitochondrial DNA (mtDNA) mutations and decline in respiratory chain function (Soong et al., 1992; Corral-Debrinski 1992). Tissues particularly subjected to this decline are heart, skeletal muscle, colonic crypts and neurons. Moreover, Respiratory-chain-deficient cells are prone to apoptosis and increased cell loss is likely a relevant consequence of age-associated mitochondrial dysfunction (Trifunovic and Larsson, 2008).

An oxidative independent protein alteration is for example protein carbamylation, a post-translational modification that occur throughout the whole life span, leading to accumulation of carbamylated proteins (Gorisse et al., 2016) which is considered a hallmark of molecular ageing and ageing-related diseases (Verbrugge et al., 2015). Another ageing biomarker in this category is the accumulation of the Advanced glycation end products (AGEs), a heterogeneous group of bioactive molecules formed by non-enzymatic glycation of proteins, lipids, and nucleic acids (Semba et al., 2010), that leads to inflammation (Thorpe et al., 1996), apoptosis (Hanssen et al., 2014), obesity (Savej et al., 2016) and other age-related disorders (Brownlee et al., 1995).

More in general, a hallmark of many age-related diseases is the dysfunction in protein homeostasis (proteostasis), leading to the accumulation of protein aggregates. In healthy cells, proteostasis is provided by molecular chaperones, proteolytic machineries and their regulators. These factors coordinate protein synthesis assisting polypeptide folding, the conservation of protein conformation and proper protein degradation. However, sustaining proteome balance is a challenging task influenced by various external and endogenous stresses that accumulate during ageing. These stresses lead to

the decline of proteostasis network capacity and proteome integrity. The resulting accumulation of misfolded and aggregated proteins affects, in particular, postmitotic cell types such as neurons, leading to disease (Hipp et al., 2019). A prominent role in the regulation of proteostasis and in other processes that influence ageing such as cell proliferation, senescence and apoptosis is the nucleolus as discussed in paragraph 1.13.

Figure 1.7: The hallmarks of ageing. Adapted from Lopez-Otin et al., 2013.

1.12 Heterochromatin and ageing

As described in the previous section ageing can be affected by a variety of external and internal factors, including diet, metabolic dysfunction, genome

instability. These ageing factors shape transcriptome changes related to the aging process through chromatin remodeling. Many epigenetic regulators, such as histone modification, histone variants, and ATP-dependent chromatin remodeling factors, play roles in chromatin reorganization during ageing (Lee et al., 2020).

Generally, a gradual loss of heterochromatin was proposed as a major factor in generating alterations in gene expression with ageing, mainly because of the consequences of aberrant de-repression of specific genes or genomic portions that should be kept silenced in a specific differentiated cell type (Villeponteau,1997). Moreover, different studies suggested that the aged cell nucleus show a general loss and disorganization of histones. This is assumed to lead to the dysregulation of the underlying genes. In fact, it seems that overexpression of the histones could dramatically extend lifespan in yeast (Feser et al. 2010). Concerning humans, it was demonstrated, for instance, that in individuals affected by Hutchinson-Gilford progeria syndrome (HGPS), a disease which determines precocious and abnormal aged phenotype, the altered Progerin expression leads to rapid and widespread loss of heterochromatin (Chojnowski et al. 2020). More in detail, nuclei from HGPS patients show a loss of peripheral heterochromatin and of the relative histone modifications H3K9me3, H3K27me3, while an opposite behavior was observed for H4K20me3, which was found upregulated (Arancio et al. 2014). On the contrary, it was also reported, a progressive “heterochromatinization” of the nucleus over time, which would have however detrimental effects, leading to a decrease in the repair processes and increase in the frequency of chromosomal aberrations. In fact, it was proposed that the higher degree of chromatin condensation in aged cells would act as a sort of obstructive barrier to the access of the repairing enzymes to DNA (Lezhava 1984; Lezhava et al. 2012). Moreover, age-related DNA hypermethylation was observed at specific genomic regions, while hypomethylation at others and, for instance, global H3K27me3 level increases with age in mice skeletal muscle stem cells (Liu et al. 2013), while it decreases with age in *C. elegans* (Ni et al. 2012). Therefore, the changes in the heterochromatin organization seem to be influenced by the locus- and cell-type-specific dynamics.

1.13 Nucleolus and ageing

Ageing research has recently been focused on the identification of genes that alter the ageing rate when mutated. The highly repeated structure of the ribosomal DNA (rDNA) and its high rates of transcription make it particularly vulnerable to genome instability and damage. Multiple studies have reported a link between rDNA stability and cellular ageing, as well as the association

of proteins involved in genome integrity transiting the nucleolus. Several nucleolar localized proteins including tumor suppressor ARF and Nucleophosmin, which assist ribosomal protein assembly, regulate cellular senescence by modulating the stability of p53 (Ko et al., 2016) (Colombo et al., 2002). Aged cells show alterations in nucleolar morphology. In particular, pre-senescent cells exhibit multiple small-sized nucleoli, while senescent cells show a single enlarged nucleolus (Bemiller and Lee, 1978). It was observed that ageing in yeast is accompanied by nucleolar enlargement and fragmentation. Concordantly, the premature ageing disorder HGPS leads to nucleolar expansion and increased ribosome biogenesis. Ribosome biogenesis is one of the most energy demanding processes in the cell. It requires about 80% of cellular energy reserves. Major perturbations in the cell have repercussions at the level of ribosome biogenesis and conversely, factors involved in ribosome biogenesis can regulate other processes. Due to its crucial role in ribosome biogenesis, the nucleolus actively determines the metabolic state of a cell (Tiku and Antebi, 2018). Recent literature highlights the crosstalk of different nucleolar functions with some well-established hallmarks of ageing such as genomic instability, telomere attrition, epigenetic modifications, and perturbations in proteostasis (Lopez-Otin et al., 2013). Lemos and Wang using whole-genome sequencing and reduced-representation bisulfite sequencing methods search for methylation profiles comparing samples from different organisms. From the mouse datasets, they identified CpG sites in the rDNA that showed increased methylation with age. This led to propose a model in which rDNA CpG methylation could be used as age molecular clock. This molecular clock was subsequently tested in human and roughly correspond with age of human samples (Wang and Lemos, 2019). A modest reduction in protein synthesis is known to extend lifespan (Tiku and Antebi, 2018). Downregulation of genes encoding multiple ribosomal proteins has been also connected to a longer lifespan in yeast and *C. elegans* (Hansen et al., 2007; Syntichaki et al., 2007). Multiple factors involved in ribosome biogenesis have been implicated in ageing. A study reported the role of nucleolar GTPase NOG-1 in regulating lifespan in *C. elegans.* Nog-1 is critical for the maturation of the 60S ribosomal subunit. RNAi against Nog-1 significantly increased the lifespan of worms while overexpression of this gene led to a reduction in lifespan (Kim et al., 2014). Also, the nucleolar methyltransferase Fibrillarin, which is required for rRNA maturation, was found to be downregulated in different longevity models of *C. elegans,* Drosophila, and mouse, as well as humans undergoing modest dietary restriction and exercise (Tiku et al., 2017). Additionally, the reduction in the levels of the rRNA methyltransferase NSUN5 was associated with increased stress tolerance and lifespan in yeast, worms, and flies (Schosserer et al., 2015). More in general, trends of reduction in nucleolar size, rRNA levels, and ribosomal proteins have been reported in different

long-lived organisms like worms and flies, suggesting that smaller nucleoli and reduced ribosome biogenesis can be considered as cellular hallmarks of longevity (Tiku and Antebi, 2018).

Several scientific studies mentioned in this dissertation show how the molecular dynamics of the nucleolus and chromatin influence and are profoundly influenced by cell stress and ageing. For this reason, in this study, we wanted to investigate some aspects of these nuclear processes by analyzing specific cell stress conditions that can contribute positively or negatively to ageing and which will be introduced in the following sections.

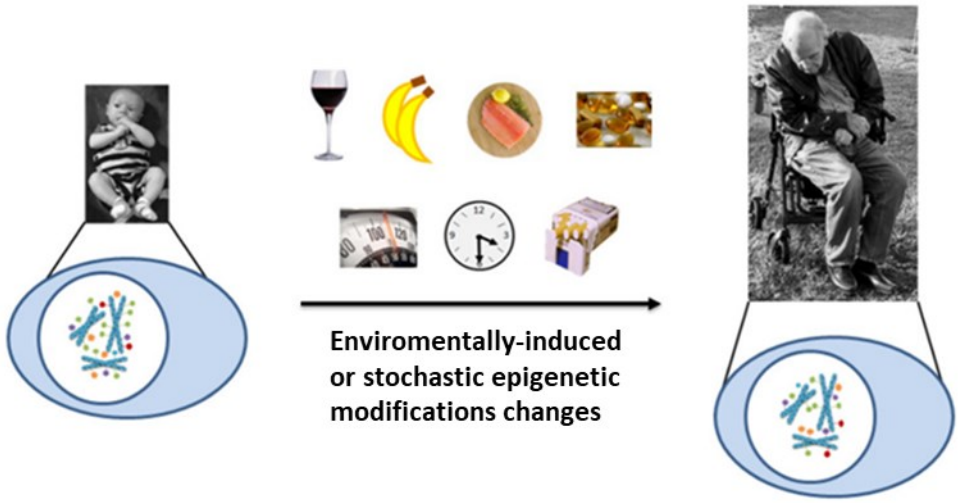

Figure 1.8: Different environmental stimuli can accelerate or slow down ageing progression affecting epigenetics and genome organization. Modified from Pennington et al., 2015.

1.14 The toxicity of mercury chloride and its effects on liver

Mercury is a highly toxic element, which represents one of the main agents responsible for environmental pollution and it is the third most dangerous heavy metal, after arsenic and lead, according to the Agency for Toxic Substance and Disease Registry (ATSDR) (Zhang et al. 2017).

Mercury toxicity and its exposure is a global concern because it is widespread in the environment and induces severe alterations and a broad range of adverse effects on health. Its industrial, domestic, agricultural, medical and technological applications have led to its wide distribution (Altunkaynak et al. 2015). Both humans and animals in fact are exposed to various chemical forms of mercury, mainly as elemental mercury (Hg0), organic mercury

(mainly methylmercury), and inorganic mercury mainly mercury chloride ($HgCl_2$) (Aleo et al., 2002).

It is toxic and corrosive, once absorbed into the bloodstream it can bind to the plasma proteins or enters the erythrocytes. Moreover, it crosses biological membranes and easily forms organo-mercury complexes with proteins (Uzunhisarcikli et al. 2016).

$HgCl_2$ is metabolized primarily in the liver and accumulates in the kidneys; consequently, these are considered the main target organs for mercury damage (Abdel Moneim, 2015).

Since mercury has a strong affinity for endogenous biomolecules associated with –SH group, it combines with thiol-containing proteins, peptides and amino acids, leading to a profound deterioration of fundamental metabolic processes (Wiggers et al., 2008). In fact, $HgCl_2$ liver accumulation induces oxidative stress, depletion of glutathione, and mitochondrial depolarization, due to interference of intracellular mercury with enzyme functions, disturbing ATP production and protein synthesis (Joshi et al., 2017; Agarwal et al., 2007). Cell physiology and integrity are altered due to decreased GSH and GSH depending enzyme activity, leading to an increase in ROS, which provokes lipid, protein, and DNA oxidation (Abarikwu et al., 2018). In addition, $HgCl_2$ is a potent apoptosis inducer, through cytochrome c release, activation of p38 mitogen-activated protein kinases (MAPK) and increase in nuclear factor kappa-B (NF-κB) level (Yang et al., 2016).

In the clinic, chelating agents are used for medical treatment of mercury toxicity, because they form chelation compounds with toxic metal ions, thus eliminating them from the body easily by the excretory system. However, these treatments show some toxicity and are ineffective in repairing tissue damage (Moneim, 2015; Yang et al., 2016; Joshi et al., 2017).

1.15 The epigenetic interplay between nutrition and ageing

Ageing is often associated with oxidative stress and a decreased effectiveness of metabolic pathways. However, different studies have suggested that calorie restriction (CR) could reduce these aberrations (Sohal and Weindruch, 1996; Li et al., 2011). Epigenetic mechanisms have also been determined to be major contributors to nutrition-related longevity (Li and Tollefsbol, 2011; Mercken et al., 2013). The food intake quantity plays a pivotal role in the prolonging of life-span and influencing the development of various diseases, but also the quality of diet has a great impact on these

processes. Moreover, the environmental factors can have marked effects on the epigenome and they can be modulated partly by diet. Because diet can influence epigenetic changes, utilizing dietary compounds to target, treat and even prevent certain diseases has become an area of great interest (Dzau et al., 2019).

Nutrition affects global DNA methylation status throughout lifespan with different effects in different tissues. Changes in the global DNA methylation status may represent an epigenetic mechanism by which age and nutrition influence each other and cell plasticity. In mammals, nutrient availability has been shown to induce epigenetic modifications at both global and locus-specific levels through a variety of molecular mechanisms. For instance, the bioavailability of S-adenosylmethionine (SAM), the substrate for the methyltransferase reactions, is regulated by the dietary intake of vitamin B2, B6, and B12 (Kim et al., 2009; Feil and Fraga, 2012). Moreover, some studies reveal that rodents subjected to a diet deficient or supplemented with methyl donors show a global DNA hypo-methylation and hyper-methylation profile, respectively (Waterland et al., 2008; Pogribny et al., 2009; Li et al., 2015; Farias et al., 2015). More in general, CR leads to alterations in DNA methylation patterns likely by modulating DNMT activities (Li et al., 2011; Maegawa et al., 2017).

Some organisms show rapid ribosomal DNA amplification at specific times or under specific nutrient conditions. For example, TOR signaling was reported to stimulate ribosomal DNA (rDNA) amplification in budding yeast, linking external nutrient availability to rDNA copy number. This amplification is regulated by Sirt1, Hst3, and Hst4 histone deacetylases, which control homologous recombination- dependent and non homologous recombination-dependent amplification pathways, to mediate rapid ribosomal DNA copy number change (Jacka et al., 2015).

Ageing, CR and fat source are all factors that influence apoptotic signaling in liver, an organ that plays a central metabolic role in the organism. Apoptotic index (DNA fragmentation) and mean nuclear area increase in aged animals except for calorie-restricted mice. This suggests possible protective changes in hepatic homeostasis with ageing in the calorie-restricted animal (López-Domínguez et al. 2014).

1.16 Dexamethasone

Glucocorticoids are a class of Corticosteroids. They are synthesized in the adrenal cortex and their name derives from their role in the regulation of glucose metabolism and their steroidal structure.

Glucocorticoids show anti-inflammatory properties. Therefore, they are used in medicine to treat a variety of autoimmune disorders, allergies, asthma, and sepsis. They have many diverse (pleiotropic) effects, including the potentially harmful side effect (Rhen and Cidlowski, 2005).

When bind to their receptor, glucocorticoids activated glucocorticoid receptor-glucocorticoid complex that up-regulates the expression of anti-inflammatory proteins in the nucleus and represses the expression of proinflammatory proteins in the cytosol (Cain and Cidlowski, 2017).

Glucocorticoid effects may be classified into two major categories: immunological and metabolic. Additionally, they play important roles in fetal development and body fluid homeostasis.

Glucocorticoids affect especially glucose metabolism. Cortisol in the fasted state stimulates several processes that collectively increase glucose in the blood (Kuo et al., 2015). Their metabolic effects include stimulation of gluconeogenesis, especially in the liver, by activating the synthesis of glucose from non-hexose substrates, such as amino acids and glycerol and by increasing the expression of the enzymes involved in this process (Kuo et al., 2015). Additionally, Glucocorticoids mobilize amino acids from extrahepatic tissues which are used as substrates for gluconeogenesis (Kuo et al., 2015). Glucocorticoids inhibit glucose uptake in muscle and adipose tissue and stimulate fat breakdown in adipose tissue used for the production of energy in tissues like muscle (Kuo et al., 2015).

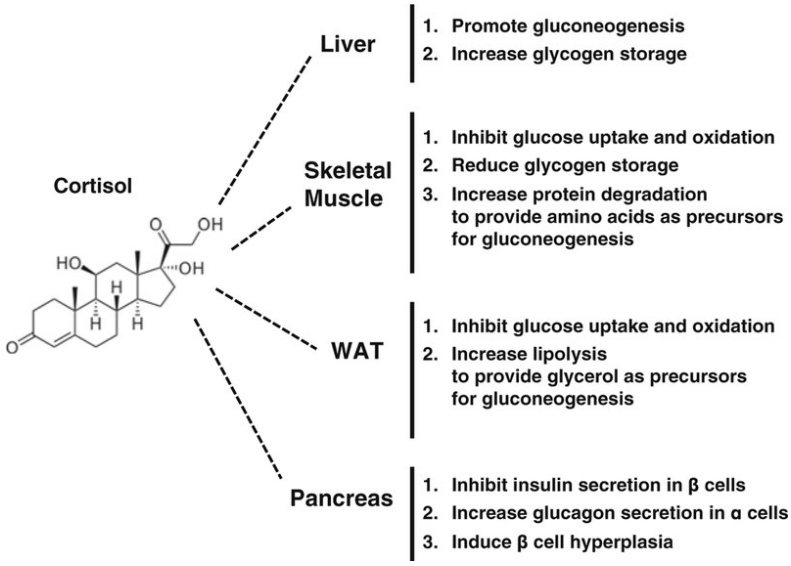

Figure 1.9: Cortisol effects on glucose homeostasis in peripheral tissues. Adapted from Kuo et al., 2015.

Dexamethasone (DEX) is a synthetic glucocorticoid. It is on the World Health Organization's List of Essential Medicines. Dexamethasone has been used as a potent immunosuppressive therapeutic agent for several inflammatory diseases, as it suppresses the expression of inflammatory genes including TNF-α, cyclooxygenase-2, and inducible nitric oxide synthase via the inhibition of NF-kB activation (Jobe et al., 2020). Furthermore, DEX has been shown to inhibit apoptosis in human and rat hepatocytes (Bailly-Maitre et al. 2001) or induce apoptosis in other cells including thymocytes (Marchetti et al. 2003) and lymphocytes (Ruiz-Santana et al., 2001). The antiapoptotic effect by DEX is regulated by several sets of genes, the best characterized of which are the Bcl-2 family such as Bcl-2 and Bcl-xL, which prevent spontaneous apoptosis of cultured primary hepatocytes (Bailly-Maitre et al. 2001). It is also known that DEX abolishes TNF-α-induced cytoxicity of several tumor cell lines via inhibition of phospholipase A2 activity (Messmer et al., 2001). People with cancer undergoing chemotherapy are often given dexamethasone to counteract certain side effects of their antitumor treatments. In brain tumors (primary or metastatic), dexamethasone is used to counteract the development of edema, which could eventually compress other brain structures. (Jessurun et al., 2019). Dexamethasone is also used as a direct chemotherapeutic agent in certain hematological malignancies, especially in the treatment of multiple myeloma, in which dexamethasone is given alone or in combination with other chemotherapeutic drugs.

Recently, Dexamethasone has been recommended by the National Health Service in the UK and the National Institutes of Health (NIH) in the US for

patients with COVID-19 who need either mechanical ventilation or supplemental oxygen, otherwise, it is not recommended. (Horby et al., 2021; Theoharides and Conti, 2020; Vecchiè et al., 2021).

Finally, it may be given to women at risk of delivering prematurely to promote maturation of the fetus' lungs. This administration, given from one day to one week before delivery, has been associated with low birth weight, although not with increased rates of neonatal death (Bloom et al., 2001). The long-term use of dexamethasone may result in thrush, bone loss, cataracts, delayed wound healing, or muscle weakness and increased risk of infection (medically reviewed, 2021, https://www.drugs.com/sfx/dexamethasone-side-effects).

1.17 Senescence

Senescence is the gradual deterioration of functional characteristics in living organisms. Senescence refers to cellular senescence or to whole organism senescence. Organismal senescence involves an increase in death rates and/or a decrease in fecundity with increasing age, at least in the latter part of an organism's life cycle. Cellular senescence is a stable cell cycle arrest that can be triggered in normal cells in response to various intrinsic and extrinsic stimuli, as well as developmental signals (Di Micco et al., 2006; Kuilman et al., 2010; Passos et al., 2010; García-Prat et al., 2016; Mikula-Pietrasik et al., 2020). Senescence is a highly dynamic, multi-step process, during which the properties of senescent cells continuously evolve depending on the context (Van Deursen, 2014; Boisvert et al., 2018). Senescent cells remain viable, but have dramatic alterations in metabolic activity and in gene expression and develop a complex senescence-associated secretory phenotype (Kumari and Jat, 2021). Cellular senescence can compromise tissue repair and regeneration, contributing to ageing (Campisi et al., 2011). The senescence phenotype is often characterized by the activation of a chronic DNA damage response (DDR), the engagement of various cyclin-dependent kinase inhibitors (CDKi), enhanced secretion of proinflammatory and tissue-remodeling factors, induction of antiapoptotic genes, altered metabolic rates and ER stress. The alterations in these pathways lead to structural aberrations, such as enlarged and more flattened morphology, altered composition of the plasma membrane, accumulation of lysosomes and mitochondria and nuclear changes (Hernandez-Segura et al., 2018).

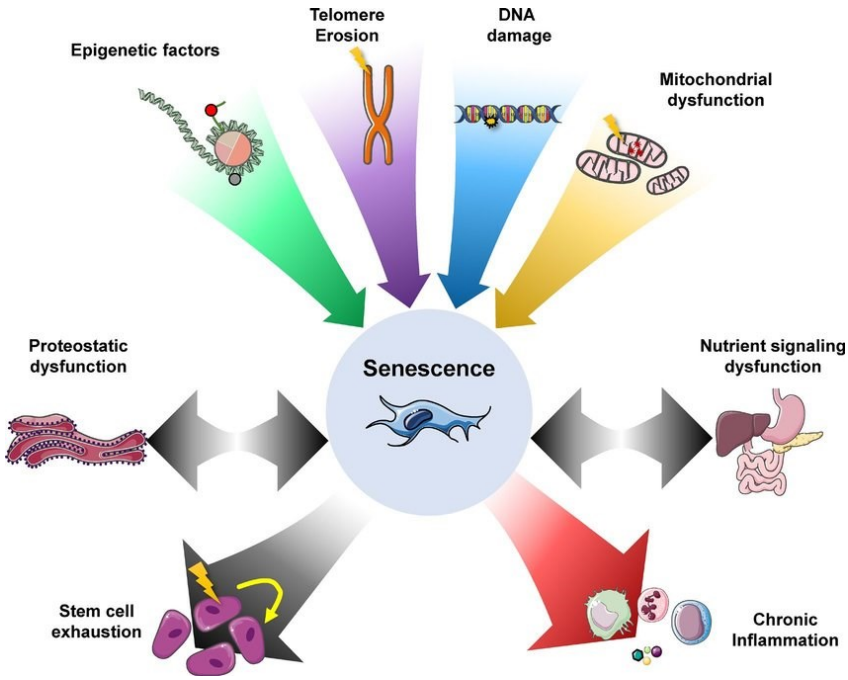

Figure 1.10: Causes and consequences of senescence. Adapted from López-Otín et al., 2013.

2. AIM

Ageing is a multi-factorial process in which the organism continuously adapts the progressive accumulation of damages to the system maintenance over time.

The purpose of my PhD project was to study the effects of ageing and of various stressful conditions that could affect this process by accelerating or slowing it down in hepatocytes. This study was conducted on the murine model, both on mouse hepatic tissue and on the mouse hepatocyte cell line AML12.

We investigated the effects of cell stress and ageing on the nucleus with a specific focus on the changes induced in the heterochromatin organization and the nucleolar activity.

Many studies have described the effects of stressful cues and liver exposure to toxicants at the level of the entire tissue or focusing on cytoplasmic metabolic processes, while, often, little information is found about the effects on the nucleus.

Although investigating tissue macro-alterations and changes in metabolic pathways is important, it should be considered that variations in the quantity or activity of the enzymes involved in these pathways or changings in tissue features are only secondary to alterations of molecular processes that occur in the nucleus, the primary center of control of cell metabolism.

For some cell stress conditions examined in this study, there are wider amount of data in the scientific literature even focused on nuclear features and molecular processes; however, most of these are obtained through molecular biology approaches, while there are still poor direct observations of nuclear dynamics at the ultrastructural level. For this reason, this study was mainly carried out by microscopy methodologies and especially through electron microscopy.

Finally, it seemed important to us to focus on the dynamics of heterochromatin domains because this provides information on the general gene expression rate in a given condition. On the other hand, investigating the nucleolar activity provides indications on the next step of protein synthesis, since the nucleolus is primarily involved in the production of ribosomes that are necessary for mRNA translation into proteins. Furthermore, as described in the introduction, given the profound influence of nucleolar activity on cell metabolism and vice versa, obtaining information on

this parameter is an important element in understanding the effects of ageing and cell stress.

3. MATERIALS AND METHODS

3.1 Mouse liver tissue

3.1.1 Young and old mice liver tissue

Liver was isolated from 3 months old (young) and 24 months old (old) male and female mice, strain B6D2F1. Liver tissue samples were quickly collected in the fixation solution of 4% PFA in Sörensen phosphate buffer at pH 7.2 for 2 hours at 4°C. Then, after PBS washes and NH_4Cl incubation for 30 minutes, samples were directly dehydrated in graded ethanol to be embedded in LRWhite resin. Finally, the embedded samples were polymerized at 60° for 24h and thin sections were collected on formvar-carbon-coated nickel grids (300 Mesh) for transmission electron microscopy. However, the described procedure was not directly carried out since these embedded samples were present in the material archive of Prof. M. Biggiogera from the University of Pavia and Lausanne.

3.1.2 Liver tissue exposure to the toxicant $HgCl_2$

Four 5-week-old female and 6-month-old male B6C3F1 mice were purchased from Charles River (Como, Italy). Animals were maintained under controlled room conditions (22 °C, with 60% air moisture, and 12L:12D photoperiod). Liver was isolated from a 3 months old mouse of the resulting F1 offspring. Liver was cut into small pieces and immersed in DMEM F12 culturing medium added with 10μM $HgCl_2$ (treated tissue) or without $HgCl_2$ as untreated control for 1h at 37°C with 5% CO_2. Time and doses of $HgCl_2$ treatments were chosen on the basis of previous studies (Niemen et al., 1990; Palmeira and Madeira, 1997).

3.2 Cell cultures

3.2.1 AML12

AML12 mouse hepatocytes were grown in 25 cm^2 flasks according to the manufacturer's instructions: in DMEM F12, supplemented with 10% fetal bovine serum (FBS), 10 μg/ml insulin, 5.5 μg/ml transferrin, 1X Penicillin / Streptomycin, 5 ng/ml selenium and 40 ng/ml (0,1μM) Dexamethasone in a

5% CO_2 humidified atmosphere at 37°C. When 90% of confluence was reached cells were detached through mild trypsinization.

3.2.2 AML12 exposure to the toxicant $HgCl_2$

We exposed AML12 hepatocytes to increasing dosages of $HgCl_2$: 1µM, 5µM and 10µM by adding it in the complete cell culture medium for 1h and maintaining the cell according to their growth protocol at 37°C with 5% CO_2 in air atmosphere.

3.2.3 AML12 serum depletion

To mimic a condition of nutriment deprivation, we cultured AML12 cells with 0.1% FBS for 5 days, instead of 10% FBS as for the AML12 control cell line (CTRL). Then cells were harvested and collected.

3.2.4 AML12 Dexamethasone treatment

We exposed AML 12 hepatocytes to 1µM Dexamethasone (10 fold more than the recommended dose used for the AML12 CTRL cells) by adding it in the cell culture media for 2h. Then cells were harvested for the downstream experimental procedures. Times and concentrations of Dexamethasone for this treatment were chosen on the basis of previous studies (Oh et al., 2006; Kimura et al., 2011).

3.2.5 AML12 senescence induced hepatocytes

AML12 cells were grown according to Singh et al. protocol to induce senescence in this cell line (Singh et al., 2020). When 50% confluency was reached, hepatocytes were treated with 1 mM H_2O_2 on day 1 and 750 µM H_2O_2 for the subsequent 5 days in serum-free DMEM:F12 medium, for 1 h each day. After treatment, serum-free DMEM:F12 medium containing H_2O_2 was replaced with complete DMEM:F12 medium (containing 10% FBS, 1x ITS, 0.1µM Dexamethasone, and 1x penicillin and streptomycin) for a 23 h period of recovery each day. This cycle was repeated 6 times.

3.3 Sample preparation for transmission electron microscopy

3.3.1 Liver tissue sample preparation

Tissue samples were fixed with 4% paraformaldehyde in PBS 1X pH 7.2-7.4 at 4°C for 2h, incubated 30 minutes in NH_4Cl 0,5 M at 4°C to block free aldehyde groups and rinsed 3 times using PBS 1X pH 7.2-7.4.

In all the experimental procedures in this study we used PBS 1X at pH 7.2-7.4, indicated in the following parts as PBS.

Physical dehydration with a graded ethanol series was performed prior the embedding in LR White acrylic resin, tissue samples were then incubated 30 minutes in 50% ethanol and 50 % LR White; an overnight infiltration with LR White at 4°C follows. Tissue samples were finally embedded in gelatine capsules and resin polymerization was carried out at a temperature of 60 °C for 24 hours.

Thin sections of 70–80 nm were cut with an ultramicrotome and collected on formvar-carbon-coated nickel grids (300 Mesh) for transmission electron microscopy.

3.3.2 AML12 hepatocytes sample preparation

Cells were harvested, centrifuged at 800 rpm for 10 minutes and fixed in 4% paraformaldehyde for 30 minutes at room temperature and 1 hours and 30 minutes at 4 °C and then rinsed with PBS. Cells were centrifuged again at 1200 rpm for 10 minutes. Pellets were stored at -80°C for RNA extraction and RT-qPCR analysis or pre-embedded in agar for immunocytochemistry at TEM. Pre-embedding in agar is necessary to avoid sample loss in the following steps of sample preparation, which were the same reported for mouse liver tissue (paragraph 3.3.1).

3.4 Immunocytochemistry at transmission electron microscopy

The grids carrying samples ultrathin sections were floated on a drop of normal goat serum diluted 1 : 50 in PBS for 5 min at R.T. and then incubated overnight at 4 °C with the primary antibody diluted in Tween20 0,05% / PBS. The following day, after two rinses in tween20 0,05% / PBS and two rinses in in PBS, the incubation in NGS was repeated as in the first step, following by incubation with secondary antibody conjugated with 12nm colloidal gold grain, diluted in PBS, for 30 min at R.T. Finally, sections were rinsed two times in PBS and two in distilled water (dH_2O) and allowed to dry. As negative control, the same experimental procedure was performed using an equal volume of Tween20 0,05% / PBS without the primary antibody. A counterstaining to increase the contrast of cells and tissue structure is required. For immunocytochemistry sections were counterstained by EDTA regressive technique described below.

The primary antibodies used in this study were: GTX128960 Histone H4K20me3 (trimethyl Lys20), GTX121184 Histone H3K27me3 (Tri-methyl

Lys27) and GTX121677 Histone H3K9me3 (Tri-methyl Lys9) from GeneTex, Inc. Biotechnology Irvine, California. All the primary antibodies were diluted in tween20 0,05% / PBS. The dilution rate was 1:50 for H3K27me3, 1:100 for H4K20me3 and 1:10 for H3K9me3. The secondary antibody was 12 nm Colloidal Gold AffiniPure Goat Anti-Rabbit IgG (H+L) (EM Grade) from Jackson Immunoresearch Biotechnology West Grove, Pennsylvania. The secondary antibody was diluted 1:20 in PBS 1X pH 7.2-7.4.

3.5 EDTA regressive technique

Regressive staining is a technique used to counterstain sections in transmission electron microscopy which exploits EDTA as a chelating agent to reveal with heavy contrast cell structures containing RNA, while deoxyribonucleoproteins and heterochromatin lose most of the stain (Bernhard, 1969). In detail, after a pre-staining with uranyl acetate 4% aqueous solution, the thin sections were briefly floated on EDTA 0.2 M and finally were post-stained with lead citrate. Then sections were allowed to dry and finally visualized on JEM-1400 Flash JEOL electron microscope operating at 80 kV.

3.6 HPMTs quantification and statistical analysis

The quantification of H3K9me3, H4K20me3 and H3K27me3 immunolabeling interest was calculated as follows: 100 squares (each one with an area of 100 nm^2 for hepatocytes from cell culture and 200nm^2 for hepatic tissue) were identified and the number of HPMT label, marked by gold grain and appearing as dark spots, per single area was counted. The measurement was performed considering 10 cells for each sample and 10 squares per single cell. Statistical significance was estimated by two-tailed unpaired Student's t-test. $P<0.05$ was considered statistically significant.

3.7 Immunofluorescence

Semi-thin sections about 500nm in thickness from samples embedded in acrylic LR white resin, as described in details for TEM samples preparation, were cut using an ultramicrotome and deposited on a microscope slide.

For γH2AX immunolabelling, AML 12 hepatocytes were cells were seeded on glass coverslips and left growing until 70-80% confluence. At this confluency,

cells were fixed in Methanol 100% for 20 minutes at -20°, followed by 30s in acetone and air-dried.

In both cases, after rehydration with short washes in PBS, the slides were incubated with the primary antibody overnight at 4°C. Antibody excess was removed by rinsing samples with PBS. Specimens were then incubated with the specific secondary antibody coupled with Alexa Fluor 594 for 45 minutes at R.T. The secondary antibody was diluted 1:200 in PBS. The samples were washed with PBS. Finally, after some washes, the coverslips were mounted in 90% Glycerol/PBS to be observed at the fluorescence microscope Olympus BX51 with a mercury lamp of 100 W.

The primary antibodies were the same listed in paragraph 3.4 for the EM immunocytochemistry and were used at the same dilution rate in PBS. γH2AX antibody (PA5-28778 from Thermo Fisher Scientific, Milan, Italy) dilution rate was 1:50. Secondary antibody used was F(ab')2-Goat anti-Rabbit IgG (H+L) Cross-Adsorbed Secondary Antibody conjugated with Alexa Fluor 594 (A-11072) from Thermo Fisher Scientific, dilution rate of the secondary antibody was: 1:200 in PBS.

Images were submitted to morphometric analyses using the software ImageJ (https://imagej.net/software/fiji/). The quantification of H3K9me3, H4K20me3 and H3K27me3 immunolabeling was calculated as follows: we calculated the sum of fluorescent areas (integrated density) in each nucleus, scoring 50 cells. Statistical significance was estimated by two-tailed unpaired Student's t-test. $P<0.05$ was considered statistically significant.

3.8 Nuclear staining with Hoechst 33258

For Hoechst staining, we used semi-thin sections prepared as for the immunofluorescence (paragraph 3.7). Sections were initially hydrated by 4 washes in PBS, 2 minutes each and incubated 5 minutes in Hoechst 33258 (1ug/mL in PBS) in the dark. 4 washes, 2 minutes each, followed by 1 wash for 5 minutes in PBS were then performed. Glass slide were finally mounted using 90% glycerol in PBS. Hepatic tissue and cells sections were imaged using an Olympus BX51 microscope. Images were submitted to morphometric analyses using the software ImageJ (https://imagej.net/software/fiji/). The quantification of the Hoechst signal was calculated as follows: we calculated the sum of fluorescent areas (integrated density) in each nucleus, scoring 50 cells per sample. Statistical significance was evaluated by two-tailed unpaired Student's t-test. $P<0.05$ was considered statistically significant.

3.9 Osmium ammine staining

The osmium ammine staining is used in transmission electron microscopy for the specific detection of DNA. It is based on a Feulgen-type reaction, consisting of acid hydrolysis to obtain free aldehyde groups on DNA followed by their binding to osmium ammine. Since the DNA interaction with the osmium ammine is specific, the nuclear domains characterized by high DNA concentration, like heterochromatin, appear dark on a lighter background (Biggiogera et al. 1996). The grids were laid on HCl 5N solution for 30 minutes in a well. Then, 7 quick rinses in dH2O followed by 3 rinses of 2 minutes each in dH_2O were performed. Afterward, the grids were laid on osmium amine solution for 60 minutes and finally rinsed in dH2O in order to reduce precipitates formation as follows: 7 quick rinses, 3 rinses of 2 minutes each, 3 rinses of 5 minutes each, 1 rinse of 20 minutes. At the end of each rinse, the grids were blotted on absorbent paper dish. As negative control, the reaction was also carried out by staining with osmium ammine, but avoiding the hydrolysis step with HCl 5N.

For morphometric analysis, all specimens were observed with a Jeol JEM-1200EXIII electron microscope equipped with a 30 mm objective aperture and operating at 80 kV. Images were analyzed using the software ImageJ (https://imagej.net/software/fiji/). The heterochromatin density was estimated by measuring the mean grey value of 50 heterochromatin areas for each condition. Statistical significance was evaluated by two-tailed unpaired Student's t-test. $P<0.05$ was considered statistically significant.

3.10 Nuclear staining with Toluidine Blue

Toluidine blue staining was performed by covering the tissue sections (prepared as previously described in paragraph 3.7), with a drop of the die and incubating for 5 min at 100°C. Sections were then washed thoroughly with dH_2O to remove die excess, airdried, mounted in Mowiol (Sigma Aldrich) and finally imaged using Zeiss Axioskop 2 plus microscope.

3.11 AgNOR staining

AML 12 hepatocytes were cells were seeded on glass coverslips and left growing until 70-80% confluence. At this confluency, cells were fixed in 95% ethanol / 5% glacial acetic acid and post-fixed in Carnoy's solution (absolute

ethanol: Glacial acetic acid 3:1 (vol/vol)) for 30 min. Subsequently, cells were hydrated through graded alcohols to dH_2O. A solution of 0.66% gelatin in dH_2O was prepared, to which formic acid was added at a final 0.33% concentration. This solution was pre-warmed at 37°C and silver nitrate was dissolved in the gelatin–formic acid solution at a final 33% concentration. The slides covered with the fixed hepatocytes were immersed in the silver nitrate-formic acid-gelatin solution and put in an incubator at 37°C for 25 minutes. Afterward, the solution was poured off and the slides were washed in several baths of dH_2O. Cells were then treated with 5% sodium thiosulfate solution, prepared extemporaneously, for 7 minutes and rinsed twice in dH2O. Coverslips were finally mounted using 90% glycerol in PBS and imaged using an Olympus BX51 microscope. Images were submitted to morphometric analyses using the software ImageJ (https://imagej.net/software/fiji/). We measured the NORs area of 50 nuclei per sample. Statistical significance was evaluated by two-tailed unpaired Student's t-test for the comparison of two groups or ANOVA test when comparing multiple conditions. $P<0.05$ was considered statistically significant.

3.12 RT-qPCR

5 million AML12 cell for each condition were cultured and collected as previously described. RNA was extracted from cell pellet using TriZol Ultra Pure Invitrogen kit and then subjected to DNase treatment using DNase I, RNase-free (Thermo Fisher Scientific, Milan, Italy), (1500 ng per sample were treated). 800 ng per sample were retrotranscribed using the RevertAid First Strand cDNA Synthesis Kit (Thermo Fisher Scientific, Milan, Italy) according to the manufacturer's suggestions. Quantitative real-time polymerase chain reaction (qRT-PCR) was carried out with the Maxima SYBR Green qPCR Master Mix (2X; Thermo Fisher Scientific) according to supplier's indications, using a Rotor-Gene 6000 PCR apparatus (Corbett Robotics Pty Ltd, Brisbane, Queensland Australia). Amplification conditions were as follows: denaturation at 95 °C for 10 min, 45 cycles of 95 °C for 15s and 60 °C for 30s, final extension at 72 °C for 30 s. Oligonucleotide primers are listed in Table 3.1 below. Primers were designed using Primer3 (http://www.bioinformatics.nl/cgi-bin/primer3plus/primer3plus.cgi/) and further verified with Oligo Analyzer (https://eu.idtdna.com/calc/analyzer). B2m and Tbp were used as reference genes to normalize gene target quantification, as they were validated by Gong and colleagues (Gong et al., 2016).

The raw, background-subtracted, fluorescence data provided by the Rotor-Gene 6000 Series Software 1.7 (Corbett Robotics) was used to estimate PCR efficiency and threshold cycle number (Ct) for each transcript quantification.

The REST2009 Software V2.0.13 (Qiagen GmbH, Hilden, Germany) and the Pfaffl method (Pfaffl et al., 2002) were used for relative quantification of the transcripts expression. Statistical significance was evaluated by two-tailed unpaired Student's t-test for the comparison of two groups or ANOVA test when comparing multiple conditions. $P<0.05$ was considered statistically significant

Table 3.1

Gene	Primer sequence
Ezh2 Fw	TGGAGTTGGTAAATGCTCTTGG
Ezh2 Rev	CGGTGCCCTTATCTGGAAAC
Kmt5B Fw	CTGGAAGAACTGGCTCCTG
Kmt5B Rev	GGATGAGACCCTGGCAAATC
Suv39h1 Fw	AGGGGAGGAAGAAGTGGAAC
Suv39h1 Rev	CCAAGGGCAGGACAAGAAAG
18S FW	CGTTGATTAAGTCCCTGCCC
18S R1	GGTTCACCTACGGAAACCTTG
18S R2	CGCTCCTCCACAGTCTCC
5.8S F1	CGCTCACACCCGAAATACCGA
5.8S F2	GGTGGATCACTCGGCTCGTG
5.8S Rev	CAACCGACGCTCAGACAGGC
28S F1	CGTGTCCCCCCTTTCTGAC
28S F2	CGACCTCAGATCAGACGTG
28S Rev	GTCTTCCGTACGCCACATTT
Ubtf Fw	TGAGTCCAGCAGTGAAGATGA
Ubtf Rev	AGAATCCGAAGAGTCCCCTG
Baz2a Fw	GAGGAGGAGAGAGAGGTGG
Baz2a Rev	TGGGAAGGCGGGAATAAAC
Rrp9	GTGAGTTCTTCGGGGTAGC
Rrp9	CTCTTCATTCATTTTGCCGCC
Rps18 Fw	CGGAAAATAGCCTTCGCCAT
Rps18 Rev	ATCACTCGCTCCACCTCATC
Rpl19 Fw	AGACCAAGGAAGCACGAAAG
Rpl19 Rev	AAGAGGGCAACAGACAAAGG
p16INK4a Fw	GATGGTGTCTTGGGGGC
p16INK4a Rev	GGATGTTTGGGGCTGGAG
Tp53 Fw	GCTTTGAGGTTCGTGTTTGTGC
Tp53 Rev	CTTTTGCGGGGGAGAGGC
Map1lc3b Fw	AACCTTGACAGCCACGAATG
Map1lc3b Rev	CGAACTCAGAAATCCGCCTG

4. RESULTS

4.1 NADs are highly methylated heterochromatin domains

In most interphase eukaryotic cells, heterochromatin is distributed mainly close to the nucleolus forming the NADs and to the nuclear lamina forming the LADs (Németh et al. 2010; Kind et al. 2013; Ragoczy et al. 2014). More than one nucleolus can be observed in the cell nucleus, depending on the cell type and activity. Moreover, is unknown the mechanism that regulates the localization of nucleoli after mitosis; so they could be located in a central position in the nucleoplasm or more peripherally. Sometimes they are so close to nuclear envelope, that NADs and LADs are partially overlapping. Due to this partial overlapping and because they share some molecular features, many scientific studies consider these domains as the same and assume them to be randomly distributed at each mitosis (van Koningsbruggen et al. 2010; Kind et al. 2013).

Investigations on NADs and LADs molecular properties are usually carried out with the support of bioinformatics tools which predict, based on a series of biological inferences, that a particular sequence belongs to NADs or LADs (Vertii et al. 2019) or by immunofluorescence. Instead, although in a smaller number of nuclei, TEM allows one to visualize directly NADs and LADs in finer details than fluorescence microscopy and there is no need to make inferences to gain information. Considering the advantages of this technique, we decided to compare NADs and LADs for the distribution and density of three epigenetic modifications:H3K9me3, H3K27me3, H4K20me3. We chose these latter since NADs and LADs are heterochromatin domains and being these HPTMs for long established to have important roles in the heterochromatin formation and gene silencing. To localize their positions in the nucleoplasm we ran immunocytochemistry at TEM on mouse liver sections. Hepatocytes were stained by the EDTA regressive technique which allows appreciating and clearly distinguish a pretty continuous heterochromatin domain above the nuclear lamina, the LADs, and large patches of heterochromatin surrounding each nucleolus, the NADs. We carried out this study on 3 months old mice, both male and female.

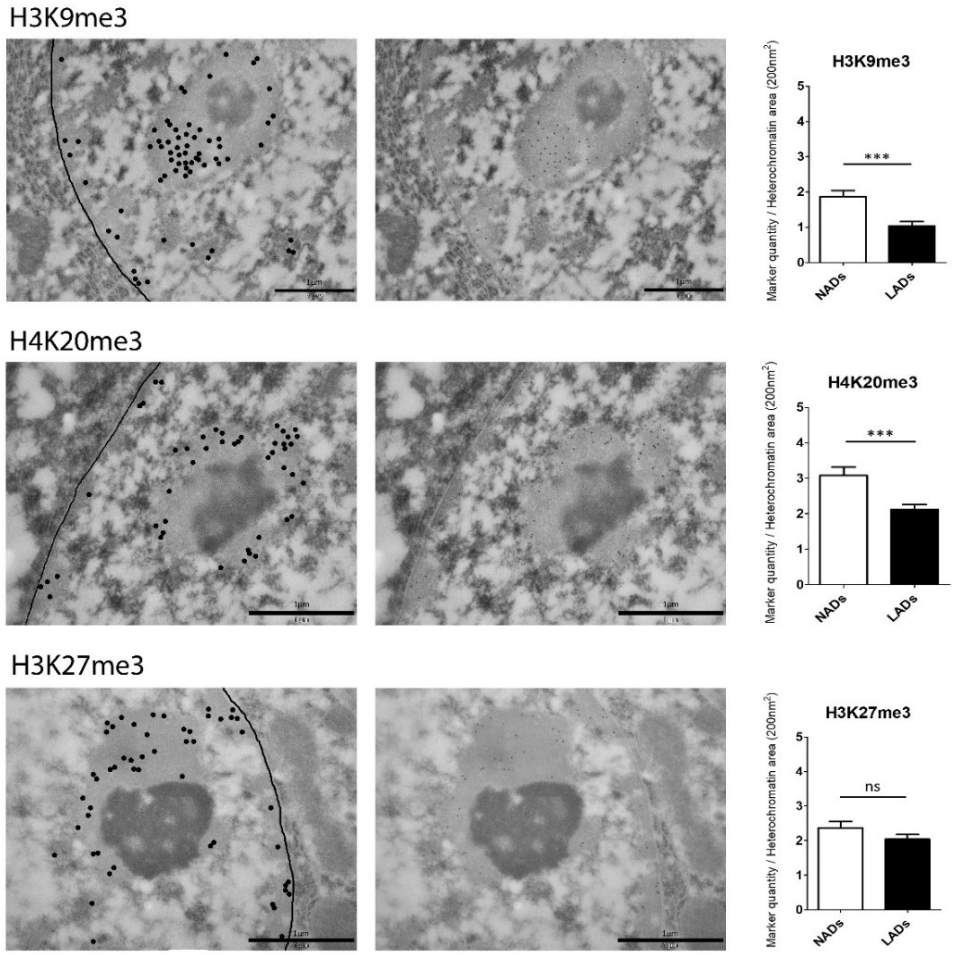

Figure 4.1.1: HPTMs distribution and quantification in male mouse hepatocyte nuclei.
The micrographs show the localizations of the HPTMs H3K9me3, H4K20me3 and H3K27me3 labelled by gold grains appearing as black spots in immunocytochemistry at TEM. On the left HPTMs localizations are highlighted by big black dots, the line stands for the nuclear envelope; the original image for comparison is on the right. Bar: 1µm.
The histograms show the mean ± SEM of the number of the HPTMs in heterochromatin areas of 200nm^2 in NADs (white) and LADs (black). Two-tailed unpaired Student's t-test was used to evaluate the difference between the two groups, which was considered statistically significant for p-value<0.05.

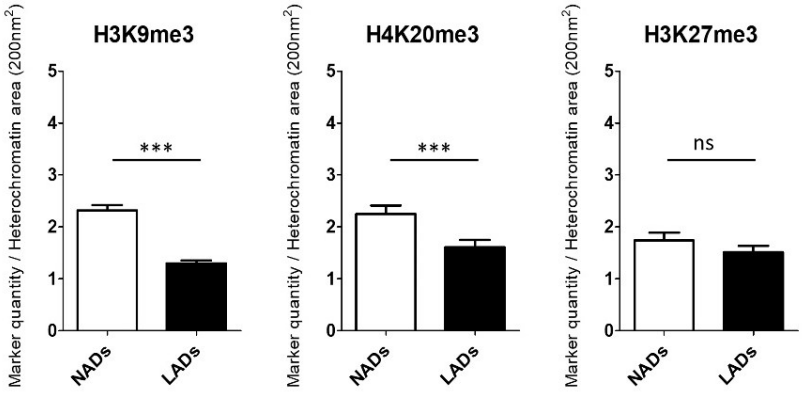

Figure 4.1.2: HPTMs quantification in female mouse hepatocyte nuclei. The histograms show the results of the same analysis conducted in figure 4.1.1 in a female mouse.

Our analysis shows that NADs are highly methylated domains when compared to LADs. They are significantly enriched in H3K9me3 and H4K20me3, which are markers of constitutive heterochromatin; while H3K27me3, associated to facultative heterochromatin, is more evenly distributed in all heterochromatin domains. In fact, even if this latter seems to be fairly more present in NADs, no statistically significant difference between NADs and LADs was detected. Results were comparable in males and females.

We further investigated the features of these heterochromatin domains by staining with Hoechst semi-thin sections of liver tissue from the same samples prepared for TEM analysis. Hoechst staining highlights mainly the heterochromatin because when bound to DNA its fluorescence increases many times (Latt et al. 1976). Since the nuclear areas where chromatin is tightly packaged, the heterochromatin, contain locally a major density of DNA, they result in brighter Hoechst signals. NADs can be recognized in these sections because they appear as a ring or patches surrounding an unstained round-shape area, which corresponds to the nucleolar components composed of unstained rRNA and ribosomal proteins. Looking at the images in figure 1.2 is quite evident that NADs are usually brighter than LADs, so they are probably organized in a more condensed conformation. We made a quantitative estimation of this difference by measuring the mean fluorescence intensity of selected areas of heterochromatin of NADs and LADs domains in 10 different cells. These measurements confirmed that on average NADs are more intensely stained by Hoechst than LADs, likely due to a higher degree of chromatin packaging.

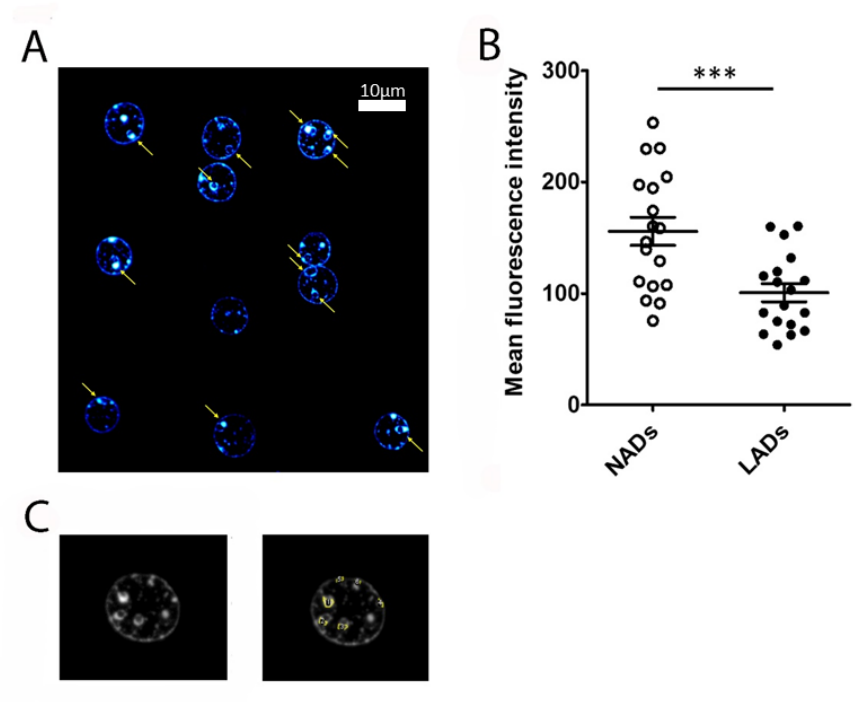

Figure 4.1.3: Hoechst staining confirms that NADs adopt tightly compact heterochromatin conformation
A: Representative image of liver tissue semi-thin sections stained by Hoechst 333258 which highlights the heterochromatin domains inside the nuclei. NADs are pointed out by the yellow arrows. Bar: 10µm. B: The graph shows the mean ± SEM of the mean fluorescent intensities measured for fluorescent dots falling into NADs or LADs. Two-tailed unpaired Student's t-test was used to evaluate the difference between the two groups. p-value<0,05 was considered statistically significant. C: Examples of areas selected to measure the mean fluorescent intensity of NADs and LADs.

4.2 Heterochromatin organization changes over time? The effects of ageing.

The results described so far concern 3-month-old mice. We, therefore, wondered whether the NADs in the nuclei of the hepatocytes kept this methylation profile unchanged even during ageing and more generally whether the organization of the heterochromatin domains would undergo evident changes over time. To answer these questions we performed the same TEM immunocytochemistry analyses, comparing liver samples from 3-month-old mice with liver samples from 24-month-old mice.

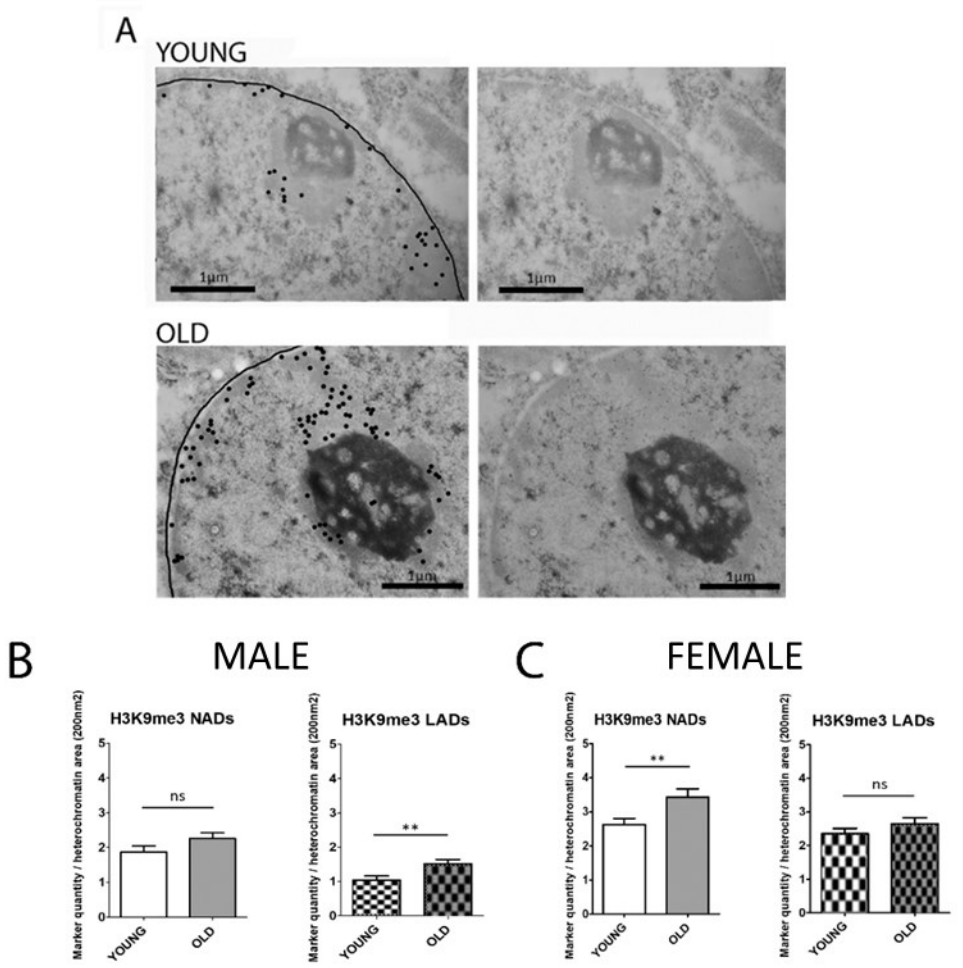

Figure 4.2.1: H3K9me3 distribution and quantification in young and old mice. A: The micrographs are representative of the distribution of H3K9me3 in young (upper) and old (bottom) female mice, labelled by gold grains at TEM. On the left HPTMs localizations are highlighted by big black dots, the line stands for the nuclear envelope. The original image for comparison is on the right. Bar: 1µm. B: The histograms show the mean ± SEM of the number of the HPTMs in heterochromatin areas of 200nm^2 in NADs (solid bars) and LADs (scattered bars) for young (white) and old (grey) male mice. Two-tailed unpaired Student's t-test was used to evaluate the difference between the two groups, which was considered statistically significant for p-value<0.05. C: the same as in B, on female mice.

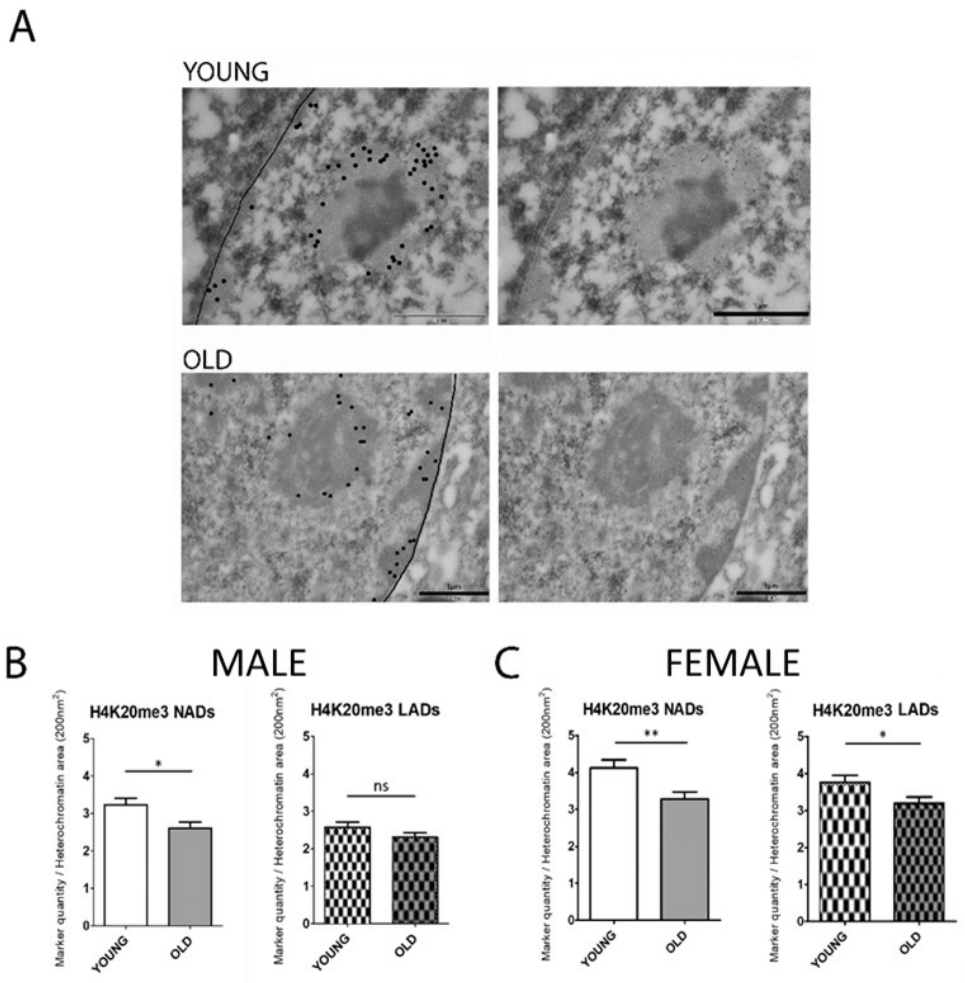

Figure 4.2.2: H4K20me3 distribution and quantification in young and old mice. Same analysis as in figure 4.2.1.

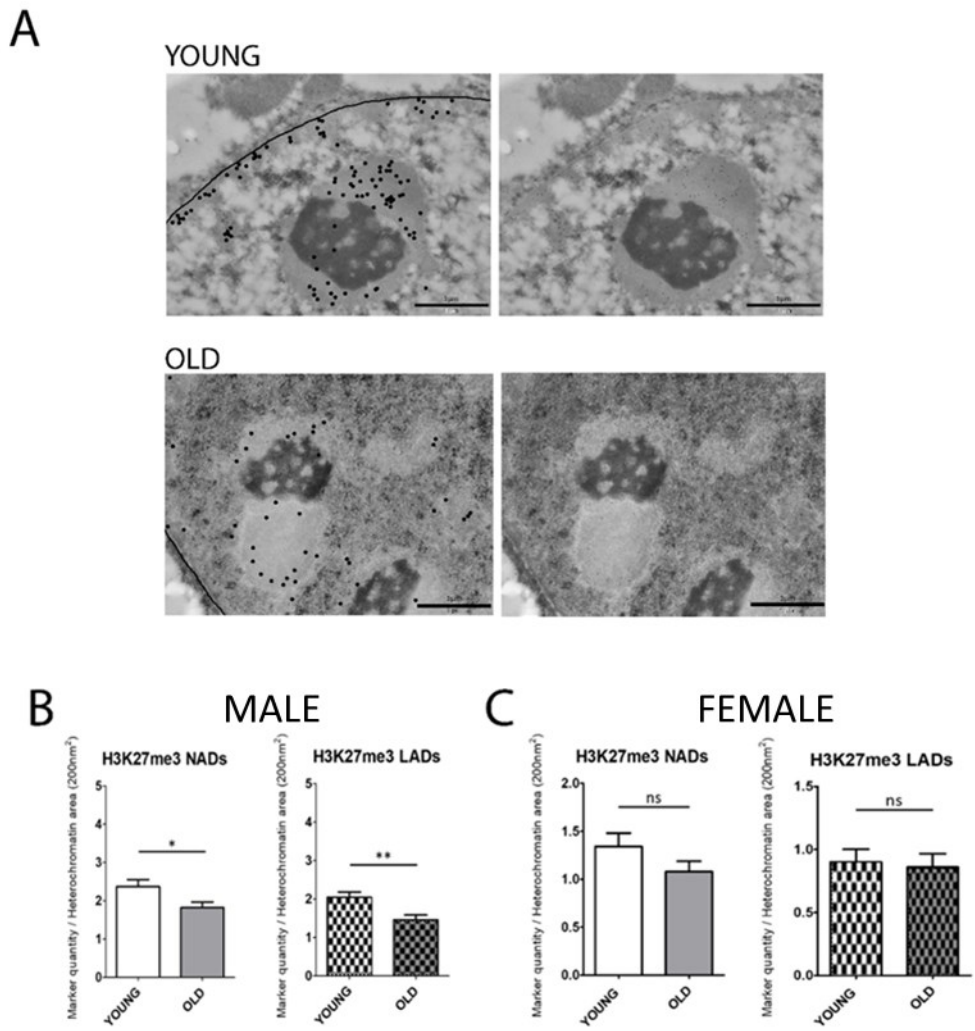

Figure 4.2.3: H3K27me3 distribution and quantification in young and old mice. Same analysis as in figure 4.2.1.

Overall the comparison between young and old mice showed more or less comparable changes of the levels of these histone modifications in male and female individuals studied, during ageing. At least similar trends can be individuated with few differences in LADs and NADs domains. Specifically, this analysis highlights an increase in H3K9me3 level and opposite trends for H4K20me3 and H3K27me3, whose levels tend to go down in hepatocytes from old mice compared to the young mice.

Since these HPTMs are all markers of heterochromatin, there seem to be no unique direction of changing of the chromatin conformation and activity during ageing. We could say in terms of heterochromatin condensation that the increase in the repressive marker H3K9me3 is counterbalanced by the decreases in H4K20me3 and H3K27me3.

To further confirm these changes on a larger number of cells, we run also immunofluorescence on liver semi-thin sections for each HPTM.

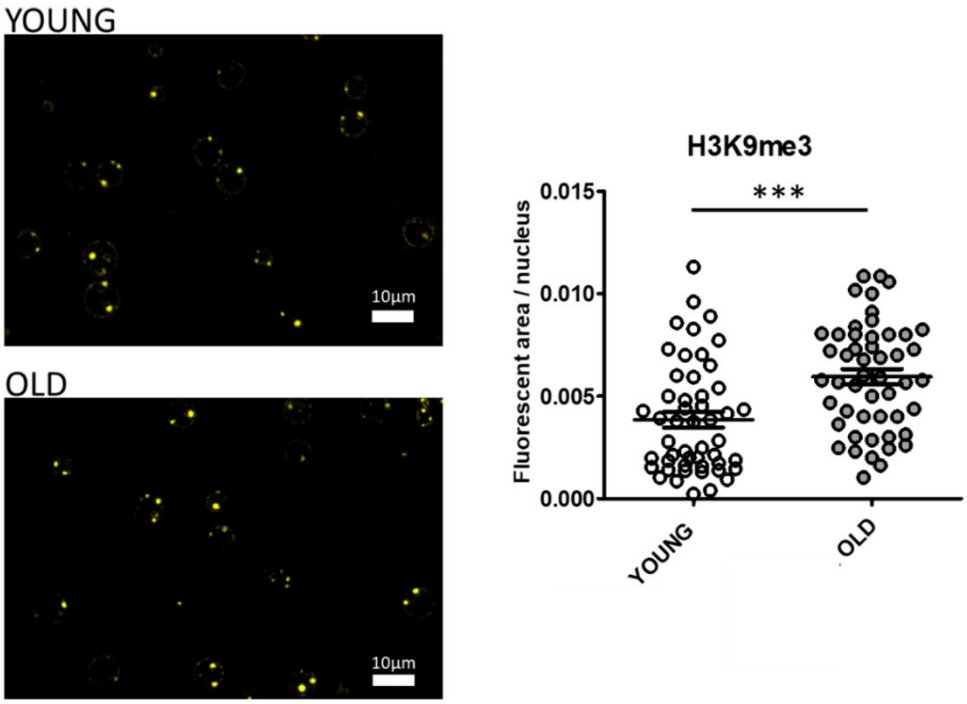

Figure 4.2.4: Immunofluorescence labelling of H3K9me3 in liver tissue sections. Images show H3K9me3 distribution in hepatocytes nuclei labelled by fluorescent signals, in young (top) and old (bottom) mice. Bar: 10µm. The graph plots the area of the total fluorescent signal per nucleus, as the sum of the fluorescent dots detected in each nucleus. Statistical significance was evaluated using two-tailed unpaired Student's t-test. Bar: mean ± SEM.

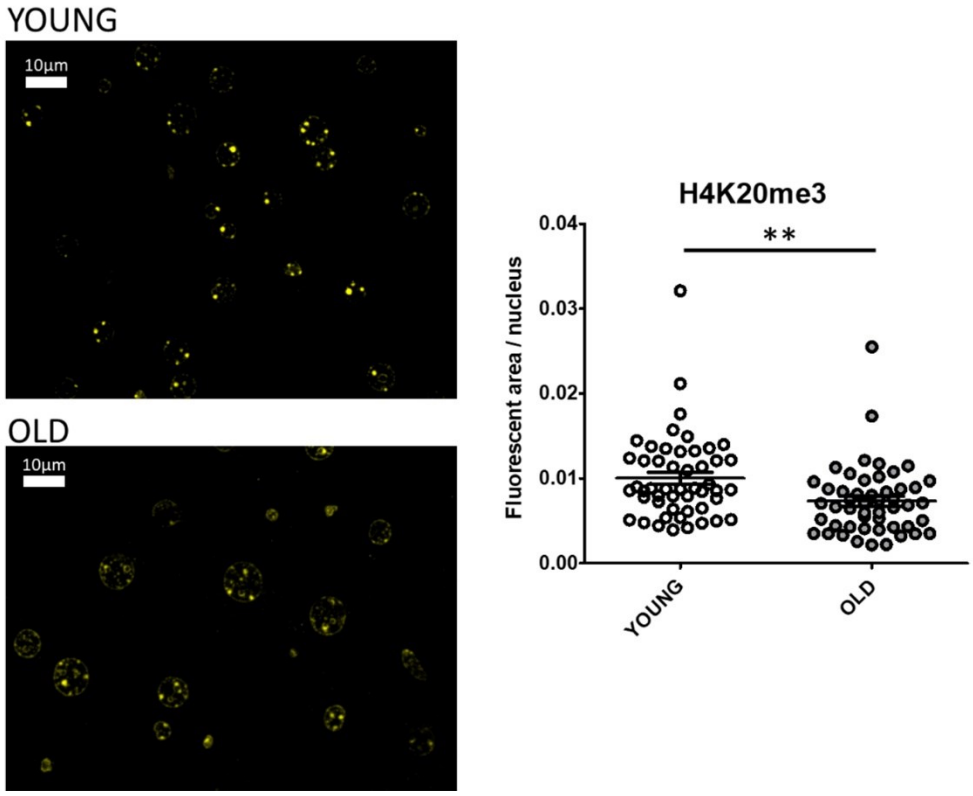

Figure 4.2.5: Immunofluorescence labelling of H4K20me3 in liver tissue sections. Images show H4K20me3 distribution in hepatocytes nuclei labelled by fluorescent signals, in young (top) and old (bottom) mice. Bar: 10µm. Graph: same analysis as in figure 4.2.4.

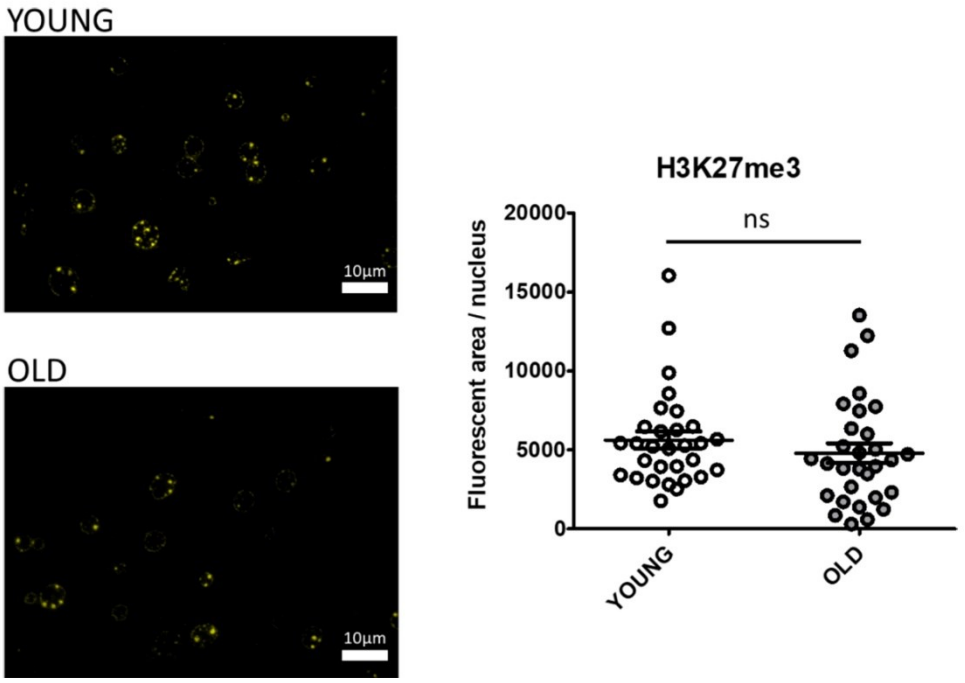

4.2.6: Immunofluorescence labelling of H3K27me3 in liver tissue sections. Images show H3K27me3 distribution in hepatocytes nuclei labelled by fluorescent signals, in young (top) and old (bottom) mice. Bar: 10µm. Graph: same analysis as in figure 4.2.4.

Immunofluorescence analysis upholds the trends observed by immunocytochemistry at TEM, demonstrating an increase in the histone marker H3K9me3 and a decrease in H4K20me3.

As in the immunocytochemistry analysis on the female mice, the decrease in the level of H3K27me3 is not statistically significant. However, unfortunately, we had run this analysis in a smaller number of cells (30 cells) due to the minor efficiency of the antibody against H3K27me3 in immunofluorescence.

Considering these results, which indicate divergent trends for the different heterochromatin markers, we decided to evaluate if there was an evident change in the total heterochromatin amount and density during ageing, by using Hoechst and osmium ammine staining, respectively.

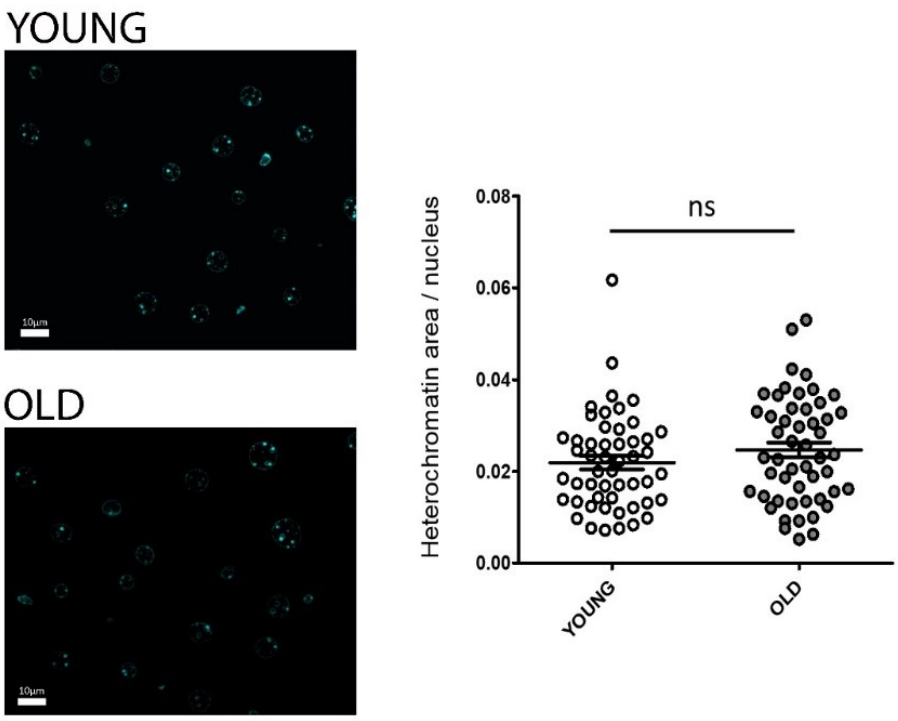

Figure 4.2.7: Hoechst staining to estimate the relative heterochromatin amount. Images show Hoechst fluorescence in hepatocytes nuclei, in young (top) and old (bottom) mouse liver tissue. Bar: 10µm. In the graph is plotted the heterochromatin area per nucleus estimated as the sum of the areas of the fluorescent dots inside each nucleus. Statistical significance was evaluated using two-tailed unpaired Student's t-test. Bar: mean ± SEM.

This analysis shows no significant differences between hepatocytes from young and old mice (Figure 4.2.7). Concordantly, immunocytochemistry suggested an increase of H3K9me3, but at the same time a decrease of the marker H4K20me3, both considered important epigenetic modifications for the formation of constitutive heterochromatin. Furthermore, even by simply observing the liver tissue sections, contrasted with EDTA regressive staining, no obvious morphological changes or difference in other features of the nucleoplasm organization were noticed and neither when observing larger portion of tissue sections at lower magnification stained by Toluidine blue (Figures 4.2.8 and 4.2.9).

YOUNG

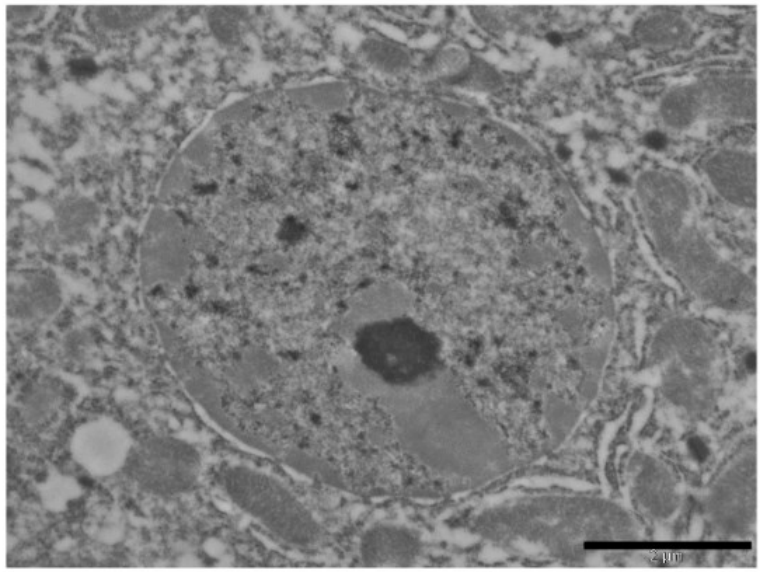

OLD

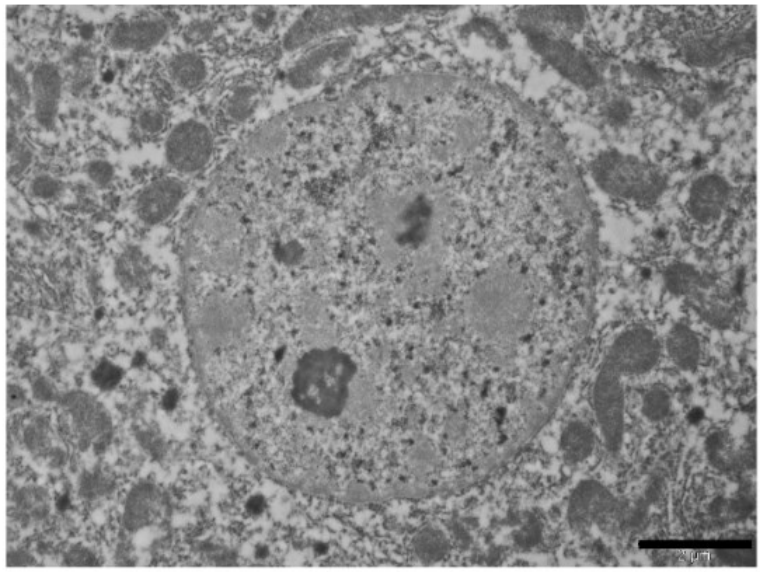

Figure 4.2.8: Sections of liver tissue from young and old mice at TEM stained by EDTA regressive technique. Bar: 2µm

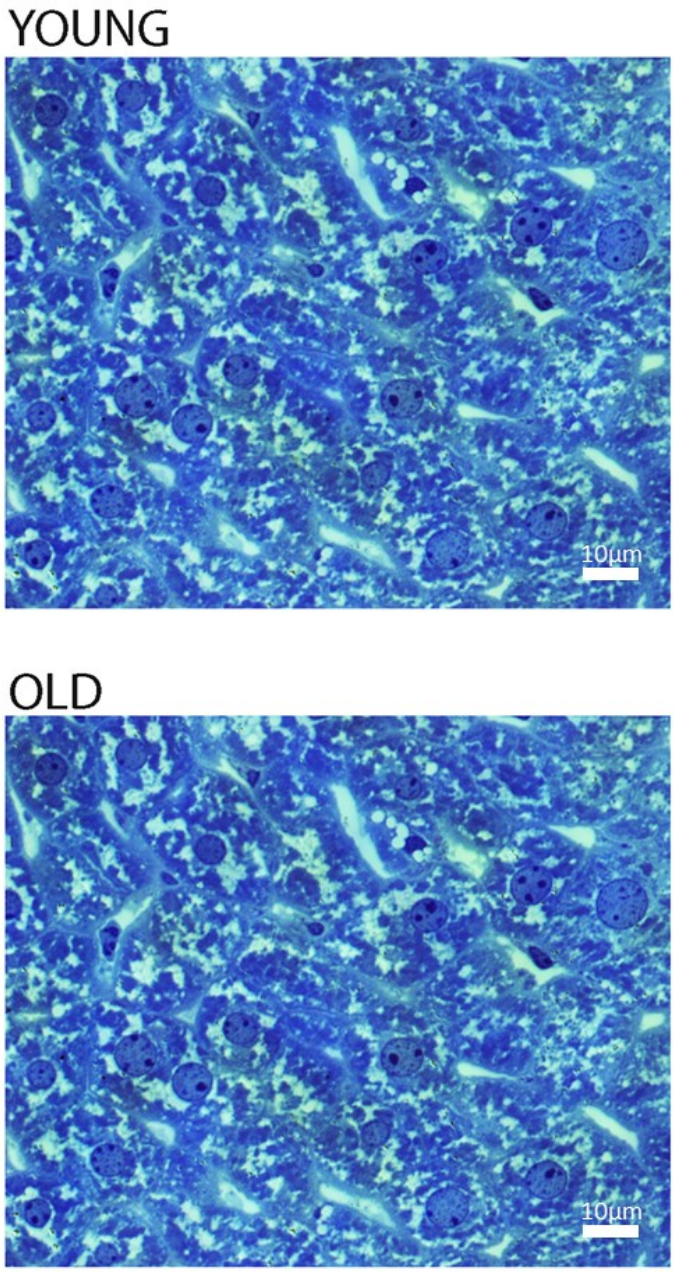

4.2.9: Semi-thin sections (500nm) of liver tissue from young and old mice stained by Toluidine blue

However, we finally decided to evaluate if any differences in the heterochromatin density can be detected through the osmium ammine staining. This technique allows the specific detection of DNA in the cell nucleus, therefore, heterochromatin appears highly contrasted on a lighter background, due to its high degree of condensation. (This analysis and each osmium ammine staining experiment presented in this study were carried out on thin sections having the same thickness of 70 nm).

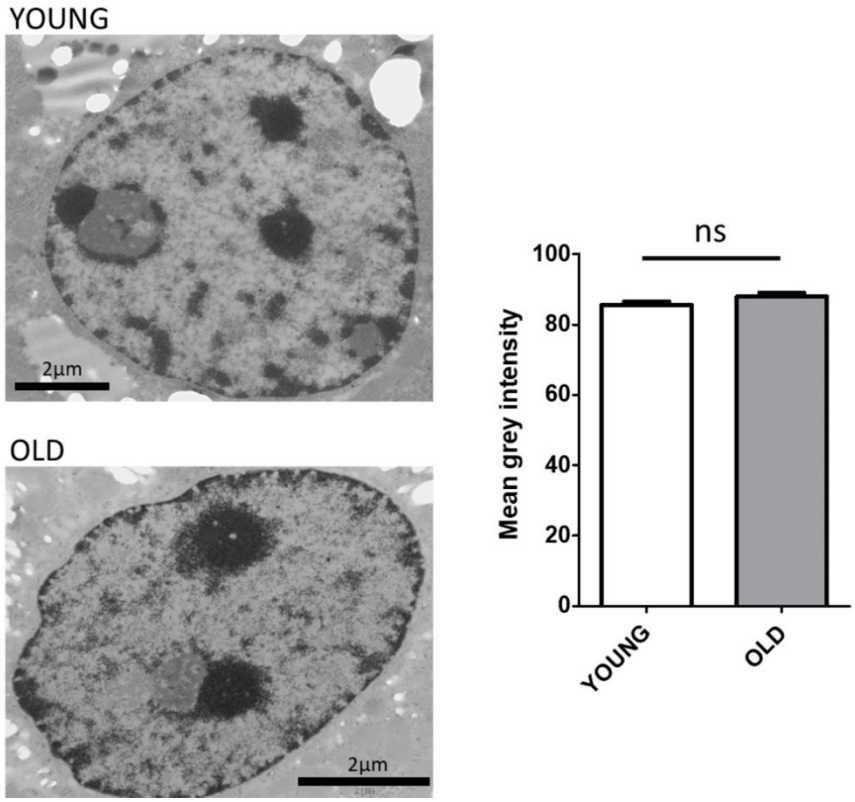

4.2.10 Osmium ammine staining of mouse liver sections: young (top) and old (bottom). Bar: 2µm. The graph shows the heterochromatin mean grey value ± SEM. Statistical significance was evaluated using two-tailed unpaired Student's t-test.

The osmium ammine staining further confirms that there were no important differences in the heterochromatin organization between young and old mice. Accordingly, the measurements of the heterochromatin mean grey value, reveal that heterochromatin domains have more or less the same density in all mice analyzed (Figure 4.2.10).

In conclusion, the lack of strong evidence of heterochromatin changes in these very old mice was quite surprising for us. It must be considered that

unfortunately, we were unable to carry out our analyses on a large number of individuals and that these mice were grown in a controlled and aseptic environment protected from many environmental damaging stimuli. Actually, being in such a controlled environment, mice are very useful although “artificial” model. A better solution would be to use wild mice, in this case the variability due to “lifestyle” would play a major role.

We next wanted to investigate whether the exposure of liver tissue to stressful conditions, which may have a contribution to ageing processes, would cause changes in the heterochromatin domains. We treated hepatocytes with mercury chloride since liver is the organ of our body primarily involved in detoxification processes from xenobiotics and given the widespread environmental diffusion and high toxicity of this chemical compound.

4.3 Mercury Chloride toxicity on hepatocytes nucleus

We ran the same analysis described above to compare liver tissue from a 3 months old mouse, subjected to $HgCl_2$ 10µM exposure for 1h to the control samples placed in the same culture medium but without the toxic agent. Tissue samples were collected and fixed just after the treatment, without a recovery period.

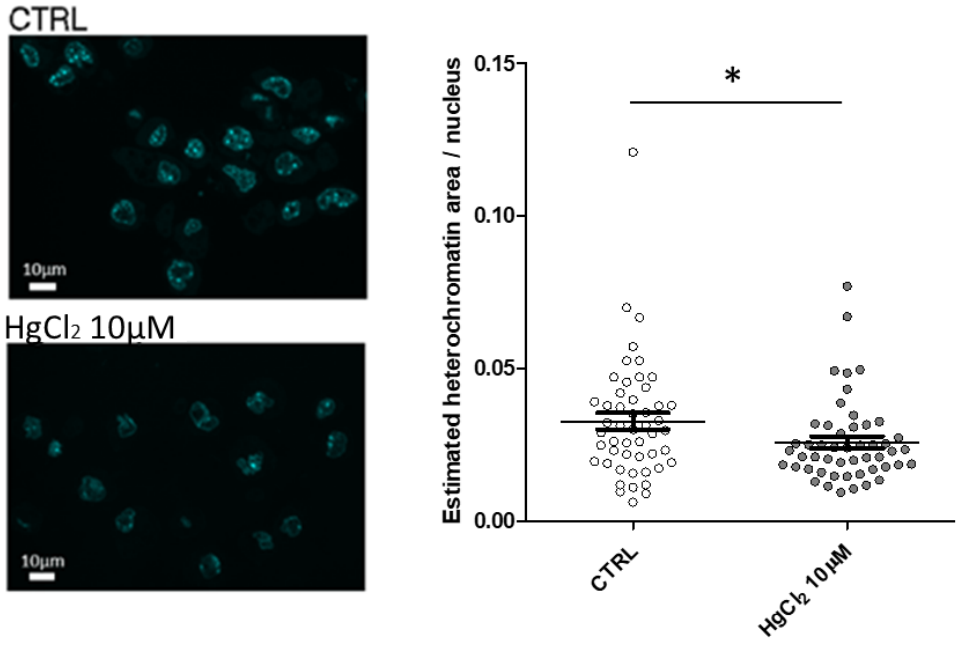

Figure 4.3.1: Hoechst staining to estimate the relative heterochromatin amount in liver tissue. Images show Hoechst fluorescence in mouse hepatocytes nuclei, in control (top) and after $HgCl_2$ treatment (bottom). Bar: 10µm. In the graph: the heterochromatin area per nucleus estimated as the sum of the areas of the fluorescent dots inside each nucleus. Statistical significance was evaluated using two-tailed unpaired Student's t-test. Bar: mean ± SEM.

Hoechst staining reveals in this case a significant decrease in the amount of heterochromatin in the hepatocytes exposed to $HgCl_2$ damages (Figure 4.3.1).

Next, liver sections were stained with osmium ammine to evaluate if the decrease of the Hoechst signal was determined by a decrease in the degree of heterochromatin condensation in $HgCl_2$ treated cells.

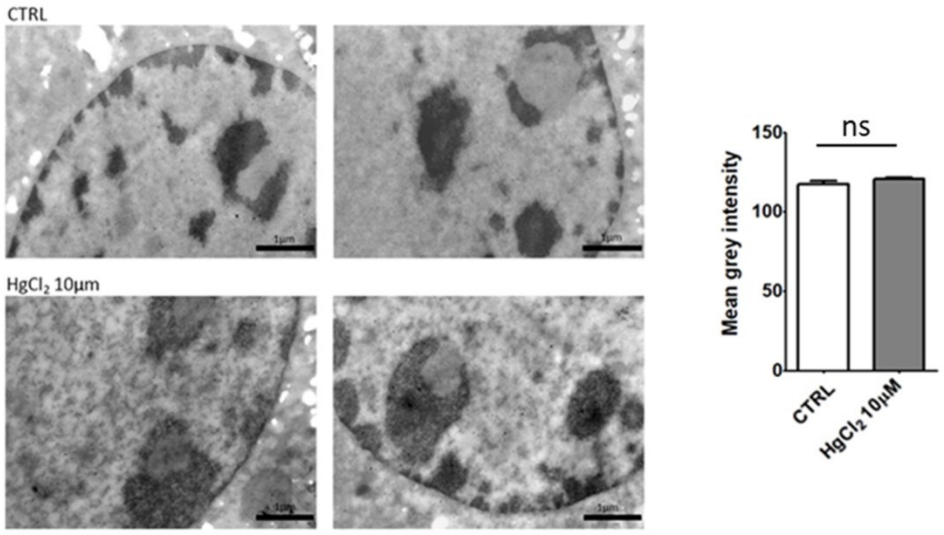

Figure 4.3.2: Osmium ammine staining of mouse liver sections: control (top) and after $HgCl_2$ treatment (bottom). Bar: 1µm. The graph shows the heterochromatin mean grey value. Statistical significance was evaluated using two-tailed unpaired Student's t-test. Bar: mean ± SEM.

The analysis of liver sections stained with osmium ammine suggests there was no significant difference in the heterochromatin density between the two conditions. In fact, the measurements of the mean grey intensity of the areas of heterochromatin in $HgCl_2$ treated cells suggest they are only fairly lighter compared to the control. However, it can be noticed in this representative micrographs that heterochromatin seems to adopt more granular and less compact conformation in $HgCl_2$ treated cells (Figure 4.3.2). This feature becomes actually more evident and statistically significant in cell culture hepatocytes subjected to mercury chloride treatment that will be presented later in this dissertation.

Finally, we analyzed, as previously, possible $HgCl_2$ effects on the epigenetics markers H3K27me3, H4K20me3 and H3K9me3 in NADs and LADs.

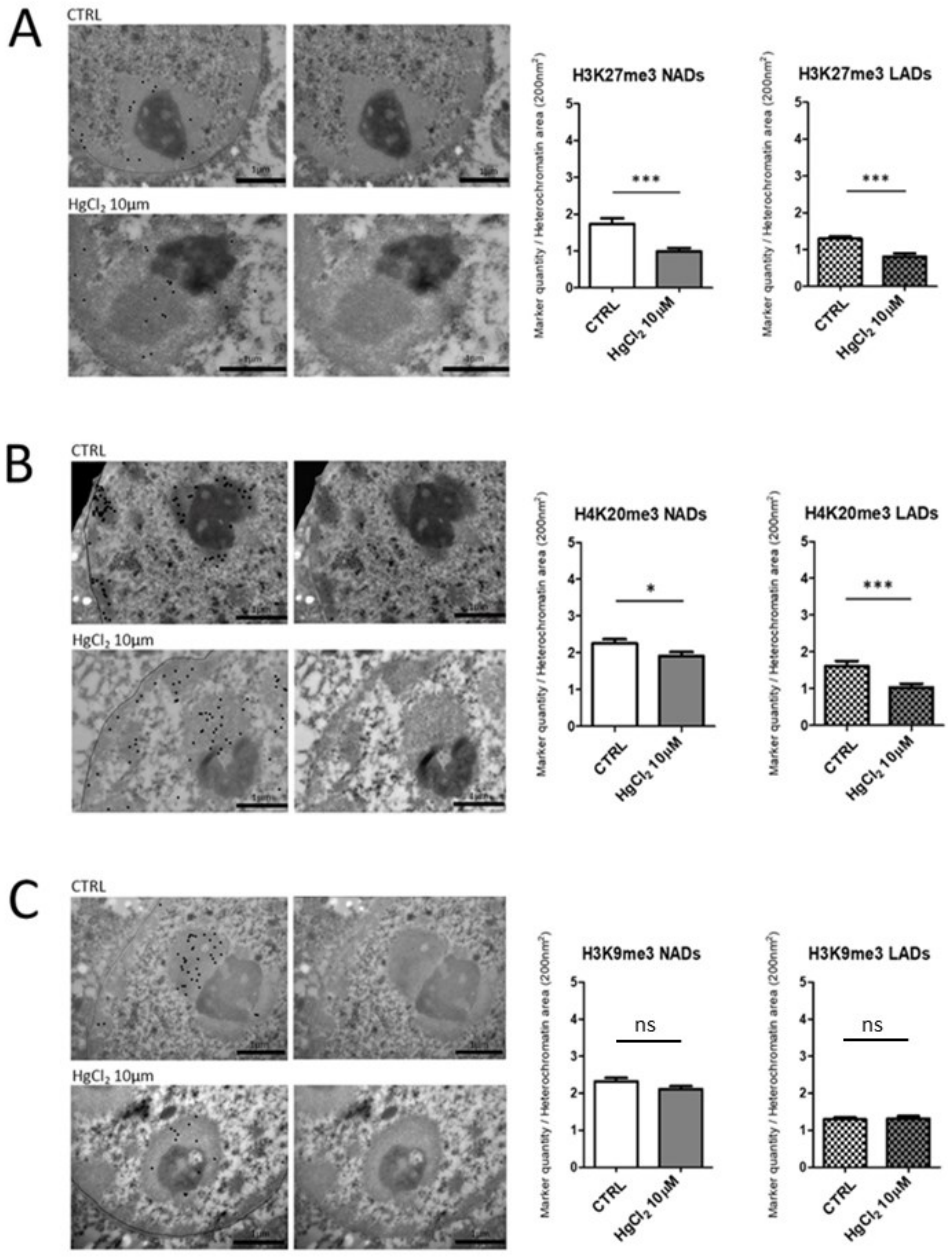

Figure 4.3.3: Immunocytochemistry at TEM of H3K27me3, H4K20me3 and H3K9me3. The micrographs show the localizations of H3K27me3 (A), H4K20me3 (B) and H3K9me3 (C) in mouse hepatocytes nuclei in liver tissue, which are highlighted by black dots, the line stands for nuclear envelope (left). The corresponding original images are shown on the right. Histograms show the mean ± SEM of the HPTM quantity per heterochromatin area (200nm^2) in NADs and in LADs for control and $HgCl_2$ treated cells. Statistical significance was evaluated using two-tailed unpaired Student's t-test.

Immunocytochemistry at TEM revealed that $HgCl_2$ treatment induces an important decrease of these three HPTMs compared to the control in all heterochromatin areas (Figure 4.3.3). Again this effect was more pronounced on hepatocytes in cell culture (shown below), even if also present when treating liver tissue. The histone marker which was subjected to less variation was H3K9me3. This could be quite expected, being H3K9me3 an epigenetic modification assumed to be more stable. The highly significant decrease in H327me3 and H4K20me3 after $HgCl_2$ treatment suggests activation of gene expression, maybe to produce those proteins and factors necessary for the detoxification.

4.4 Heterochromatin organization under cell stress in murine cell culture hepatocytes model

We began our analysis in liver tissue and then we moved to murine hepatocytes in cell culture. Tissue represents a more physiological environment compared to cell culture. In fact, some differences can be noticed in the heterochromatin organization and more in general in nuclear morphology between the hepatocytes in the liver tissue and the cell culture hepatocytes. This probably occurs because cell culture can reproduce only partially the organism environment both from a chemical and physical point of view. On the other hand animal maintenance to retrieve tissue samples is very costly and there is less possibility to see directly and in a short time the effects of the hepatocytes exposure to toxicants or other cell stress conditions. Specifically, we were interested in analyzing the effects of stressful stimuli which may contribute to liver ageing processes. Therefore, in line with the previous investigation in liver tissue, we treated hepatocytes with increasing doses of mercury chloride, to gain further evidence in a condition that exposes directly the cells to the toxicant. Afterward, considering the fundamental role of the hepatocytes in glucose and fat metabolism, we analyzed the consequences of calorie restriction, mimicked by serum starvation. Moreover, we investigated if a high dose of the corticosteroid Dexamethasone, a synthetic drug that shows anti-inflammatory properties, could have a beneficial role in slowing down ageing. Finally, a condition that mimics ageing was also analyzed: hepatocytes were induced to senescence following the protocol published by Singh and colleagues (Sing et al., 2020).

4.4.1 Mercury chloride toxicity on mouse hepatocytes in cell culture

As shown in the previous chapter, mercury chloride exposure induces a conspicuous decrease in the epigenetic modifications H3K27me3, H4K20me3 and to a lesser extent in H3K9me3, which are all HPTMs that exert an important role in chromatin condensation (Figure 4.3.3). The analysis by Hoechst staining revealed a decrease in the amount of the tightly condensed heterochromatin areas in $HgCl_2$ treated cells, even though the osmium ammine staining to evaluate heterochromatin density showed no clear difference compared to the control (Figures 4.3.1 and 4.3.2).

As discussed above cell culture experiments allow one to see more directly the effects of a particular stimulus on the cell.

Indeed, by exposing hepatocytes in cell culture to increasing doses of mercury chloride, we saw important rearrangement of the heterochromatin organization, which undergoes an extensive decondensation. Hoechst staining reveals a significant decrease of the heterochromatin domains in hepatocytes treated with 10μM $HgCl_2$ for 1h (Figure 4.4.1). The statistical analysis on the Osmium ammine staining also confirm, in this case, the Hoechst trend and allows one to clearly appreciate at ultrastructural level the changing in heterochromatin organization, which is evidently less dense and less compact compared to the control (Figure 4.4.2).

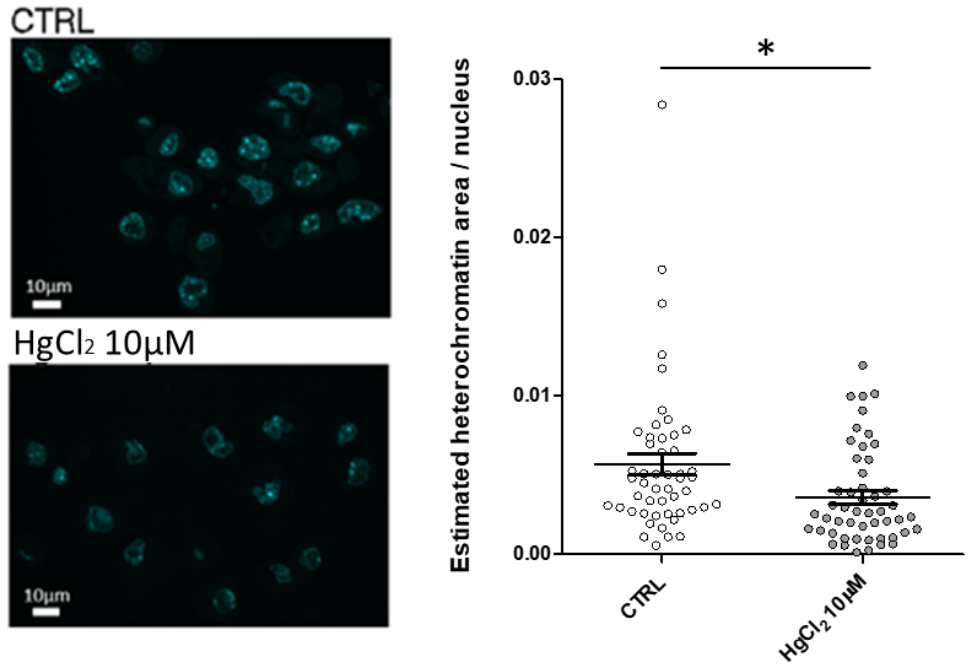

4.4.1: Hoechst staining to estimate the relative heterochromatin amount. Images show Hoechst fluorescence in AML12 hepatocytes nuclei, in control (top) and after $HgCl_2$ treatment (bottom). Bar: 10μm. In the graph: the heterochromatin area per nucleus estimated as the sum of the areas of the fluorescent dots inside each nucleus. Statistical significance was evaluated using two-tailed unpaired Student's t-test. Bar: mean ± SEM.

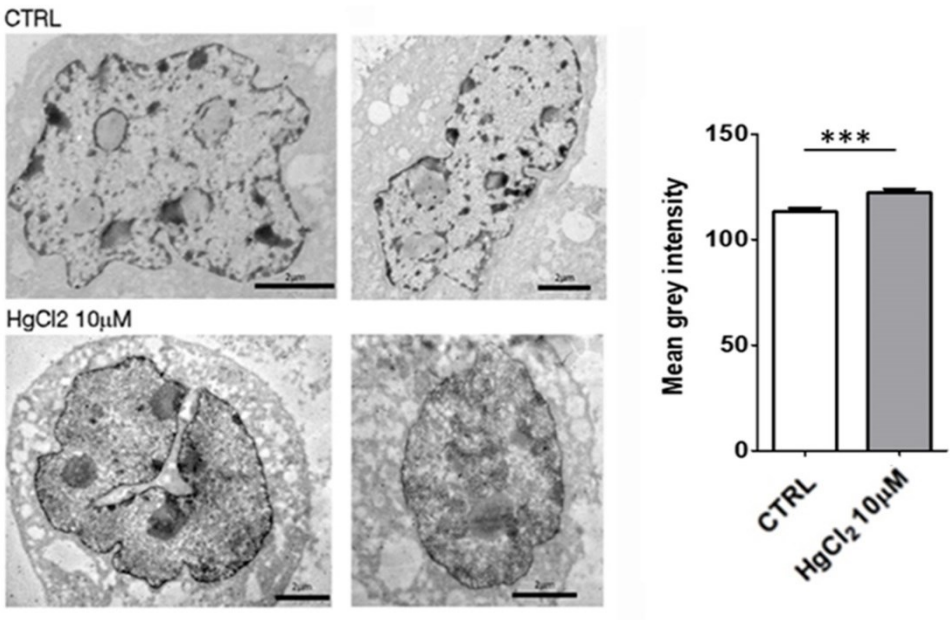

Figure 4.4.2: Osmium ammine staining reveals different degrees of heterochromatin density in mouse hepatocytes nuclei, in control (top) and after $HgCl_2$ treatment (bottom). Bar: 2μm. The graph shows the heterochromatin mean grey value ± SEM. Statistical significance was evaluated using two-tailed unpaired Student's t-test. Bar: 2μm. $HgCl_2$ treated hepatocytes has lighter heterochromatin domains which reflect less packaged hetero-chromatin conformation.

Just as the effects on the degree of chromatin condensation were much more evident on hepatocytes in cell culture, so too were the effects on the heterochromatin epigenetic markers. In fact, we detected a major decrease of H3K27me3 and H4K20me3 (Figure 4.3 A and B) and an evident, albeit minor, decrease in H3K9me3 (4.4.3 C).

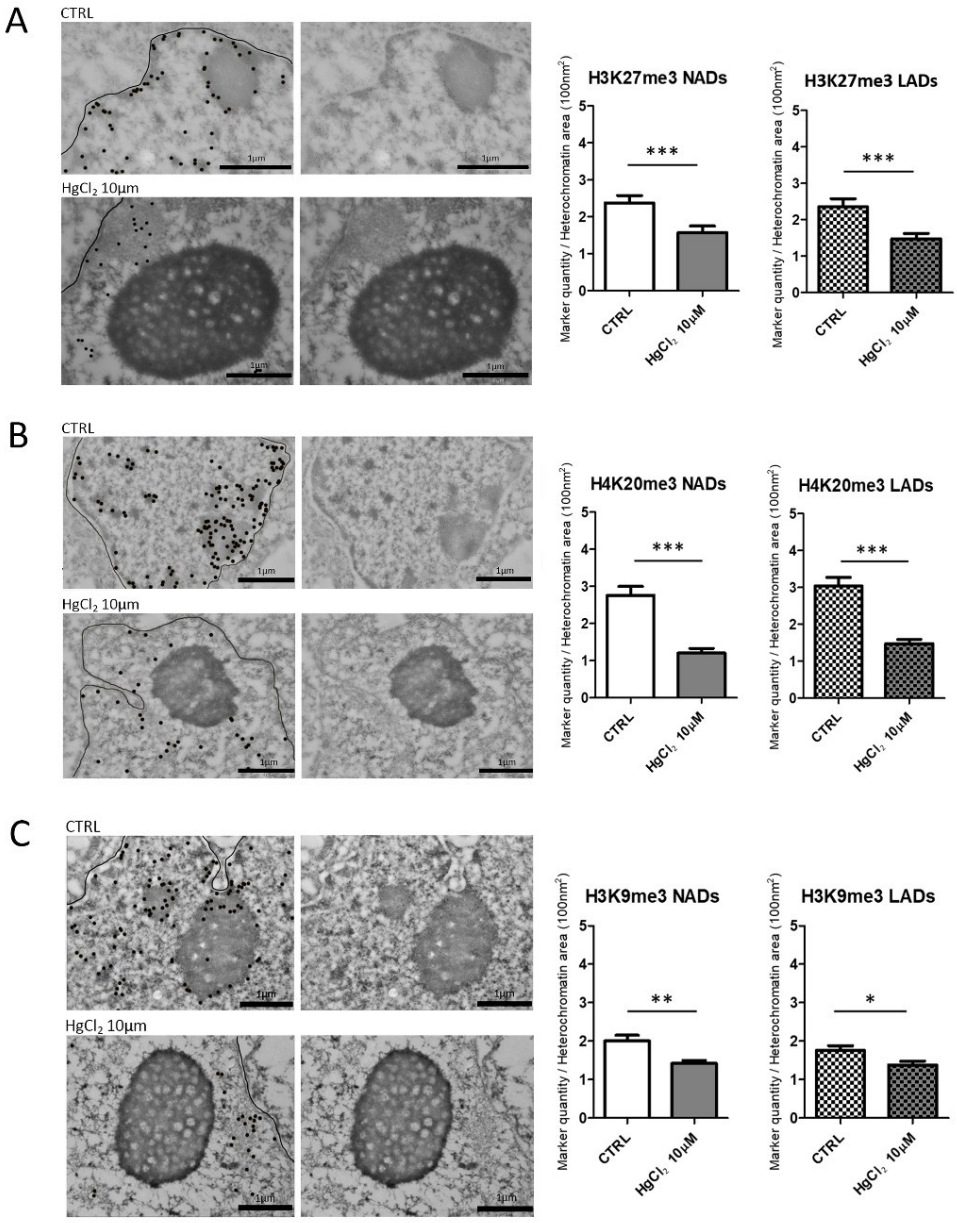

Figure 4.4.3: Immunocytochemistry at TEM of H3K27me3, H4K20me3 and H3K9me3. The micrographs show the localizations of H3K27me3, H4K20me3 and H3K9me3 in mouse hepatocytes in culture, highlighted by black dots, the line stands for nuclear envelope (left). The corresponding original images are shown on the right. Histograms show the mean ± SEM of the HPTM quantity per heterochromatin area (100nm2) in NADs and in LADs for control and $HgCl_2$ treated cells. Statistical significance was evaluated using two-tailed unpaired Student's t-test.

In order to confirm these trends, we decided to quantify the expression of the methyltransferases majorly implicated in the establishment of the three HPMTs analyzed. Kmt5b is the histone methyltransferase responsible for the mono-, di- and tri-methylation of H4K20 to produce respectively H4K20me1, H4K20me2 and H4K20me3 which regulate transcription and maintenance of genome integrity. This methyltransferase mainly functions in pericentric heterochromatin regions, thereby playing a central role in the establishment of constitutive heterochromatin (Bromberg et al. 2017). Suv39h1 is the Histone methyltransferase that specifically trimethylates H3K9, using H3K9me1 as substrate. H3 'Lys-9' trimethylation represents a specific tag for epigenetic transcriptional repression by recruiting HP1 (CBX1, CBX3 and/or CBX5) proteins to methylated histones (Lehnertz B. et al. 2003). EZH2 is a Polycomb group protein, the catalytic subunit of the PRC2 complex, which methylates 'Lys-27' of histone H3 (H3K27me), leading to transcriptional repression of the affected target gene. It is able to mono-, di- and trimethylate H3K27 to form H3K27me1, H3K27me2 and H3K27me3 respectively, but plays a major role in forming H3K27me3, which is required for embryonic stem cell identity and proper differentiation. The PRC2 complex may also serve as a recruiting platform for DNA methyltransferases, thereby linking two epigenetic repression systems (Lanzuolo and Orlando, 2012).

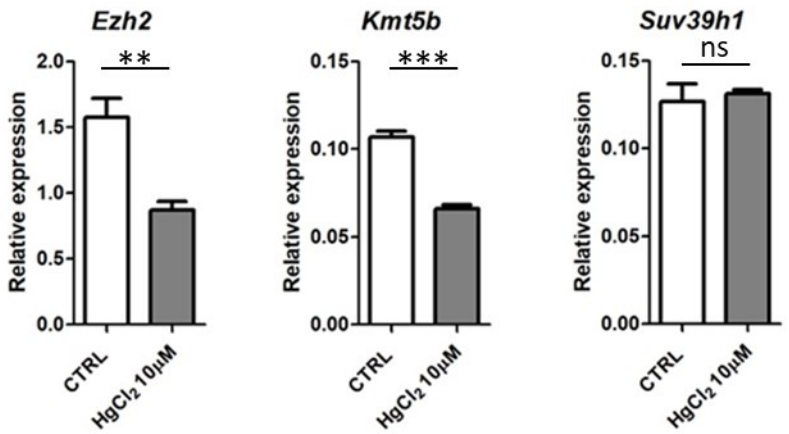

Figure 4.4.4: RT-qPCR analysis to quantify the expression of histone methyltransferases ezh2, kmt5b and suv39h1. Histograms show the relative expression of the gene coding for ezh2, kmt5b and suv39h1 which are involved in the establishment of H3K27me3, H4K20me3 and H3K9me3 respectively, in control versus $HgCl_2$ treated hepatocytes. Bar: mean ± SD.

The RT-qPCR analysis revealed that both *Kmt5b* and *Ezh2* expression decrease in hepatocytes exposed to $HgCl_2$ 10μM (Figure 4.4.4). This is in agreement with the results obtained at immunocytochemistry, which suggested a decrease in both products of these methyltransferases. Suv39h1 expression was not significantly distinct between treated and control cells, concordantly immunocytochemistry showed less degree of variation of H3K9me3 both in hepatocytes from cell culture (Figure 4.3.3) and liver tissue (Figure 4.4.3).

4.4.2 The effects of calorie restriction on heterochromatin

Many studies in various model organisms show how the reduction of calorie intake, without malnutrition, can lead to an improvement in health and a consequent increase in life span (Weindruch and Sohal 1997; Fontana and Klein 2007; Longo et al. 2021). However, many molecular mechanisms through which the beneficial effects of calorie restriction are realized have not been elucidated. In particular, in our opinion, it remains of fundamental importance to study caloric restriction influence on the nucleus. In fact, understanding changes at the systemic level is important, but these only follow the changes that occur at the cellular level. Likewise, although the enzymes involved in the various biochemical processes of metabolism play a key role in the final effects of caloric restriction, the variations in their activity or expression are necessarily secondary to variations that occur at the level of the nucleus, the primary control center of cell metabolism. Therefore, we studied if calorie restriction was able to induce variations in the degree of chromatin condensation and, as shown later, on the nucleolus, which plays a key role in regulating the rate and extent of protein synthesis.

We therefore carried out the same analyses performed previously.

Hepatocytes nuclei stained with Hoechst revealed that serum depletion for 5 days (serum 0.1%) causes an increase of the amount of condensed heterochromatin compared to the control cells, grown in a complete medium (serum 10%) (Figure 4.5). However, the osmium amine staining did not show a significant difference in the density of the heterochromatin domains (Figure 4.4.6).

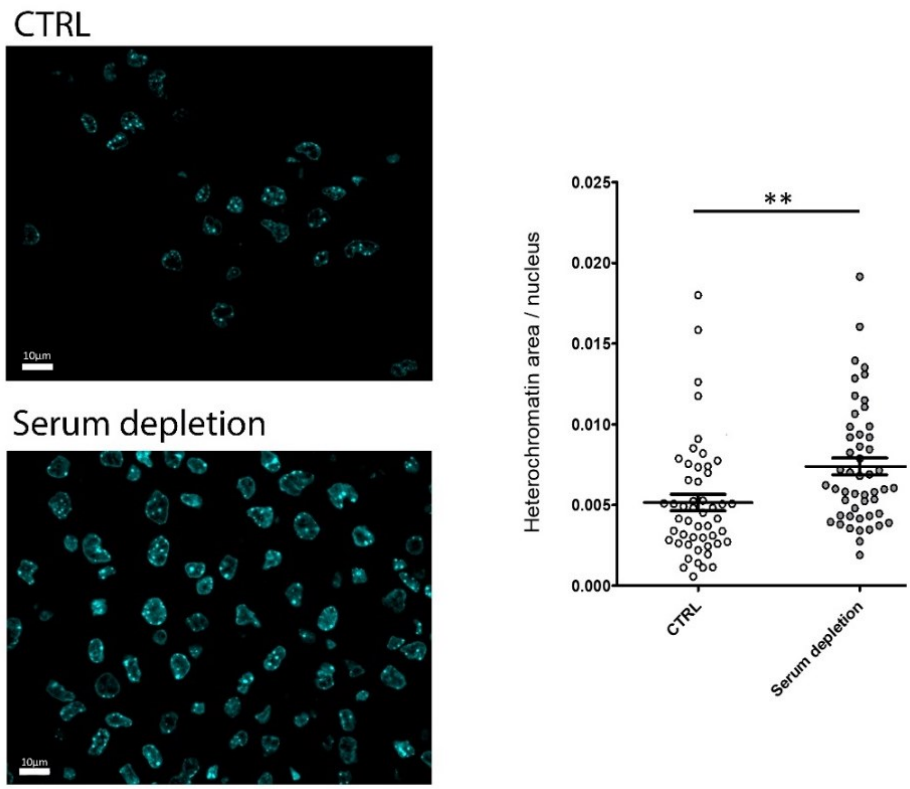

Figure 4.4.5: Hoechst staining to estimate the relative heterochromatin amount. Images show Hoechst fluorescence in mouse hepatocytes nuclei, in control (top) and after five days of serum depletion (bottom). Bar: 10µm. Graph: same analysis as in figure 4.4.1.

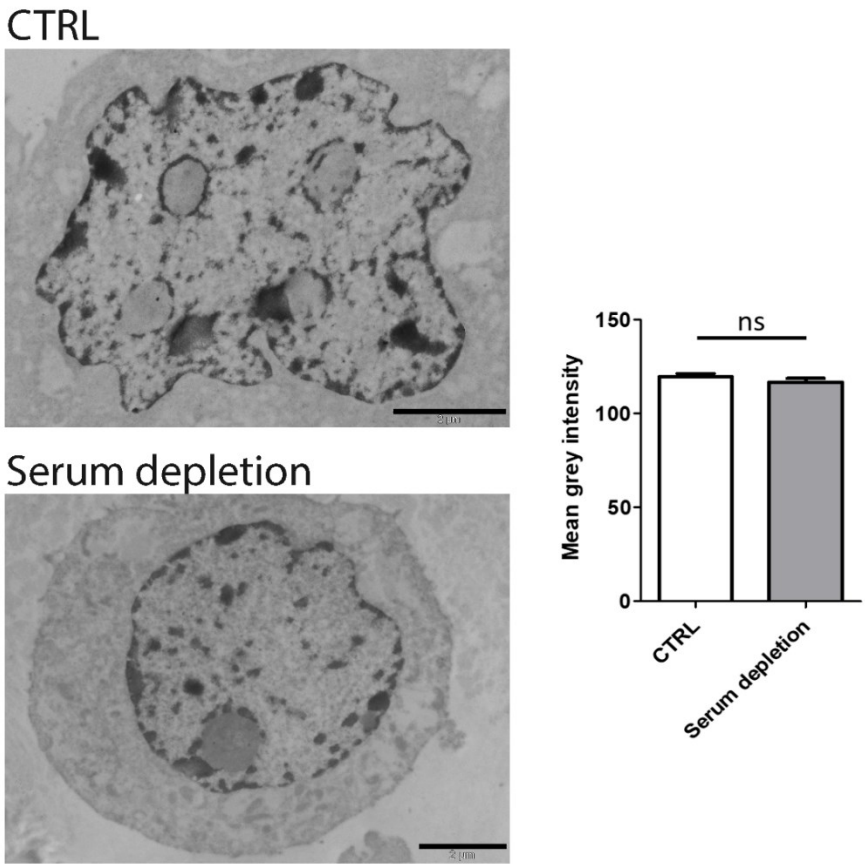

Figure 4.4.6: Osmium ammine staining of mouse hepatocytes sections: control (top) and serum depleted (bottom). Bar: 2µm. The graph shows the heterochromatin mean grey value. Statistical significance was evaluated using two-tailed unpaired Student's t-test. Bar: mean ± SEM.

Following the latter result, immunocytochemistry at TEM to evaluate variations of the quantity of HPTMs associated with heterochromatin did not demonstrate significant differences between the two conditions, except for a decrease in H4K20me3 in LADs (Figure 4.4.7).

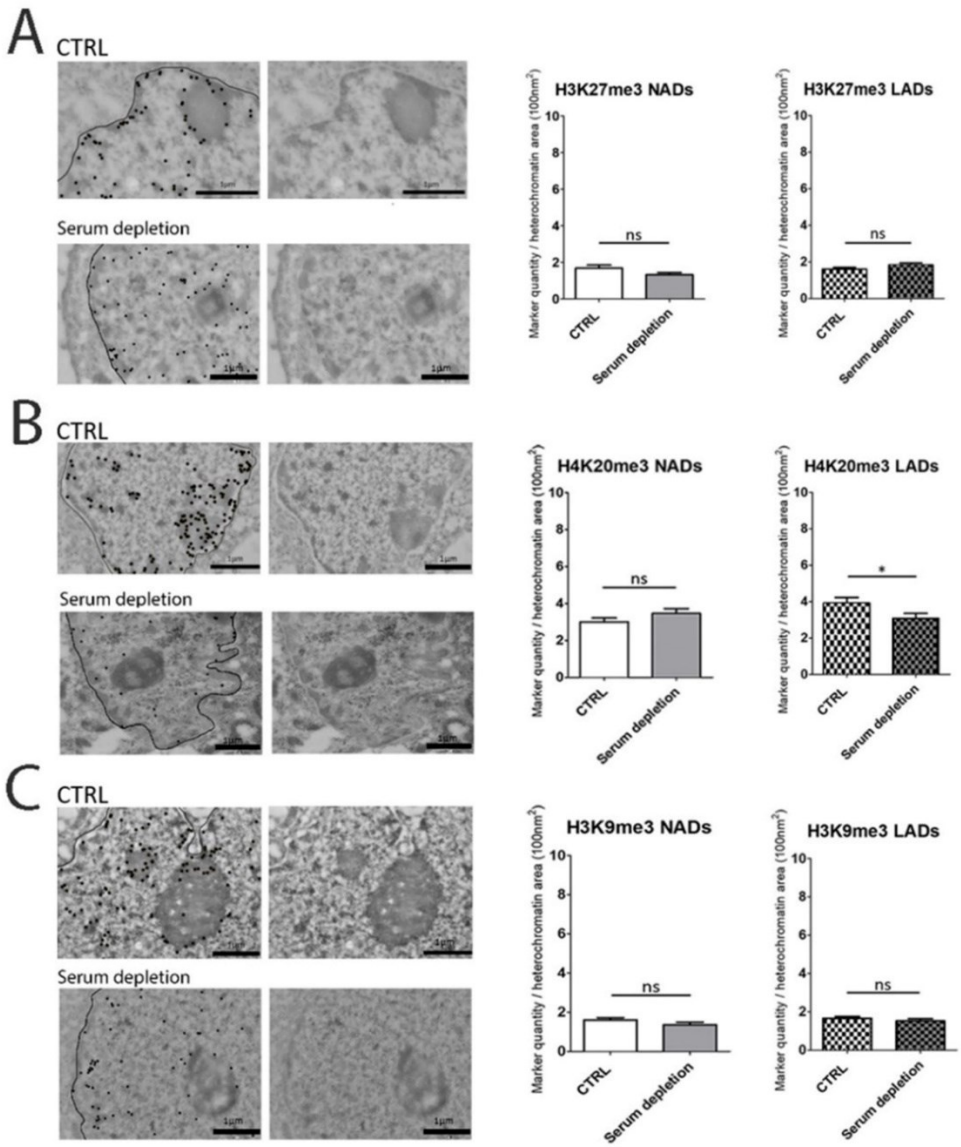

Figure 4.4.7: Immunocytochemistry at TEM of H3K27me3, H4K20me3 and H3K9me3. The micrographs show the localizations of H3K27me3, H4K20me3 and H3K9me3 in mouse hepatocytes, which are highlighted by black dots, the line stands for nuclear envelope (left). The corresponding original images are shown on the right. Histograms report the same analysis as in figure 4.4.3 comparing control versus serum depleted hepatocytes.

Moreover, this small trend of decrease was discordant with the increased expression of the methyltransferase kmt5b that we detected by RT-qPCR in serum depleted compared to the control hepatocytes (Figure 4.8). It should

be noted however that by immunocytochemistry we measured on average a small although not significant increase in H4K20me3 in NADs domains in serum depleted cells and that the increased expression of the methyltransferase precedes temporally the establishment of the corresponding HPTM. This could partly explain the discrepancy observed.

Figure 4.8

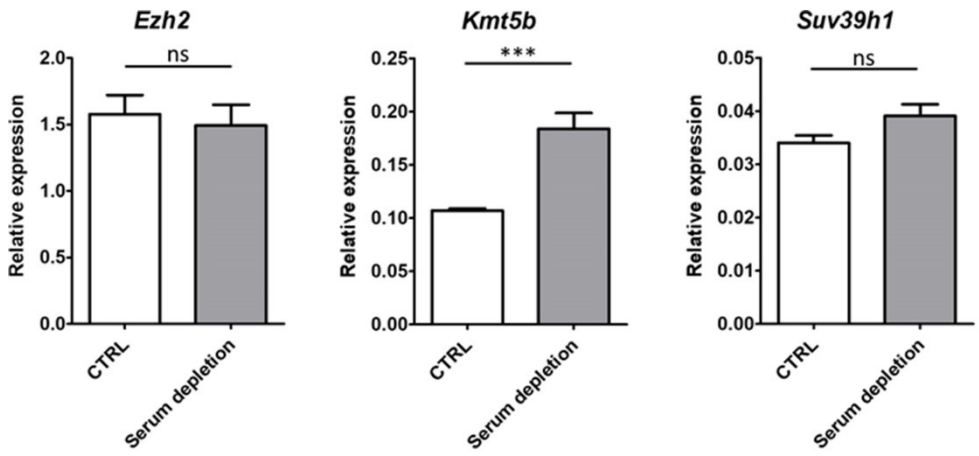

Figure 4.4.8: RT-qPCR analysis to quantify the expression of histone methyltransferases ezh2, kmt5b and suv39h1. Same analysis as in figure 4.4.4 comparing control versus serum depleted hepatocytes.

4.4.3 Dexamethasone induces reduction of the heterochromatin domains

Dexamethasone is a synthetic corticosteroid known for its anti-inflammatory properties. Our analyses revealed that treatment with a high concentration of dexamethasone (10-fold more than the concentration applied to the control hepatocytes) for 2 hours is sufficient to significantly reduce the extension of the heterochromatin domains as demonstrated by the staining of the nuclei with Hoechst (Figure 4.4.9). However, osmium amine staining did not reveal a significant change in heterochromatin density in the two conditions (Figure 4.4.10).

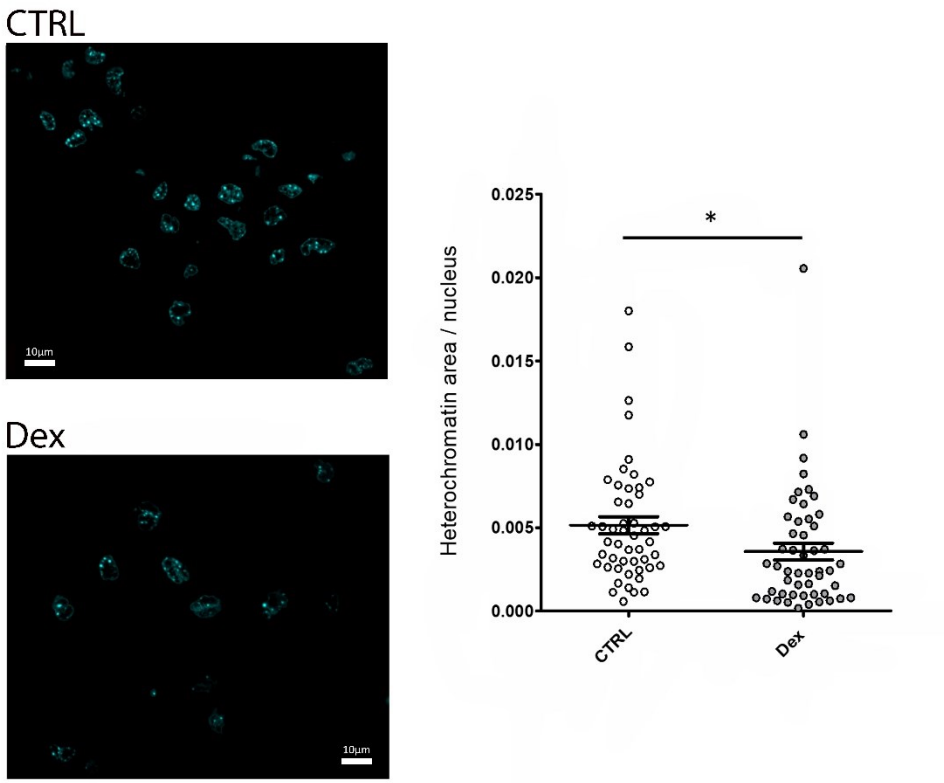

Figure 4.4.9: Hoechst staining to estimate the relative heterochromatin amount. Images show Hoechst fluorescence in mouse hepatocytes nuclei, in control (top) and after Dexamethasone treatment (bottom). Bar: 10µm. Graph: same analysis as in figure 4.4.1.

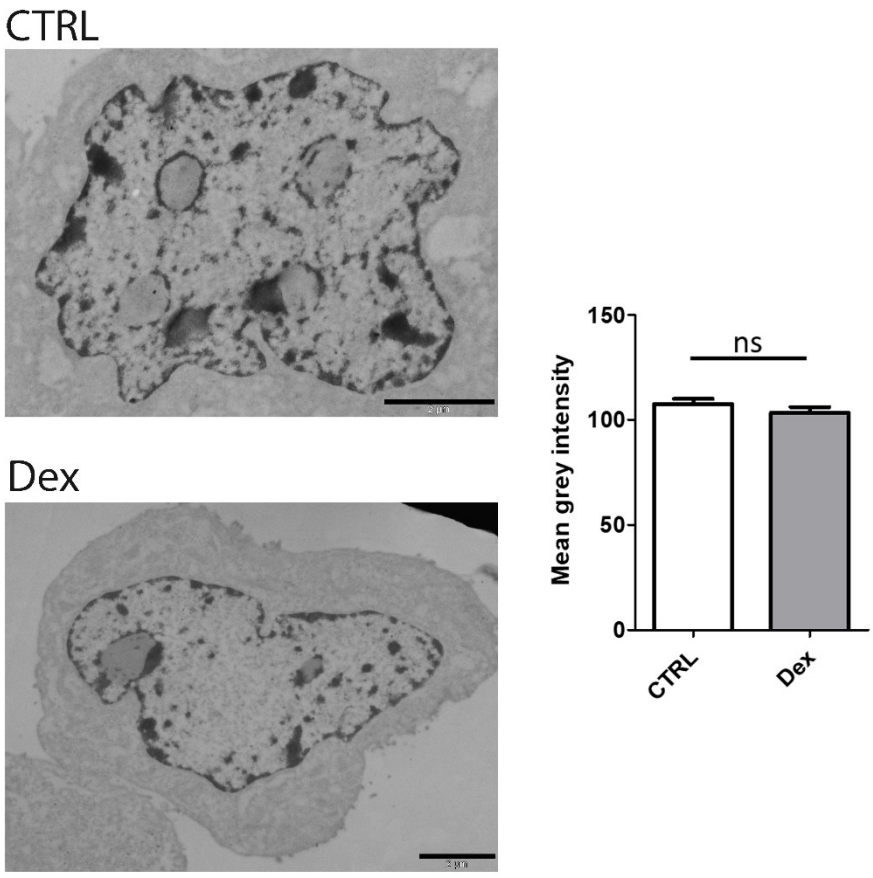

Figure 4.4.10: Osmium ammine staining of mouse hepatocytes sections: control (top) and after Dexamethasone treatment (bottom). Bar: 2µm. The graph shows the heterochromatin mean grey value. Statistical significance was evaluated using two-tailed unpaired Student's t-test. Bar: mean ± SEM.

Nevertheless, the subsequent immunocytochemistry analyses in agreement with Hoechst staining revealed an evident decrease of the markers H3K27me3 and H4K20me3 after 2h Dexamethasone treatment. Whereas, no significant variation of H3K9me3 quantity was detected compared to the control hepatocytes (Figure 4.4.11). Moreover, RT-qPCR to evaluate the expression of the methyltransferases involved in the deposition of these HPTMs confirms these trends (Figure 4.4.12).

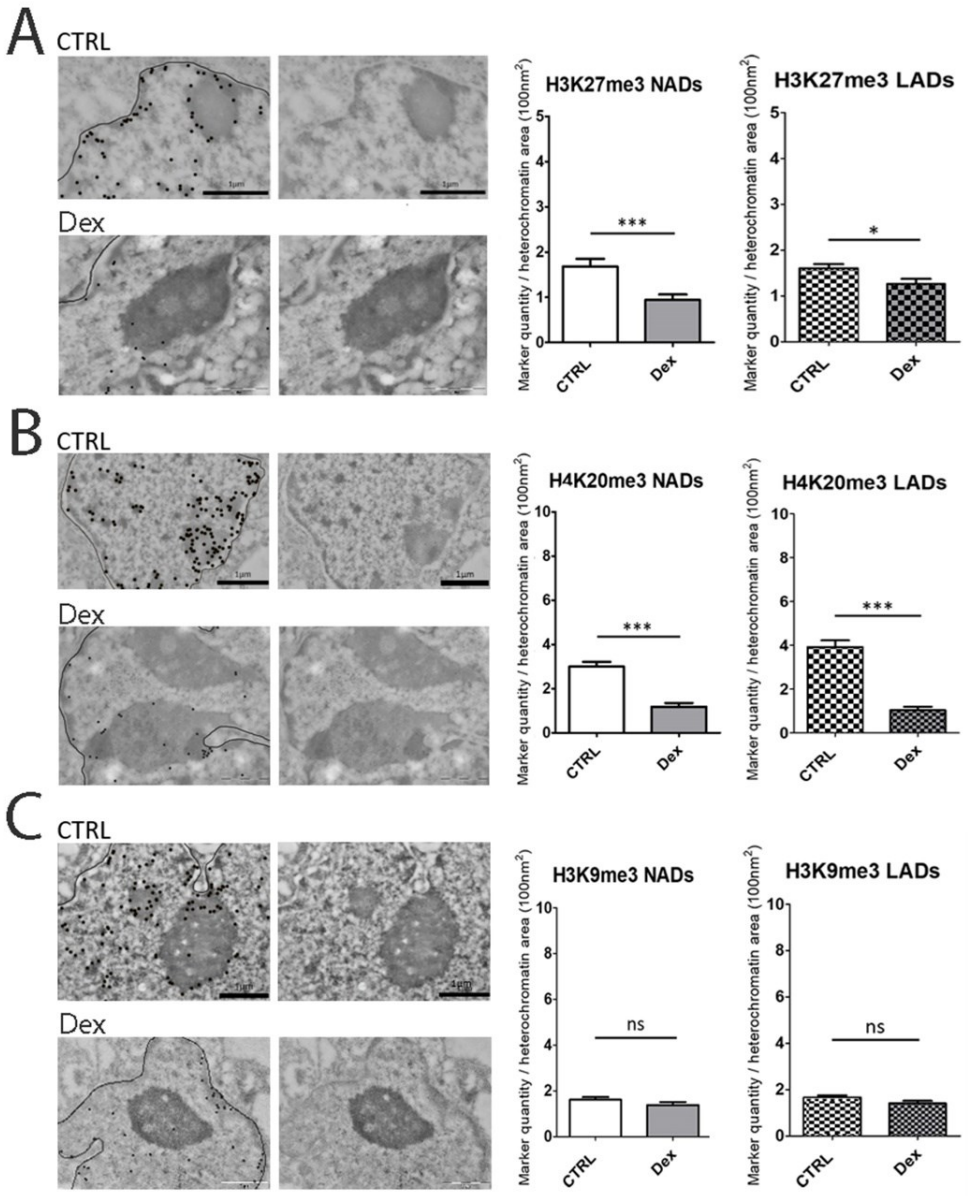

Figure 4.4.11: Immunocytochemistry at TEM of H3K27me3, H4K20me3 and H3K9me3. The micrographs show the localizations of H3K27me3, H4K20me3 and H3K9me3 in mouse hepatocytes, which are highlighted by black dots, the line stands for nuclear envelope (left). The corresponding original images are shown on the right. Histograms report the same analysis as in figure 4.4.3 comparing control versus Dexamethasone treated hepatocytes.

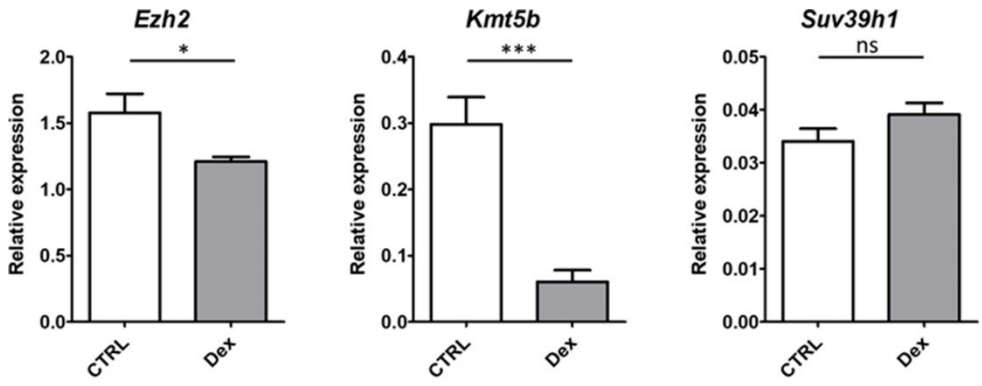

Figure 4.4.12: RT-qPCR analysis to quantify the expression of histone methyltransferases ezh2, kmt5b and suv39h1. Same analysis as in figure 4.4.4 comparing control versus Dexamethasone treated hepatocytes.

These results overall may suggest that Dexamethasone treatment induces a reduction of the heterochromatin areas as indicated by the Hoechst staining and by decreases in the quantity of the HPTMs associated to the heterochromatin, but without altering significantly the degree of heterochromatin compaction as suggested by the osmium ammine staining.

4.4.4 Heterochromatin changes in senescent hepatocytes

The condition of senescence mimics premature ageing achieved, in this case, through exposure to repeated damaging stimuli. So it can somehow be used as a term of comparison for those changes that occur in the hepatocyte in case of “unhealthy” ageing. The morphological changes observed in the general organization of the nucleus of hepatocytes induced to senescence are much more evident than in the other conditions, as showed in the figure below (Figure 4.4.13) and in the summary figure shown at the end of these last two sections (Figure 4.5.11). An increase in cell size and extension of heterochromatin domains, as well as in size of nucleoli can be immediately noted.

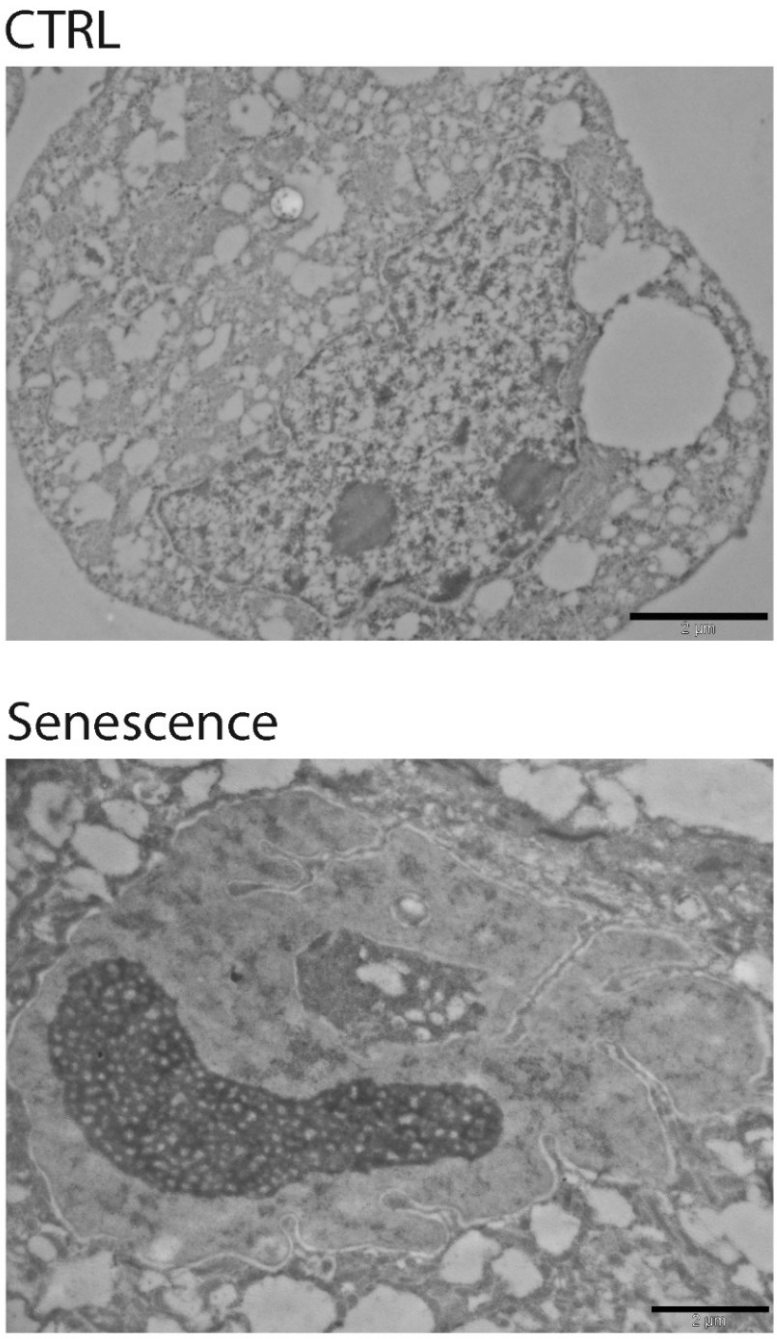

Figure 4.4.13: Sections of AML12 mouse hepatocytes at TEM stained by EDTA regressive technique. Control (top) and senescent hepatocyte (bottom).

We performed some experiments to further confirm that the cells had achieved the senescence phenotype.

We ran immunofluorescence analysis of histone γH2AX, a marker of DNA damage and senescence. γH2AX should be present in major quantity due to higher activation of DDR response typical of senescent cells and in this case also revoked by the repeated exposure to oxidative stress as reported by Singh and colleagues (Singh et al., 2020).

In the image below (figure 4.4.14) it is possible to see a higher number of positive senescent hepatocytes for γH2AX, while control hepatocytes are essentially negative. Furthermore, also in these images is possible to appreciate the increase in cell size typical of senescent cells compared to the control.

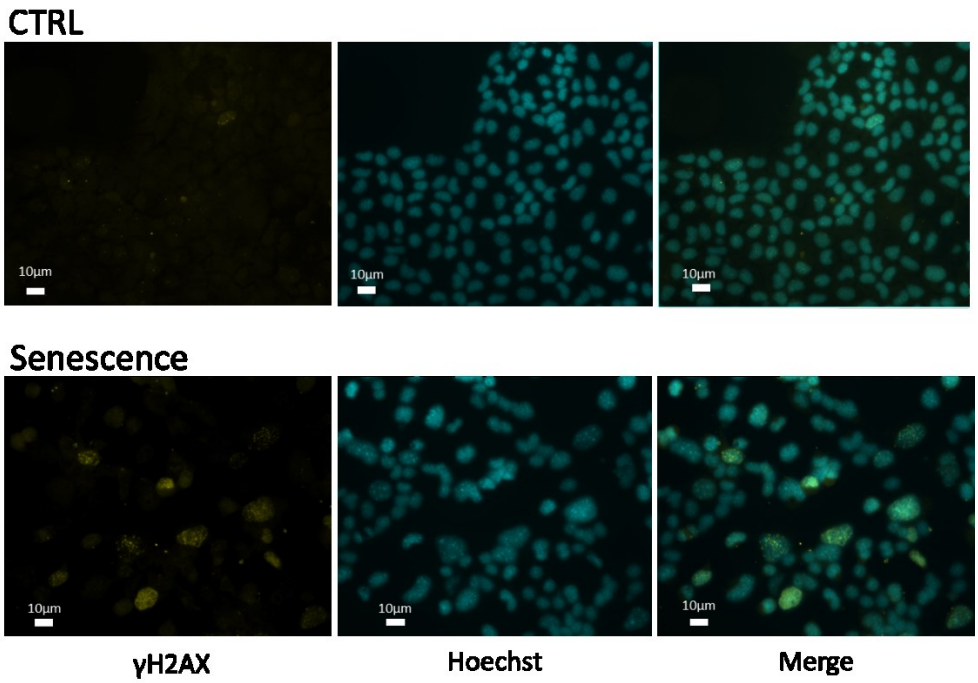

Figure 4.4.14: Immunofluorescence labelling of γH2AX in AML12 heaptocytes. γH2AX labelling is shown on the left, Hoechst staining in the middle, merge is on right, in CTRL (top) and Senescent (bottom) hepatocytes. Bar: 10µm.

Another marker of senescence is p16INK4a, whose transcriptional activation has been used extensively to report the presence of senescent cells in vivo (Burd et al., 2013; Baker et al., 2011). p16INK4a is an inhibitor of cyclin-dependent kinases 4 and 6 and a potent mediator of cell cycle arrest in

transient assays (Koh et al., 1995; Medema et al., 1995; Serrano et al., 1995). Singh and colleagues measured also an increase in the expression of p53, considered as a marker of senescence (Singh et al., 2020). Therefore we quantify the expression of these markers by RT-qPCR comparing untreated control hepatocytes to those induced to senescence. We detected an increase in the expression of both *Tp53* and *p16INK4a* in senescence induced cells (Figure 4.4.15). Moreover, as reported in the same study (Singh et al., 2020), we also measured an increased expression of the autophagy-related protein Map1lc3b compared to the control (Figure 4.4.15). In a recent review is confirmed that autophagy is currently thought to have a direct effect on triggering senescence, although autophagy and senescence relation still need to be clarified (Rajendran et al., 2019).

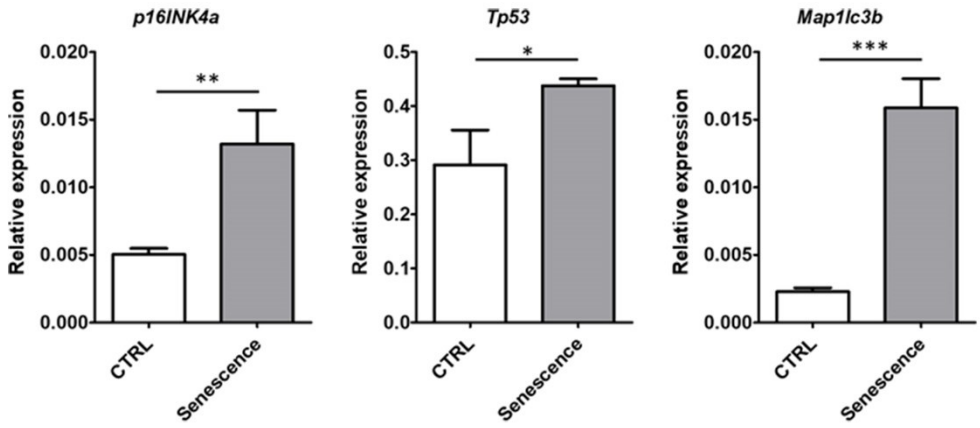

Figure 4.4.15: RT-qPCR analysis to quantify the expression of p16INK4a Tp53 and Maplc3b used as markers of senescence. Same analysis as in figure 4.4.4 comparing control versus senescent hepatocytes.

The analysis by Hoechst staining was carried out as for the other cell stress and showed a significant increase of the heterochromatin areas, although not as extreme, as it would appear from electron microscopy images.

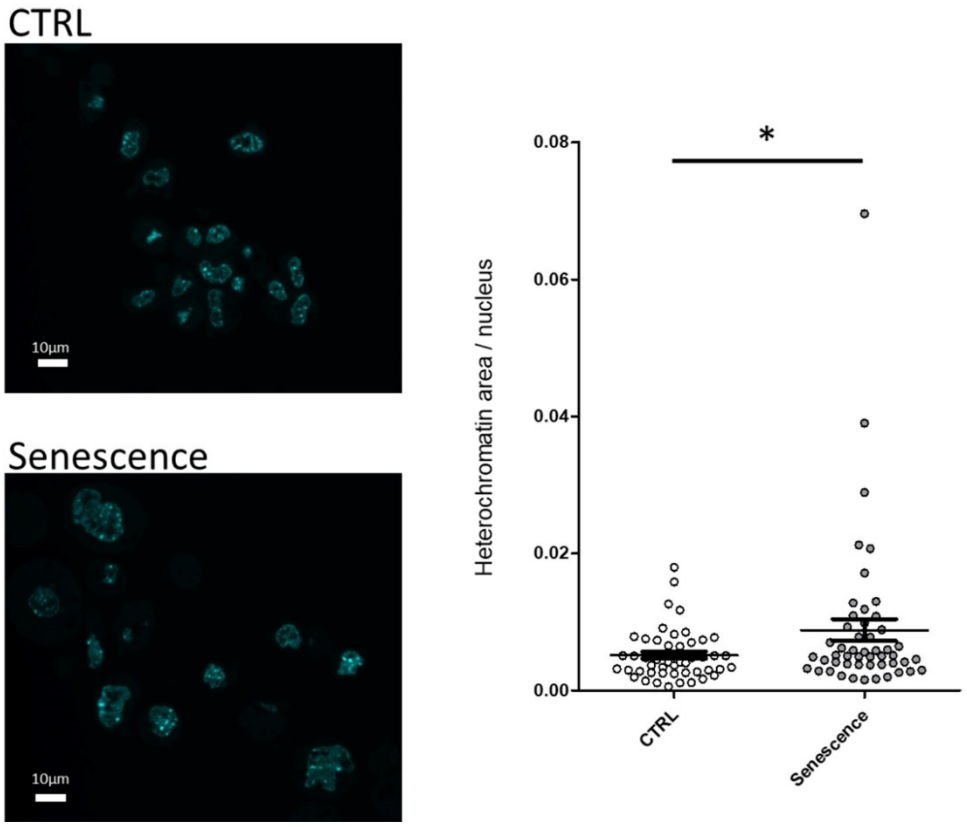

Figure 4.4.16: Hoechst staining to estimate the relative heterochromatin amount. Images show Hoechst fluorescence in mouse hepatocytes nuclei, in control (top) and senescent hepatocytes (bottom). Bar: 10µm. Graph: same analysis as in figure 4.4.1 comparing control versus senescent hepatocytes.

It may be that a general increase in the heterochromatin extension is observed through EDTA regressive staining, but this is not accompanied by an increase in the degree of heterochromatin density. This would result in a non-particularly intense Hoechst staining, which may account for the not so extreme difference observed compared to the control cells.

Moreover, immunocytochemistry analysis revealed a significant reduction in the amount of the HPTM H3K9me3 and no significant increase of H3K27me3 per area of heterochromatin in senescent cells. These data may suggest that the enlargement of the heterochromatin domains observed in senescent cells is not due to an important contribution from these HPTMs, but that a major role may be played by the increase of H4K20me3 or by other epigenetic mechanisms involved in the formation of heterochromatin as for example: the methylation of DNA, the reduction of the degree of acetylation, or the increase / decrease of other HPTMs.

Furthermore, beyond the consideration that the greater extension of heterochromatin areas observed by EDTA staining in senescent cells may not necessarily be related to a greater condensation compared to the control hepatocytes which show much smaller domains, it has also to be taken into account that the comparison between these two conditions was the most complex to analyze due to the large variation in the dimensions of the entire nucleus. A senescent cell nucleus can be more than double in size compared to a control cell and this critically influences the organization of the heterochromatin domains and the spatial relationships between nucleolus, heterochromatin and the other nuclear elements. When we analyzed the data and derived our conclusions, the effects that the dimensional differences may have on the measurements were taken into account.

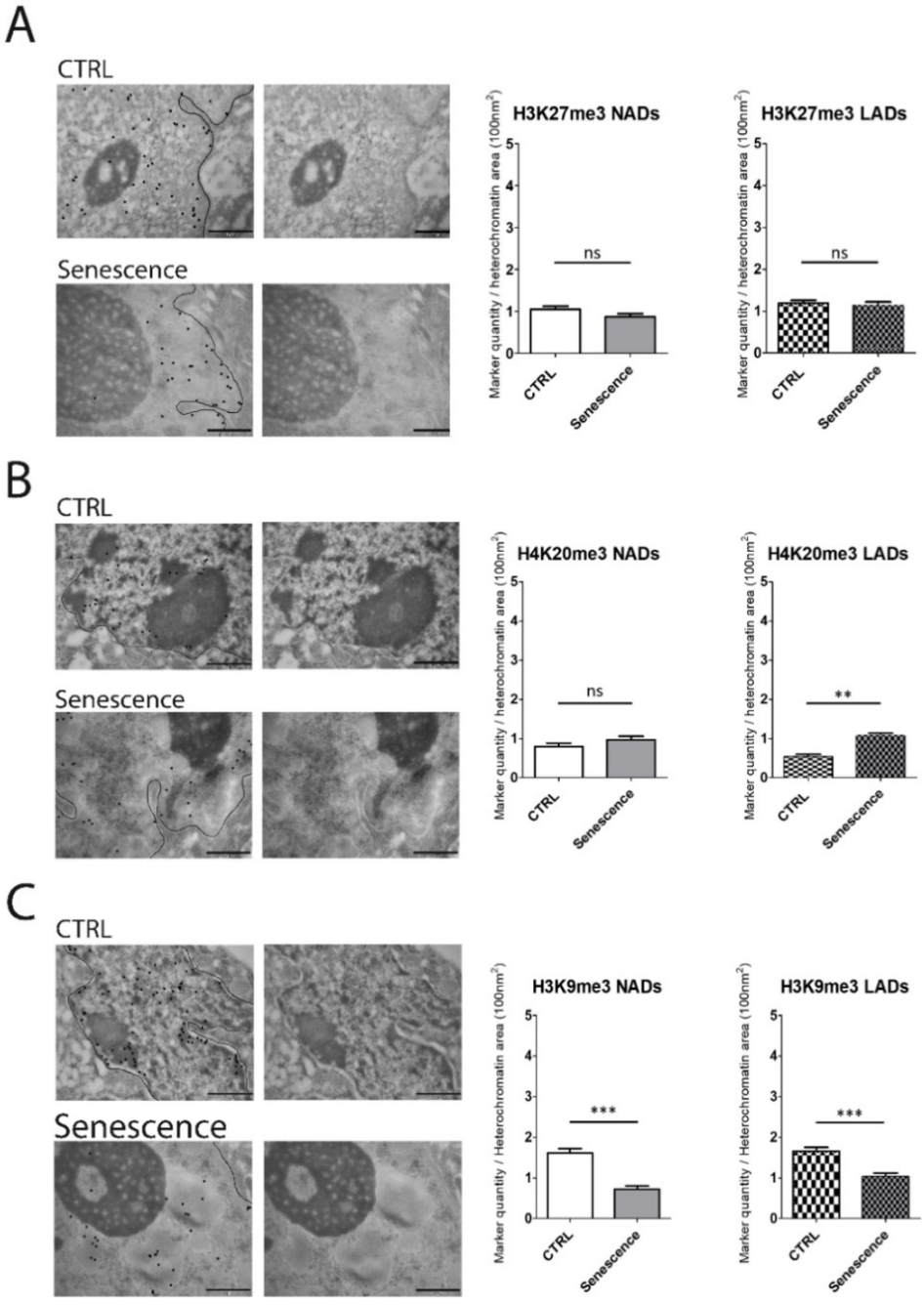

Figure 4.4.17: Immunocytochemistry at TEM of H3K27me3, H4K20me3 and H3K9me3. The micrographs show the localizations of H3K27me3, H4K20me3 and H3K9me3 in mouse hepatocytes, which are highlighted by black dots, the line stands for nuclear envelope (left). The corresponding original images are shown on the right. Histograms report the same analysis as in figure 4.4.3 comparing control versus senescent hepatocytes.

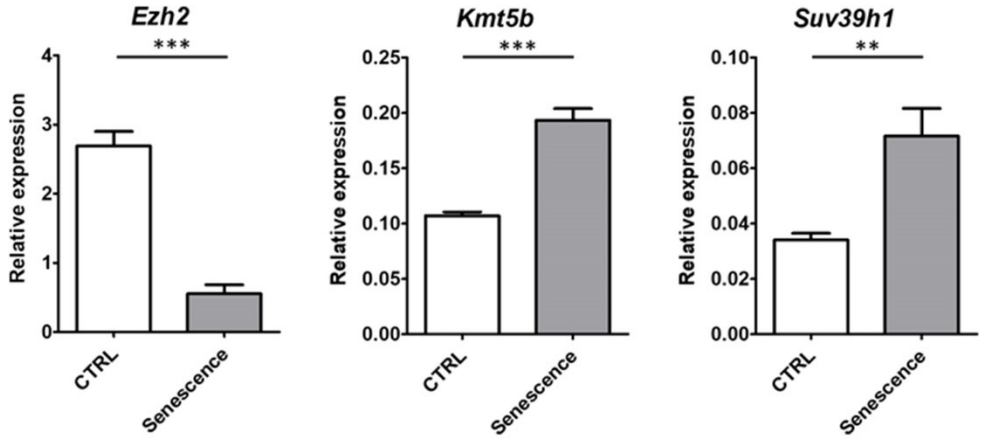

Figure 4.4.18: RT-qPCR analysis to quantify the expression of histone methyltransferases ezh2, kmt5b and suv39h1. Same analysis as in figure 4.4.4 comparing control versus senescent hepatocytes.

Even the analysis of the expression of the methyltransferases does not always seem to agree with the trends observed through immunocytochemistry. In fact, we detected a concordant increase of kmt5b expression and H4K20me3 quantity in senescent cells, but a marked decrease in the expression of ezh2, while the immunocytochemical analysis did not show significant differences for this epigenetic marker between the two conditions. Finally, we measured an increase of suv39h1 expression, while immunocytochemistry revealed a clear decline compared to the control. In this last case, it is possible to explain this difference considering that although the quantity of H3K9me3 per area of heterochromatin is lower in senescent hepatocytes, since the nucleus is much larger and a considerable amount of heterochromatin is present, there is still the need for an increased expression of the corresponding methyltransferase, because in the entire nuclear volume of senescent cells the quantity of the H3K9me3 modification could be higher than in control. More difficult to interpret is the decline in the expression of ezh2 which does not correspond to an evident decline in H3K27me3. However, once again, it must be taken into account the gap in time between the decrease of the enzyme expression and the amount of the corresponding HPTM, which may have been previously deposited and not removed by the other competent “eraser” enzymes. In fact, the quantification of the methyltransferases responsible for the deposition of these HPTMs provide only indirect information, then many factors can influence the quantity and density per heterochromatin area of a specific HPTM.

4.5 Nucleolar activity under cell stress

Finally, as a further step in the investigation of the effects of the ageing process and cell stress on the hepatocyte nucleus, we studied the changes in the morphology and activity of the nucleolus. In fact, being the nucleolus the nuclear domain where ribosome biogenesis and other important molecular processes take place (such as pathways that regulate cell proliferation and apoptosis and telomere formation), its size and activity are subjected to important changes upon different cell stress (Yang et al. 2018).

We carried out some experiments that can give us some general indications on the state of activity of the nucleolus. First of all, we investigated these features through the silver staining of the nucleolar organizer regions (NORs). These nucleolar components contain a set of argyrophilic proteins, which are selectively stained by silver methods. After staining, they are visualized as black dots localized throughout the nucleolar area, called "AgNORs" (Trerè, 2000). We measured the extension of the NORs by comparing control hepatocytes with those subjected to different stressful conditions.

Senescent hepatocytes showed a strong increase in the NORs size compared to the control. (From these images, it is possible to note, on average, also an increase of the nuclear size of senescent cells, as previously observed) (figure 4.5.1).

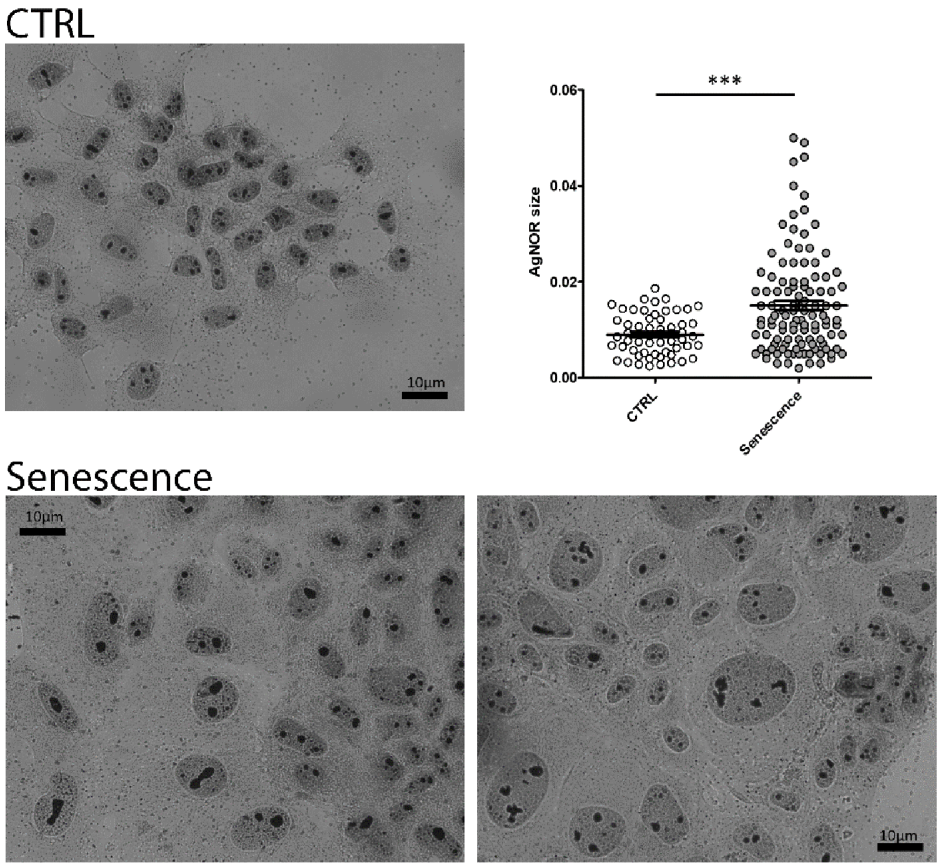

Figure 4.5.1: Silver staining of the NORs. AgNOR staining of control and senescent hepatocytes. Histograms show the size of the NORs. Bars indicate the mean ± SEM. Statistical significance was evaluated using two-tailed unpaired Student's t-test.

Considering this, we evaluated whether the other treatments induced a change of this feature in the same or in the opposite direction of that observed in the senescent hepatocytes.

The toxicity of mercury chloride seems to bring the nucleolus closer to a state similar to senescence. In fact, exposure to increasing doses causes evident extensions of the NOR size compared to the control. Surprisingly, the major increase was detected upon 1µM $HgCl_2$ exposure, the lowest dose (Figure 4.5.2). Maybe $HgCl_2$ exerts a highly toxic effect on the nucleus, so that 1µM is sufficient to evoke strong nucleolar changing, then increasing dose may determine a degree of damage which overcomes further nucleolar response.

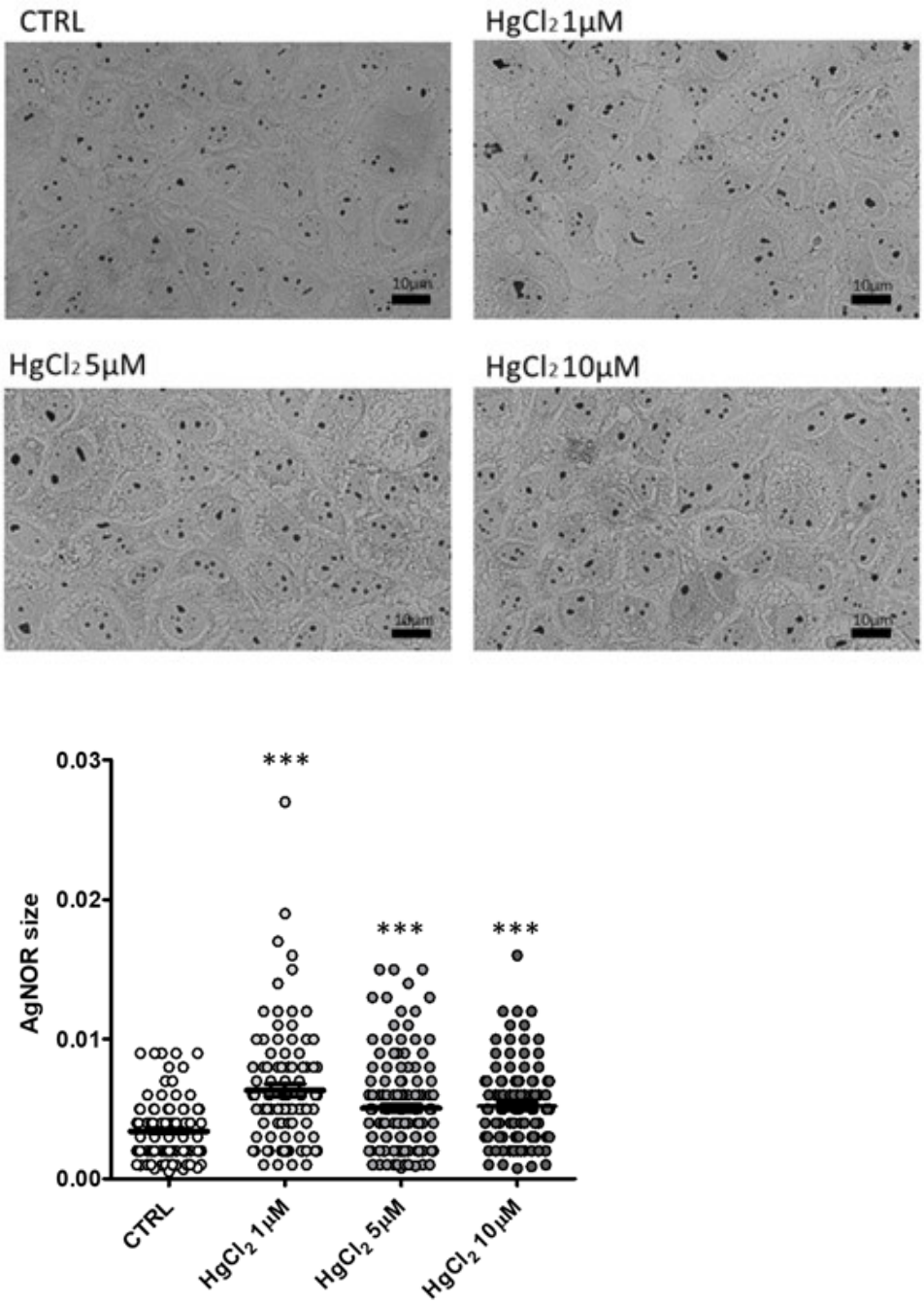

Figure 4.5.2: Silver staining of the NORs. AgNOR staining for control and hepatocytes treated with increasing doses of $HgCl_2$. Histograms show the size of the NORs. Bars indicate the mean size ± SEM. Statistical significance was evaluated using One Way ANOVA test.

Serum depletion, as well as treatment with Dexamethasone, on the other hand, induce an opposite change. In fact, in these two conditions, the hepatocytes showed smaller nucleoli than the control (Figures 4.5.3 and 4.5.4).

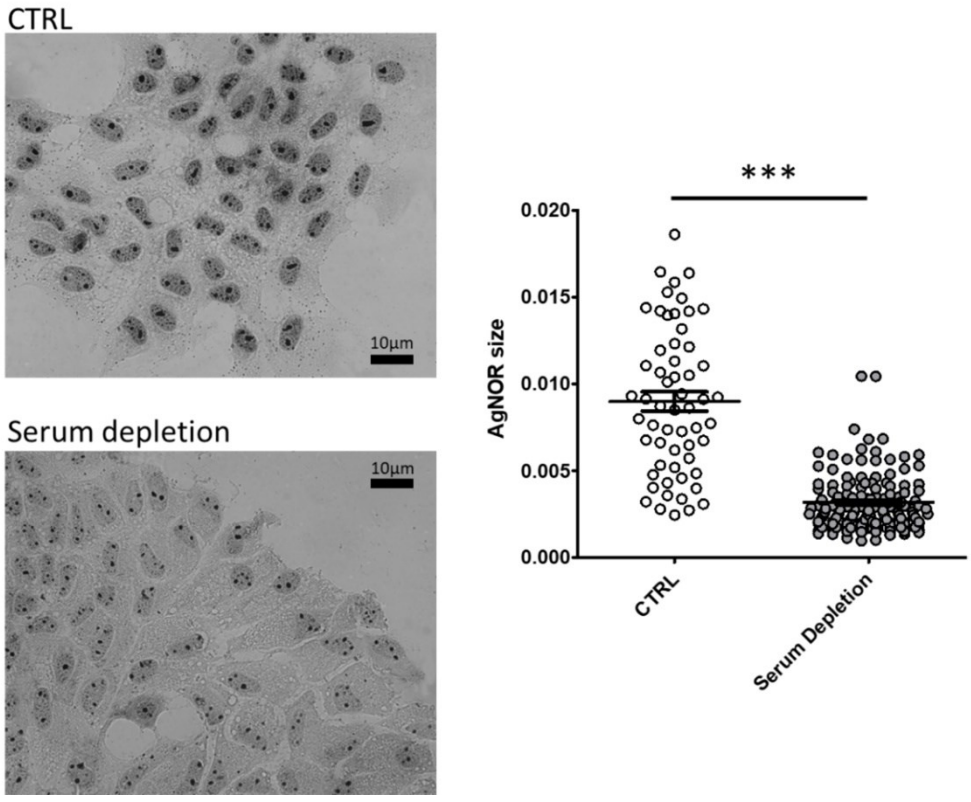

Figure 4.5.3: Silver staining of the NORs. AgNOR staining for control hepatocytes (top) and those subjected to five days of serum depletion (bottom). Histograms show the size of the NORs. Bars indicate the mean ± SEM. Statistical significance was evaluated using two-tailed unpaired Student's t-test.

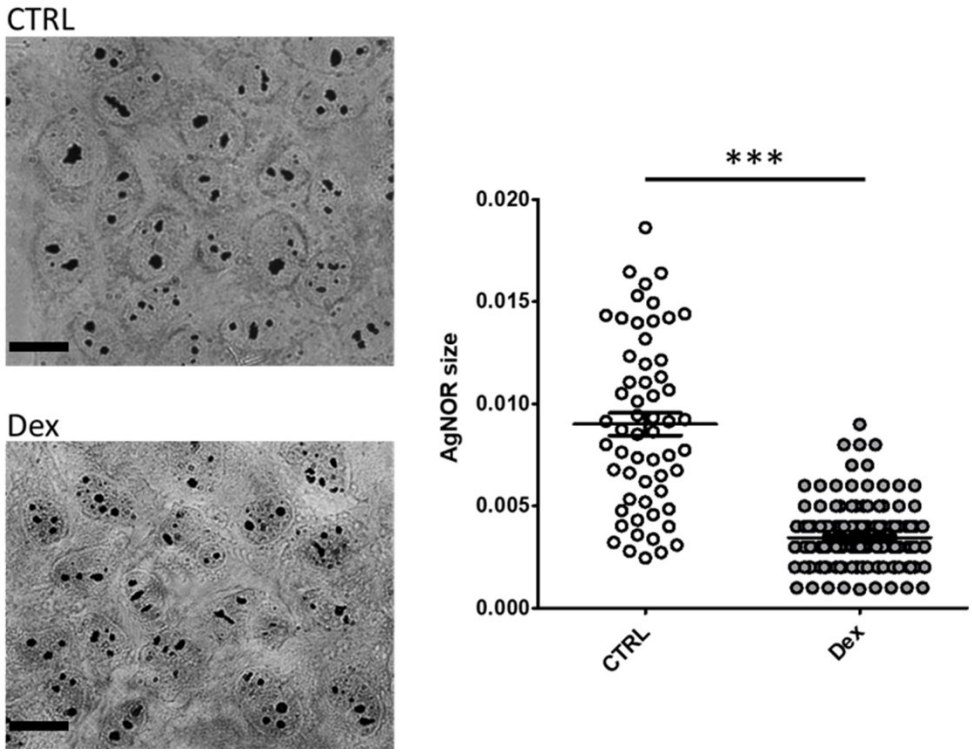

Figure 4.5.4: Silver staining of the NORs. AgNOR staining for control hepatocytes (top) and those treated with Dexamethasone 1μM (bottom). Bar: 10μm. Histograms show the size of the NORs. Bars indicate the mean ± SEM. Statistical significance was evaluated using two-tailed unpaired Student's t-test.

We could expect that lower calorie intake induces a slowdown in cell metabolism, which is reflected in a lower nucleolar activity because of less need for enzymes synthesis.

The reduction in the nucleolar size observed after Dexamethasone treatment finds a less immediate interpretation. We could hypothesize that Dexamethasone exerts its anti-inflammatory action, slowing down cell metabolism and cell activation in response to external stimuli, by limiting ribosomes production.

To obtain complementary evidence on the nucleolar activity under cell stress, we measured the rRNA synthesis evaluating the quantity of the mature and some precursor transcripts in control hepatocytes compared to the other different stressful conditions, through relative RT-qPCR. The image below schematizes the design of the primer used in this study for the detection of

the rRNAs quantity and their relative position along the full-length 45S transcript (Figure 4.5.5). All primer sequences are reported in table 3.1, chapter 3 Material and Methods.

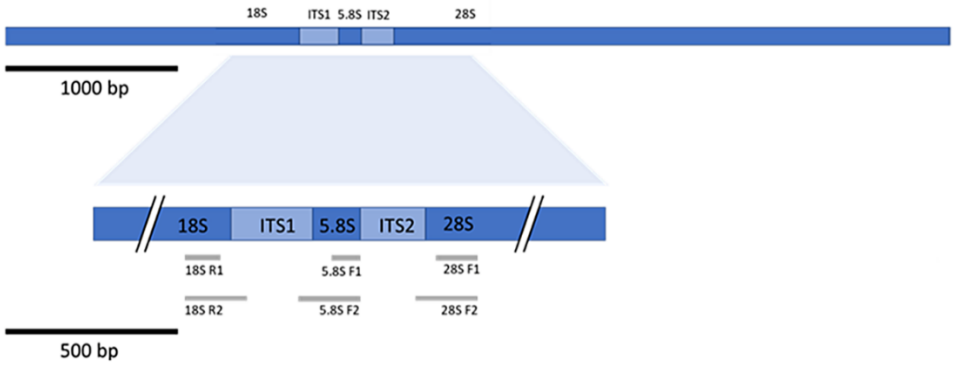

Figure 4.5.5: Schematic representation of primers design for rRNAs quantification by RT-qPCR.

The RT-qPCR to compare control hepatocytes to those treated with increasing doses of mercury chloride revealed, in agreement with the morphological analysis after agNOR staining, that ribogenesis increases after $HgCl_2$ treatment more or less in a dose-dependent manner, with some difference considering each transcript (Figure 4.5.6). This is interesting because it could reflect an impact on different moments of ribogenesis. Specifically, we detected an increase in the precursors for all three transcripts upon mercury treatment. On the contrary, for the 28S we saw an increase in the precursor, but not in the final transcript product. 18S, the first processed transcript, is evidently increased in both (Figure 4.5.6). This trend suggests an attempt of the cell to counteract $HgCl_2$ harmful stimulus by activating nucleolus, maybe to translates the enzymes necessary for detoxification and to restore the previous equilibrium. However, this initial increase seems to be not so efficient: the ribogenesis initially speeded up, but then in the final part the rate of production of the 28S is not increased. Therefore, the cells may try to trig a response against mercury chloride-induced damage, but at certain steps, this response may not be so effective.

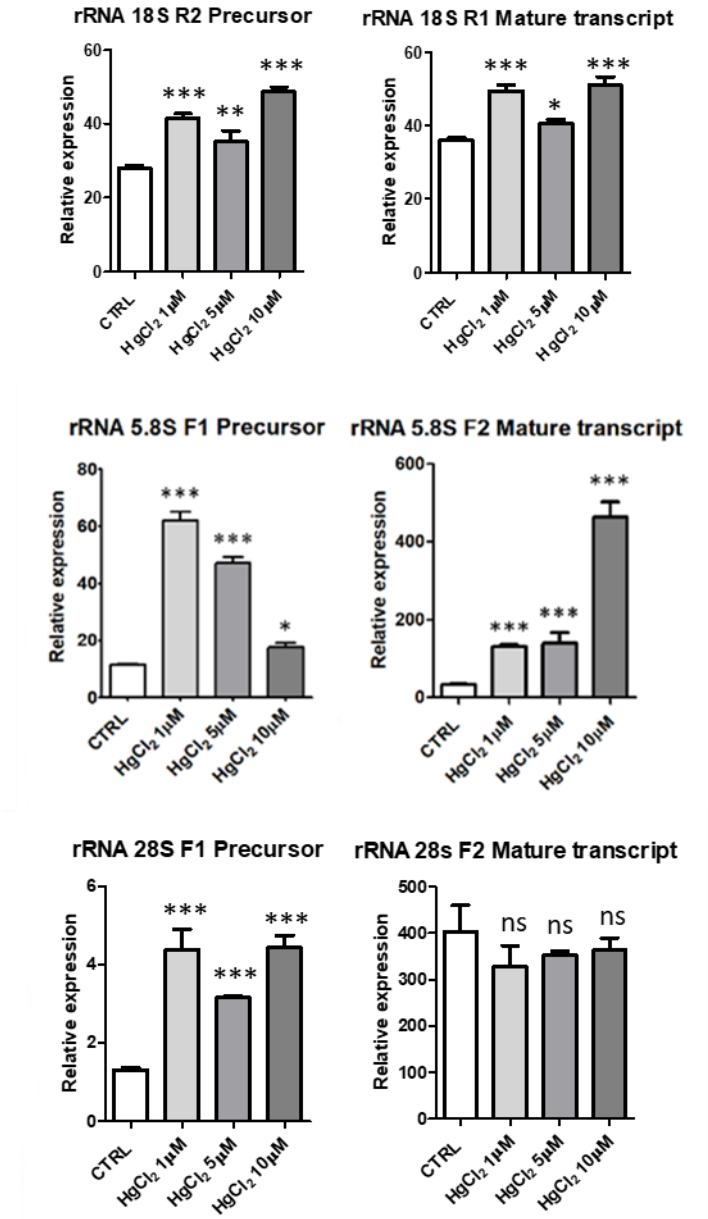

Figure 4.5.6: RT-qPCR analysis to quantify the expression of rRNAs mature and precursor transcripts. In the histograms are plotted the mean ± SD of the relative gene expression. Statistical significance was evaluated using One Way ANOVA test.

To gain further information, we also measured the variation in the expression of genes encoding proteins involved in ribosome biosynthesis. We analysed the expression of ubtf, and rrp9, as proteins that positively regulate the ribogenesis. The role of ubtf is well known and was detailed in the

introduction. While Rrp9 protein is a component of a nucleolar small nuclear ribonucleoprotein particle (snoRNP), thought to participate in the processing and modification of pre-ribosomal RNA (pre-rRNA) (Chen et al. 2016). We also evaluated the expression of the baz2a protein as a repressor of the rRNA transcription. This protein is of particular interest because it mediates the silencing of rDNA genes by promoting the deposition of H3K9me3 and H4K20me3 on these sequences (Santoro and Grummt, 2002).

Finally, as further supporting evidence of increase in ribosome production, we analyzed the expression of genes coding for one component of the small ribosomal subunit the rps18 and one protein of the large ribosomal subunit the rpl19.

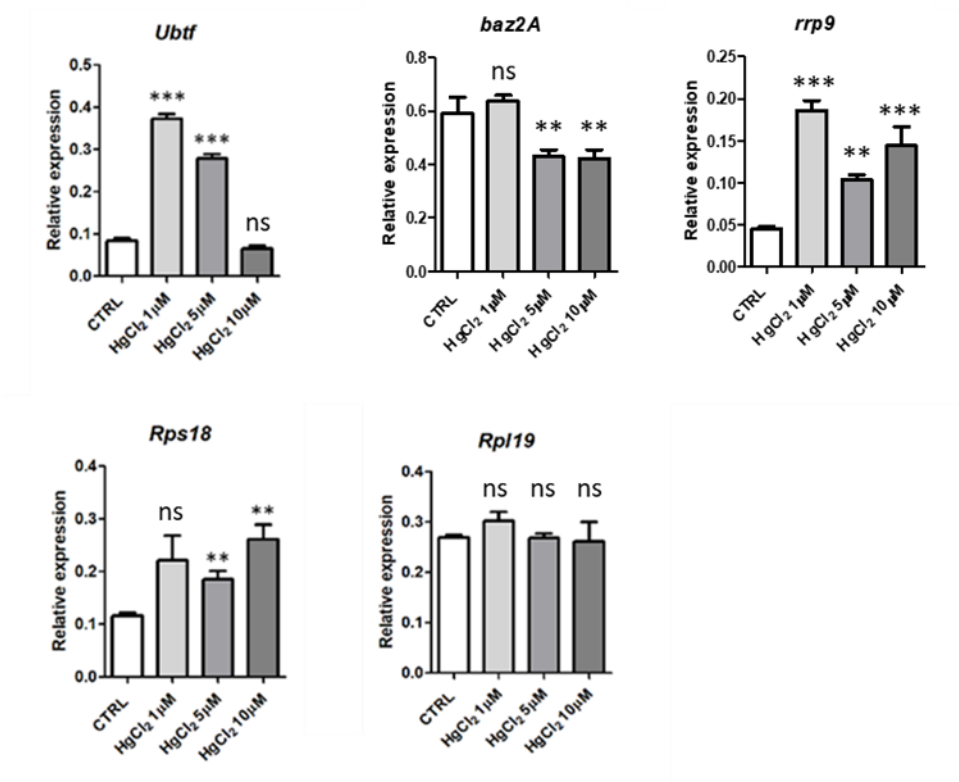

Figure 4.5.7: RT-qPCR analysis to quantify the expression of some proteins involved in the ribogenesis. In the histograms are plotted the mean ± SD of the relative gene expression. Statistical significance was evaluated using One Way ANOVA test.

We detected an increase in the expression of both *Ubtf* (although not for the highest dosage) and *Rrp9* genes and a decrease in *Baz2a* expression. These

results suggest again nucleolar activation upon $HgCl_2$ treatment. The decrease of *Baz2a* expression is also in agreement with the results of immunocytochemistry at transmission electron microscopy, where we detected a decrease in these HPMTs and especially of H4K20me3 in NADs.

Concerning the component of the small and large ribosome subunits, we detected an increase in Rps18 but not in Rpl19. Small ribosomal subunits are known to be processed and exported from the nucleus before the large ribosomal subunits (Henras et al., 2015). Once again our results suggest an increase in the speed of the first part of the ribogenesis process, while the final events, such as the 28S mature transcripts production, seemed not evidently increased.

The same RT-qPCR analyses were also carried out for the other cell stress conditions, focusing however only on some transcripts. In particular, we have chosen to monitor the 5.8S rRNA and its precursor, being the central transcript and the one present in smaller quantities and therefore less subject to normalization problems. We then decided to focus on the two transcription factors ubtf and baz2A which should exert opposite regulatory roles in promoting and limiting the transcription of rRNAs, respectively.

RT-qPCR analysis of serum depleted cells revealed decreased synthesis rate of mature 5.8s and its precursor transcript, concordantly with the reduced mean NORs size (Figure 4.5.8). In the same direction of reduction of the rRNA synthesis, we observed a decrease, albeit not significant, of the expression of ubtf and an increase of baz2a.

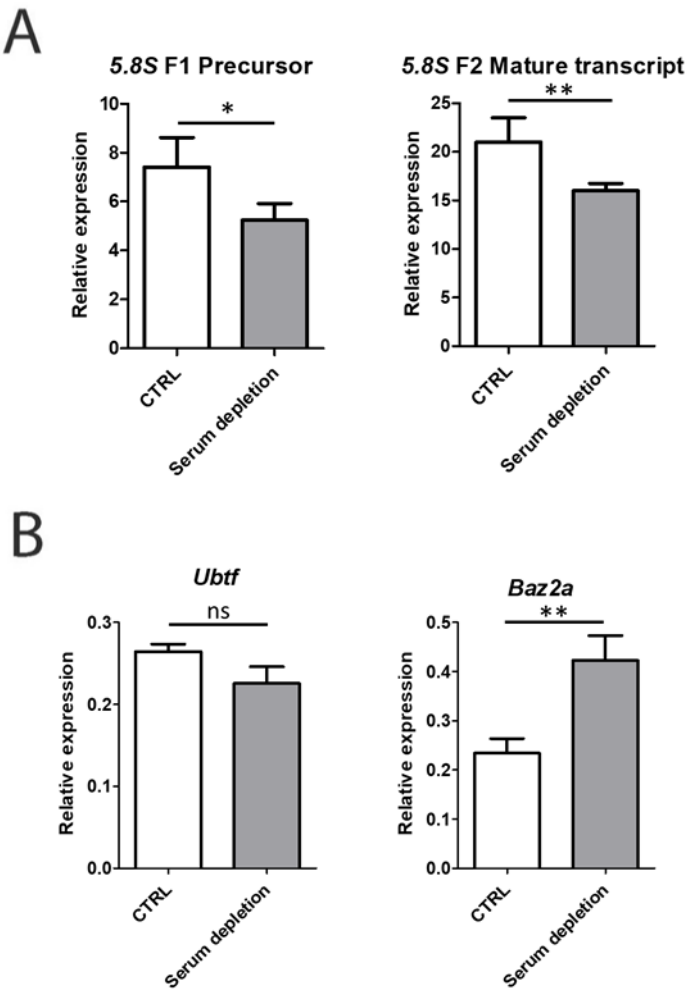

Figure 4.5.8: RT-qPCR analysis to quantify the expression of 5.8S precursor and mature transcripts (A) and the transcription factors ubtf and baz2a (B). In the histograms are plotted the mean ± SD of the relative gene expression. Statistical significance was evaluated using two-tailed unpaired Student's t-test.

For Dexamethasone treated hepatocytes we measured a decrease in the amount of the 5.8S precursor, which however did not turn out into a significant reduction of the mature 5.8S transcript compared to the control. Accordingly, the expression of ubtf also decreases, while we detected a slight but not significant increase of baz2a (Figure 4.5.9). These results suggest induction of nucleolar activity to slow down by Dexamethasone. Not having observed a consistent reduction in the mature 5.8S transcript may be because the cells were analyzed immediately after the 2h of treatment, so just after the possible

induction of rRNA transcription slowing down and therefore probably more time is needed before measuring a decrease in the final product of the process.

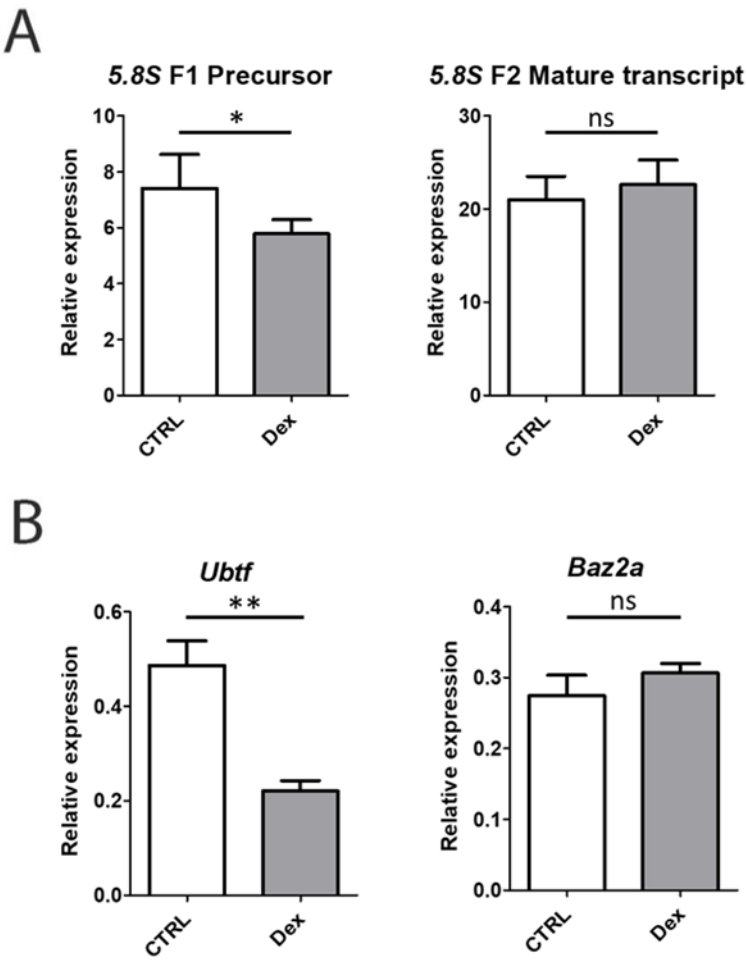

Figure 4.5.9: RT-qPCR analysis to quantify the expression of 5.8S precursor and mature transcripts (A) and the transcription factors ubtf and baz2a (B). In the histograms are plotted the mean ± SD of the relative gene expression. Statistical significance was evaluated using two-tailed unpaired Student's t-test.

The results emerged from the real-time analyses that compare senescent to control cells offers only a few suggestions. Morphological analysis at optical and electron microscopy showed extremely enlarged nucleoli with numerous fibrillar centers. In agreement we can note an evident increase in mature 5.8S

transcript and in the transcription factor ubtf. However, the precursor was not significantly increased compared to the control. Furthermore, we also observe an increase of baz2a expression (Figure 4.5.10).

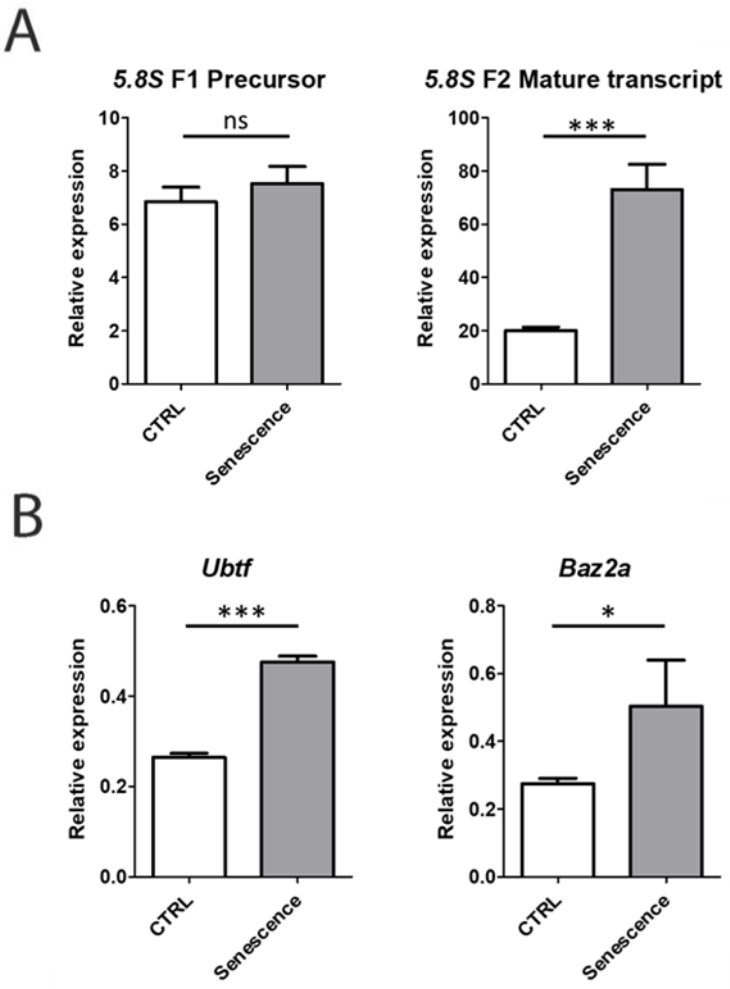

Figure 5.5.10: RT-qPCR analysis to quantify the expression of 5.8S mature and precursor transcripts (A) and the transcription factors ubtf and baz2a (B). In the histograms are plotted the mean ± SD of the relative gene expression. Statistical significance was evaluated using two-tailed unpaired Student's t-test.

We could hypothesize the increase in the 5.8S transcript is due to an accumulation of this transcript because of dysregulations and misfunctioning at some points of the ribogenesis process in senescent cells. We also observe both an increase in ubtf and baz2a. The interpretations could be

many. The great increase in cell size itself would suggest the need for higher protein synthesis. Following the measured increase in the amount of mature 5.8S rRNA, some micrographs obtained at electron microscopy showed large portions of the nucleoplasm occupied by granules that are probably ribosomal subunits, as particularly evident in Figure 4.5.11 E on the right. Additionally, in accordance with the large increase in heterochromatin observed, we could expect the observed increase in baz2a expression. However, as indicated in the introduction to this section, the morphological and qPCR analyses were intended to obtain some general information on the state of activity of the nucleolus. Since the nucleolus is the seat of many fundamental molecular processes, to draw more specific conclusions it would be necessary to adopt different approaches that go beyond the general purpose of this study.

To conclude, we show below representative images of hepatocyte nuclei in their entirety for each different cell stress condition analyzed, visualized at TEM, staining the sections by EDTA regressive technique, to better show the morphological changes in the organization of the nucleoplasm in the different conditions. In particular, senescent cells, which should mimic precocious ageing reveal a conspicuous extension of the heterochromatin domains and a strong increase in the size of the nucleoli, with the presence of numerous fibrillar centers. Evident morphological changes already highlighted in the previous sections can also be seen in the nucleus of the hepatocytes treated with mercury chloride. Note the strong reduction of the areas bleached by EDTA and the increase in the size of the nucleoli which reminds the nucleoli of senescent cells. Although in this case, we do not observe an increase in the nuclear and cell size. The morphological changes induced by serum depletion and Dexamethasone treatment are instead much less evident, maybe because these types of stress could be considered less extreme.

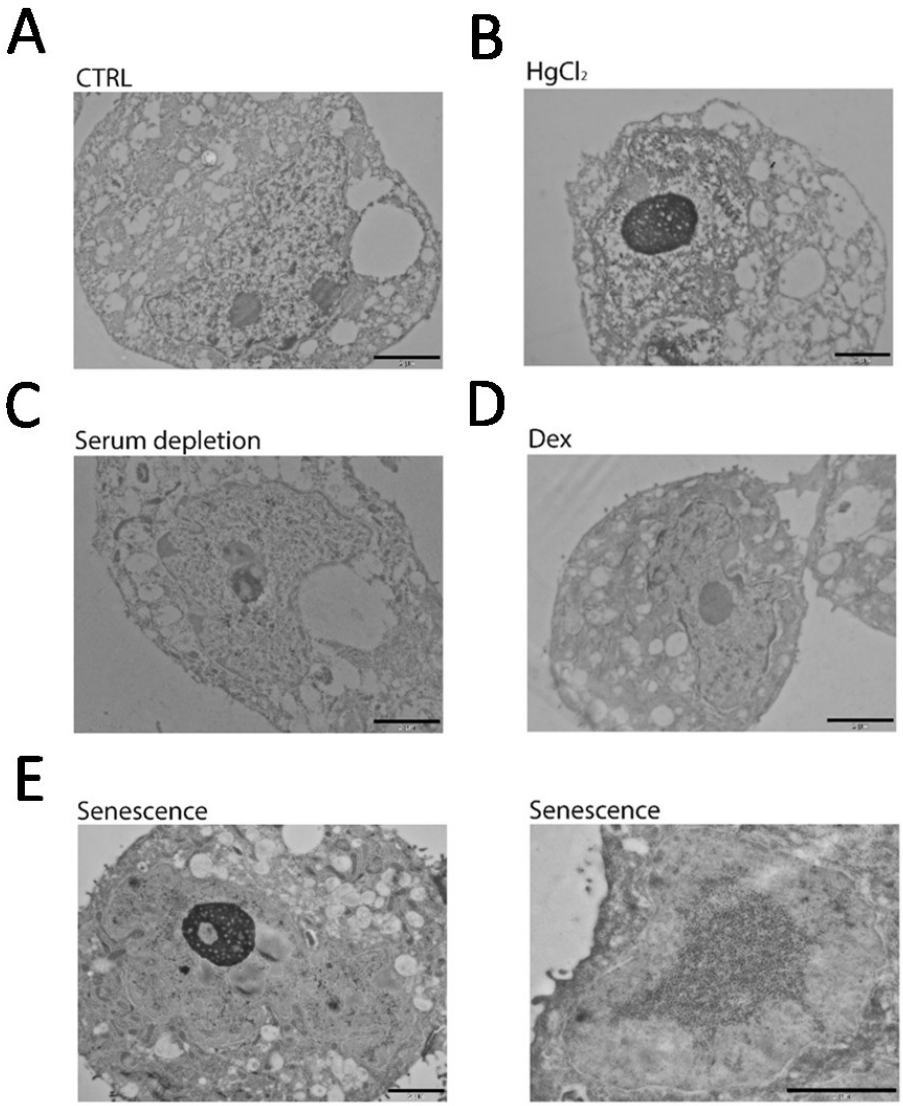

Figure 4.5.11:Sections of AML12 mouse hepatocytes at TEM stained by EDTA regressive technique. Control (A); $HgCl_2$ 10µm treated hepatocyte (B); Serum depleted hepatocyte (C); Dexamethasone treated hepatocyte (D); senescent hepatocyte (E). Bar: 2µm.

To conclude, the tables shown below summarize the average trends of change observed in the various conditions analyzed.

Liver tissue samples		Heterochromatin amount	Heterochromatin density	Histone H3K27me3	Histone H4K20me3	Histone H3K9me3
YOUNG vs :						
	OLD	=	=	↓	↓	↑
	$HgCl_2$	↓	=	↓	↓	=

Table 4.1: Summary table of the observed changes in heterochromatin domains comparing liver tissue from young mice (3 months) with samples from old mice (24 months) and liver tissue samples exposed to 10µM $HgCl_2$.

Cell culture hepatocytes		Heterochr. amount	Heterochr. density	Histone H3K27me3	Histone H4K20me3	Histone H3K9me3
CTRL vs:						
	$HgCl_2$	↓	↓	↓	↓	↓
	Serum depletion	↑	=	=	=	=
	Dexamethasone	↓	=	↓	↓	=
	Senescence	↑		=	↑	↓

Table 4.2: Summary table of the changes observed in heterochromatin domains comparing AML12 mouse hepatocytes grown according to manufacturer instructions (CTRL) and cultured AML12 mouse hepatocytes subjected to the different conditions of cell stress.

Cell culture hepatocytes		AgNOR size	rRNA synthesis
CTRL vs:			
	$HgCl_2$	↑	↑
	Serum depletion	↓	↓
	Dexamethasone	↓	↓
	Senescence	↑	↑

Table 4.3: Summary table of the observed changes in the nucleolar activity comparing AML12 mouse hepatocytes grown according to manufacturer instructions (CTRL) and AML12 cultured mouse hepatocytes subjected to the different conditions of cell stress.

5. DISCUSSION

One of the main goals of this study was to analyze the changes in the heterochromatin organization and epigenetics in hepatocytes nuclei under different cell stress conditions.

First of all, we evaluated if there were any differences between the heterochromatin domains mainly recognized and evident in interphase eukaryotic cell nucleus: the NADs and the LADs. These domains are sometimes overlapping and both are characterized by epigenetic features associated to a low level of transcription and late replicating loci (Kind et al., 2013; Ragoczy et al., 2014). However, some studies found specific genomic sequences preferentially associated to NADs and distinct from LADs (Quinodoz et al., 2018, Vertii et al. 2019). Our immunocytochemical analysis at TEM revealed that NADs are enriched in H3K9me3 and H4K20me3 compared to LADs, and provides the imaging confirmation of some evidence obtained in other studies. In accord with this latter, H3K9me3 and H4K20me3, mainly established by the NoRC complex, were shown to play an important role in silencing the fraction of inactive rDNA genes and the minor and major satellite DNA repeats, that are sequences constituting NADs (Guetg et al. 2010; Santoro et al., 2002; Zhou et al., 2002). These HPTMs are associated to constitutive heterochromatin, confirming the role of the nucleolus as an attractive hub to organize portions of the genome that should be permanently silenced (O'Sullivan et al., 2013). Accordingly, our data suggested that NADs adopt more condensed heterochromatin organization than LADs, likely occurring thanks to the enrichment in H3K9me3 and H4K20me3.

As discussed in the introduction, by Hi-C analysis it was demonstrated that NADs play important role in genome organization. Dillinger and colleagues demonstrated that interphase NADs topological organization is maintained for the most part upon senescence, with only few changes, concerning mainly the large centromeric and pericentromeric satellite repeat clusters. These clusters were found to dissociate from nucleoli in senescent cells and accordingly, H3K9me3-marked heterochromatin decreased in NADs (Dillinger et al., 2017). We utilized microscopy approaches to see what ageing entails in the organization of heterochromatin in mouse hepatocytes. Hoechst and osmium ammine staining did not reveal major changes in heterochromatin organization between the young and old mouse liver nuclei. Immunocytochemistry at TEM instead reveals only small, but significant variations of the quantity of some epigenetics markers associated to the heterochromatin formation. Specifically, a decrease of H3K27me3 and H4K20me3, particularly evident in female mice for the latter. Contrary to what was detected in the senescence cell model in the study by Dillinger et al. we

noticed a certain increase of H3K9me3 in NADs and LADs of the old mice. Of course, it must be taken into account that discrepancies between the data presented in this study compared to those of other studies can be due to the use of different cell types in different conditions. Generally, a gradual loss of heterochromatin was proposed as a major factor in generating alterations in gene expression during ageing (Villeponteau, 1997; Feser et al., 2010), but It was also reported a progressive “heterochromatinization” and an age-related DNA hypermethylation of specific DNA region (Lezhava 1984; Lezhava et al. 2012; Liu et al. 2013). Therefore, likely locus and cell-type dynamics are critical in influencing heterochromatin organization during ageing (Morris et al., 2019). However, the few changes we observed in the heterochromatin of hepatocytes from old mice were quite surprising and prompted us to evaluate whether different stimuli which may contribute to ageing, would cause evident variations or maybe the appearance of some aged associated nuclear features.

We found that $HgCl_2$ toxic effects determine a decrease in the amount and the density of heterochromatin and, concordantly, immunocytochemistry at TEM revealed a significant reduction in the epigenetic heterochromatin markers. An important contribution to reach the $HgCl_2$ induced heterochromatin changing probably derives from the significant decrease detected in H3K27me3, H4K20me3 and H3K9me3. More in detail, H3K9me3 decrease was less than those of the other two markers; but we exposed hepatocytes to the toxicant for only one hour. In such a short time probably extensive changes in heterochromatin markers assumed to constitute the core of tightly close heterochromatin domains, such as H3K9m3, are difficult to imagine. However, the toxic effects of mercury on the nucleus seem to be so powerful to induce an important decrease of H4K20me3, also associated to constitutive heterochromatin. These results, in general, suggested that even very short exposure to $HgCl_2$ is able to deeply modify nuclear architecture and gene activity.

We then analyzed the effects of calorie restriction, a condition known to slow down the effects of ageing (Weindruch and Sohal, 1997; Fontana and Klein, 2007; Longo et al., 2021). Our analyses, in this case, did not reveal marked changes in cells subjected to calorie restriction by serum depletion for 5 days: we measured an extension of the heterochromatin areas, but the analysis with osmium ammine did not reveal a significant increase in the degree of condensation and in agreement the immunocytochemistry revealed comparable quantity of histone markers associated with gene repression per heterochromatin area between control and serum depleted cells. The reduction of calorie intake would imply a decrease in cell metabolism to adapt to the new availability of nutrients (Vettor et al., 2020). Cells subjected to

caloric restriction are expected to proliferate slower (Hsieh et al.2005). It is possible that 5 days of calorie restriction were too short a period to observe major changes in these nuclear features. Alternatively, we could hypothesize that cell metabolism slows down, but, at the same time, in the first days of serum depletion, hepatocytes need to activate mechanisms to cope with this stressful condition. Therefore, we see a sort of balance between the activation of genes necessary to trigger specific molecular processes, for example, autophagy (Bagherniya et al., 2018; Peeters et al., 2019, Chung and Chung, 2019), and the decrease of metabolic rate reached through the inhibition of other categories of genes. Wang and colleagues reported that in Hela cells even only 36h of serum depletion are sufficient to induce chromatin condensation, measured using Binding Activatable Localization Microscopy (BALM), as an increase in the chromatin fibers diameter of about 70 nm. Moreover, they detected, by chromatin spreading visualized by STORM, a decrease in the number of RNA Pol II proteins on the chromatin fibers in serum-depleted cells (Wang et al., 2014). An increase of H4K20me3 was also reported in C127 mouse mammary tumor cells subjected to serum depletion for 36-48h, even though with some variability from cell to cell (Kourmouli et al., 2004). However, an increase of epigenetic markers associated heterochromatin decondensation were also reported, under serum depletion, at specific set of genes, like those coding for protein involved in autophagy process. (Peeters et al., 2019).

Finally, we analysed the effects of the anti-inflammatory drug Dexamethasone. 1 μM Dexamethasone, ten-fold more than the recommended concentration, induced a reduction of the heterochromatin areas and a substantial decrease of all histone modifications associated to gene repression considered in this study. This change was not so evident at morphological level as that induced by mercury chloride, maybe because it was not clearly accompanied by a decrease of heterochromatin condensation, as revealed by osmium ammine staining.

We also carried out experiments to investigate nucleolar activity under the different stressful conditions. In fact, the study of the organization of heterochromatin domains can give a general idea of gene activity at the transcriptional level, while analyzing nucleolar activity provides information on the next step: the biogenesis of ribosomes, which are necessary for the translation of mRNAs into proteins. Additionally, given this essential role, the nucleolus also influence other fundamental cellular processes as reported in the introduction, so it seemed to us an important feature to consider in the study of nuclear changes induced by ageing.

Silver staining showed a strong increase in the size of the NORs of senescence-induced hepatocytes. This experiment revealed a change in the same direction in hepatocytes exposed to mercury chloride, while those subjected to serum depletion or treated with 1μM Dexamethasone showed a reduced NOR size compared to the control. These results are in agreement with the transcription rate of rRNA detected by RT-qPCR which demonstrated an increasing trend for hepatocytes exposed to mercury chloride and a decrease for cells subjected to serum depletion and treatment with Dexamethasone. The changes in the expression of proteins involved in ribogenesis analyzed were also consistent with these trends.

To summarize, the study of the effect of ageing in liver tissue on mouse model in a controlled environment did not highlight major changes in the heterochromatin organization and more generally in the nuclear architecture, judging from the numerous images of nuclei obtained at different levels of resolution.

The cell model that should mimic ageing, the senescent AML12 hepatocytes, (see Singh et al., 2020 and chapter 3 Material and Methods for protocol) obtained through exposure to repeated oxidative stress, showed instead strong morphological changes of the nucleus compared to the control hepatocytes. Senescent cells, as it generally happens, have larger dimensions and, consequently, the nuclei were also enlarged. Heterochromatin domains increased their extension and in many cases occupies the largest part of the nucleoplasm. The nucleoli were very large with many fibrillar centers, it was also possible to notice several portions of the nucleoplasm full of granules that look like ribosomes. Probably such a great discrepancy between the two models: hepatocytes of elderly mice and hepatocytes induced to senescence, is due to the fact that, as previously mentioned, the laboratory mouse models, grown in a cage, are devoid of the stimuli that in wild type living conditions have an important effect on ageing. On the contrary, this mimicked ageing in senescent cells is reached in a short time, by repeatedly subjecting the cells to intense damage. In fact, if in the first case the exposure to injuries may be strongly underestimated, while in the second case, is higher and more frequent than what we might expect in normal wild life. Therefore, laboratory mouse models may represent a good model for individuals who have preserved well their state of health. Conversely, the senescent cell model may better show the effects of “unhealthy” ageing to which harmful agents have contributed.

Concerning the effects of the cell stress analyzed, the damage induced by mercury chloride seems to bring the cell to a state more similar to senescence as regards the morphology and activity of the nucleoli. However, unlike

senescent cells, those exposed to mercury chloride show extensive heterochromatin decondensation. A possible interpretation of this divergence is that hepatocytes treated with mercury chloride are subjected to higher toxic damage for a short time, while in senescent hepatocytes we observed the effect of repeated insults over time of less intensity. Mercury chloride induced changes increase the synthesis of the enzymes necessary to counteract the damages and try to reach new homeostasis. Different mechanisms may occur in senescent cells; maybe the gradual accumulation of damages could cause the cell to gradually shut down by compacting the chromatin and minimizing its activities that would be otherwise carry on in an inefficiently aberrant way.

Serum-depleted cells show a similar degree of chromatin condensation as the control cells grown in complete medium, although the total amount of heterochromatin resulted higher. This could make it appear that these cells undergo a change that brings them closer to senescent cells. However, the two conditions are notably different, because the increase in heterochromatin of serum depleted cells is clearly lower than that observed in senescent cells. Furthermore, the morphology of the nucleus and the organization of the heterochromatin domains still show a greater similarity to the control hepatocytes than to the senescent ones. It should also be noted that the nucleoli, on the other hand, have a reduced size and activity compared to the control and therefore the metabolic dynamics in the conditions of serum depletion and senescence must be different.

Finally, treatment with Dexamethasone seemed to induce changes that are different from other cell stress and in particular opposite to those observed in senescent cells, as chromatin decondensation, but at the same time a reduction in the activity and size of the nucleolus. Dexamethasone may provide some beneficial or protective effects on ageing process by preserving the hepatocytes in a condition that is more distant to the senescence. Clinically, high dose of Dexamethasone for short time seem to have no major side-effects, but unfortunately its long-term use as a possible strategy to reduce some ageing effects would not be applicable yet, due to the many undesirable consequences of today's Dexamethasone drug formulations, when assumed for long periods (Poetker and Reh, 2010).

To conclude, this study attempted to evaluate whether general trends of change could be identified regarding the quantity and the degree of condensation of heterochromatin and the size and the activity of the nucleolus during hepatocyte ageing or under specific stressful conditions.

Considered the nature and purpose of this approach, we conclude by saying that basically a trend can be identified as smaller and less active nucleoli slow down the ageing process. This is perfectly logical, being the nucleolus the site where ribosomes production occurs and thus being necessary for the synthesis of enzymes that catalyze cell metabolic reactions; any machine working more and more frequently wears out faster. Moreover, several studies also demonstrated that the size of the nucleoli is inversely related to the life span in different organisms and that, by inhibiting the activity of different nucleolar proteins, it is possible to extend the average life span of different animal models (Tiku and Antebi, 2018).

Conversely, it is more difficult to establish a general correlation between the organization of heterochromatin and ageing or the effects of cell stress. In this case, in fact, the subtle dynamics that come into play in the different conditions induce changes that seem to be hardly attributable to a single trend at the level of the total fraction of repressed chromatin and not of the specific gene locus. On the other hand, as discussed above, previous studies have also reported divergent conclusions on the variation of the heterochromatin features during ageing, which were strongly dependent on the specific context.

6. REFERENCES

1. Abarikwu SO, Njoku R-CC, Onuah CL. Aged coconut oil with a high peroxide value induces oxidative stress and tissue damage in mercury-treated rats. J Basic Clin Physiol Pharmacol. 2018;29:365–76.

2. Abdel Moneim A. The neuroprotective effect of berberine in mercury-induced neurotoxicity in rats. Metab Brain Dis. 2015;30:935-42.

3. Agarwal R, Goel SK, Chandra R, Behari JR. Role of vitamin E in preventing acute mercury toxicity in rat. Environ Toxicol Pharmacol. 2010;29:70–8.

4. Aleo MF, Morandini F, Bettoni F, Tanganelli S, Vezzola A, Giuliani R, Steimberg N, Boniotti J, Bertasi B, Losio N, Apostoli P, Mazzoleni G. In vitro study of the nephrotoxic mechanism of mercuric chloride. La Medicina del lavoro. 2002;93:267–78.

5. Allis C, Jenuwein T, Reinberg D, Hughes H: Epigentics. Cold Spring Harbor Laboratory Press. 2015;3:46-116.

6. Allshire RC, Madhani HD. Ten principles of heterochromatin formation and function. Nat Rev Mol Cell Biol. 2018;19:229–44.

7. Altunkaynak M, Akgül N, Yahyazadeh A, Altunkaynak B, Türkmen A, Akgül H, Aksak S, Ünal B. A stereological and histopathological study of the effects of exposure of male rat testes to mercury vapor. Biotechnic & Histochemistry. 2015;90:529–34.

8. Aparicio O, Geisberg JV, Struhl K. Chromatin Immunoprecipitation for Determining the Association of Proteins with Specific Genomic Sequences In Vivo. Current Protocols in Molecular Biology. 2004;65:21.3.1-21.3.23.

9. Arancio W, Pizzolanti G, Genovese SI, Pitrone M, Giordano C. Epigenetic involvement in Hutchinson-Gilford progeria syndrome: a mini-review. Gerontology. 2014;60:197–203.

10. Aumiller W, Keating C. Experimental models for dynamic compartmentalization of biomolecules in liquid organelles: Reversible formation and partitioning in aqueous biphasic systems. Advances in Colloid and Interface Science. 2016;239. 1.

11. Bagherniya M, Butler AE, Barreto GE, Sahebkar A. The effect of fasting or calorie restriction on autophagy induction: A review of the literature. Ageing Res Rev. 2018;47:183–97.

12. Bailly-Maitre B, de Sousa G, Boulukos K, Gugenheim J, Rahmani R. Dexamethasone inhibits spontaneous apoptosis in primary cultures of human and rat hepatocytes via Bcl-2 and Bcl-xL induction. Cell Death Differ. 2001;8:279–88.

13. Bajwa P, Nagendra PB, Nielsen S, Sahoo SS, Bielanowicz A, Lombard JM, Wilkinson JE, Miller RA, Tanwar PS. Age related increase in mTOR activity contributes to the pathological changes in ovarian surface epithelium. Oncotarget. 2016;7:19214–27.

14. Baker DJ, Wijshake T, Tchkonia T, LeBrasseur NK, Childs BG, van de Sluis B, et al. Clearance of p16Ink4a-positive senescent cells delays ageing-associated disorders. Nature. 2011;479:232–6.

15. Banani SF, Lee HO, Hyman AA, Rosen MK. Biomolecular condensates: organizers of cellular biochemistry. Nat Rev Mol Cell Biol. 2017;18:285–98. 1.

16. Becker JS, Nicetto D, Zaret KS. H3K9me3-Dependent Heterochromatin: Barrier to Cell Fate Changes. Trends in Genetics. 2016;32:29–41.

17. Belton J-M, McCord RP, Gibcus JH, Naumova N, Zhan Y, Dekker J. Hi-C: a comprehensive technique to capture the conformation of genomes. Methods. 2012;58:268–76.

18. Bemiller PM, Lee L-H. Nucleolar changes in senescing WI-38 cells. Mechanisms of Ageing and Development. 1978;8:417–27.

19. Bernhard W. A new staining procedure for electron microscopical cytology. Journal of Ultrastructure Research. 1969;27:250–65.

20. Bernstein BE, Mikkelsen TS, Xie X, Kamal M, Huebert DJ, Cuff J, Fry B, Meissner A, Wernig M, Plath K, Jaenisch R, Wagschal A, Feil R, Schreiber SL, Landeret ES. A bivalent chromatin structure marks key developmental genes in embryonic stem cells. Cell. 2006;125:315–26.

21. Berry J, Weber SC, Vaidya N, Haataja M, Brangwynne CP. RNA transcription modulates phase transition-driven nuclear body assembly. PNAS. 2015;112:E5237–45.

22. Biesterfeld S, Beckers S, Cadenas M, Schramm M. Feulgen Staining Remains the Gold Standard for Precise DNA Image Cytometry. Anticancer research. 2011;31:53–8.

23. Biggiogera M, Courtens J-L, Derenzini M, Fakan S, Hernandez-Verdun D, Risueno M-C, Soyer-Gobillard MO. Osmium ammine: Review of current applications to visualize DNA in electron microscopy. Biology of the Cell. 1996;87:121–32.

24. Biggiogera M, Malatesta M, Abolhassani-Dadras S, Amalric F, Rothblum LI, Fakan S. Revealing the unseen: the organizer region of the nucleolus. J Cell Sci. 2001;114 Pt 17:3199–205.

25. Blackburn EH, Epel ES, Lin J. Human telomere biology: A contributory and interactive factor in aging, disease risks, and protection. Science. 2015;350:1193–8.

26. Bloom SL, Sheffield JS, McIntire DD, Leveno KJ. Antenatal dexamethasone and decreased birth weight. Obstetrics & Gynecology. 2001;97:485–90.

27. Bloomfield VA/ C. Nucleic Acids: Structures, Properties, and Functions. U.s.a.: Univ Science Books; 2000.

28. Boisvert MM, Erikson GA, Shokhirev MN, Allen NJ. The Aging Astrocyte Transcriptome from Multiple Regions of the Mouse Brain. Cell Rep. 2018;22:269–85.

29. Boyle AP, Davis S, Shulha HP, Meltzer P, Margulies EH, Weng Z, Furey TS, Crawford GE. High-resolution mapping and characterization of open chromatin across the genome. Cell. 2008;132:311–22.

30. Bromberg KD, Mitchell TRH, Upadhyay AK, Jakob CG, Jhala MA, Comess KM, Lasko LM, Li C, Tuzon CT, Dai Y, Li F, Eram MS, Nuber A, Soni NB, Manaves V,Algire MA, Sweis RF, Torrent M,Schotta G, Sun C, Mixhaelides MR, Shoemaker AR, Arrowsmith CH,Brown PJ, Santhakumar V, Martun A, Ricd JC,Chiang GG, Vedadi M, Barsyte-Lovejoy D, Pappano WN. The SUV4-20 inhibitor A-196 verifies a role for epigenetics in genomic integrity. Nat Chem Biol. 2017;13:317–24.

31. Brownlee M. Advanced protein glycosylation in diabetes and aging. Annu Rev Med. 1995;46:223–34.

32. Brunet A, Berger SL. Epigenetics of aging and aging-related disease. J Gerontol A Biol Sci Med Sci. 2014;69 Suppl 1:S17-20.

33. Buenrostro JD, Wu B, Chang HY, Greenleaf WJ. ATAC-seq: A Method for Assaying Chromatin Accessibility Genome-Wide. Curr Protoc Mol Biol. 2015;109:21.29.1-21.29.9.

34. Bukhari H, Müller T. Endogenous Fluorescence Tagging by CRISPR. Trends Cell Biol. 2019;29:912–28.

35. Bulut-Karslioglu A, De La Rosa-Velázquez IA, Ramirez F, Barenboim M, Onishi-Seebacher M, Arand J, GaláN C,Winter GE, Engist B, Roderick BG, O'Sullivan J, Martens JHA, Walter J, Manke M, Lachner M, Jenuwein T. Suv39h-Dependent H3K9me3 Marks Intact Retrotransposons and Silences LINE Elements in Mouse Embryonic Stem Cells. Molecular Cell. 2014;55:277–90. 1.

36. Burd CE, Sorrentino JA, Clark KS, Darr DB, Krishnamurthy J, Deal AM, et al. Monitoring Tumorigenesis and Senescence In Vivo with a p16INK4a-Luciferase Model. Cell. 2013;152:340–51.

37. Caburet S, Conti C, Schurra C, Lebofsky R, Edelstein SJ, Bensimon A. Human ribosomal RNA gene arrays display a broad range of palindromic structures. Genome Res. 2005;15:1079–1085.

38. Cain DW, Cidlowski JA. Immune regulation by glucocorticoids. Nat Rev Immunol. 2017;17:233–47.

39. Campisi J, Andersen JK, Kapahi P, Melov S. Cellular senescence: A link between cancer and age-related degenerative disease? Seminars in Cancer Biology. 2011;21:354–9.

40. Cao R, Wang L, Wang H, Xia L, Erdjument-Bromage H, Tempst P, Jones RS, Zhang Y. Role of Histone H3 Lysine 27 Methylation in Polycomb-Group Silencing. Science. 2002;298:1039–1043.

41. Cavalli G, Misteli T. Functional implications of genome topology. Nat Struct Mol Biol. 2013;20:290–9.

42. Chen S, Blank MF, Iyer A, Huang B, Wang L, Grummt I, Voit R. SIRT7-dependent deacetylation of the U3-55k protein controls pre-rRNA processing. Nature Communications. 2016;7.

43. Chen S, Luperchio TR, Wong X, Doan EB, Byrd AT, Choudhury KR, et al. A Lamina-Associated Domain Border Governs Nuclear Lamina Interactions, Transcription, and Recombination of the Tcrb Locus. Cell reports. 2018;25:1729-1740.e6.

44. Chojnowski A, Ong PF, Foo MXR, Liebl D, Hor L-P, Stewart CL, et al. Heterochromatin loss as a determinant of progerin-induced DNA damage in Hutchinson-Gilford Progeria. Aging Cell. 2020;19:e13108.

45. Chung KW, Chung HY. The Effects of Calorie Restriction on Autophagy: Role on Aging Intervention. Nutrients. 2019;11:2923.

46. Clark SJ, Harrison J, Paul CL, Frommer M. High sensitivity mapping of methylated cytosines. Nucleic Acids Res. 1994;22:2990–7.

47. Colombo E, Marine J-C, Danovi D, Falini B, Pelicci PG. Nucleophosmin regulates the stability and transcriptional activity of p53. Nat Cell Biol. 2002;4:529–33.

48. Conconi A, Widmer RM, Koller T, Sogo JM. Two different chromatin structures coexist in ribosomal RNA genes throughout the cell cycle. Cell. 1989;57:753–761.

49. Coppedè F. Mutations Involved in Premature-Ageing Syndromes. TACG. 2021;14:279–95.

50. Corpas E, Harman SM, Blackman MR. Human growth hormone and human aging. Endocr Rev. 1993;14:20–39.

51. Corral-Debrinski M, Horton T, Lott MT, Shoffner JM, Beal MF, Wallace DC. Mitochondrial DNA deletions in human brain: regional variability and increase with advanced age. Nat Genet. 1992;2:324–9.

52. Cremer T, Cremer C. Chromosome territories, nuclear architecture and gene regulation in mammalian cells. Nat Rev Genet. 2001;2:292–301.

53. Crimmins E, Vasunilashorn S, Kim JK, Alley D. Biomarkers related to aging in human populations. Adv Clin Chem. 2008;46:161–216.

54. Denker A, de Laat W. The second decade of 3C technologies: detailed insights into nuclear organization. Genes Dev. 2016;30:1357–82.

55. Di Micco R, Fumagalli M, Cicalese A, Piccinin S, Gasparini P, Luise C, Schurra C, Garre' M, Nuciforo PG, Bensimon A, Maestro R, Pelicci PG, d'Adda di Fagagna F. Oncogene-induced senescence is a DNA damage response triggered by DNA hyper-replication. Nature. 2006;444:638–42.

56. Dieterlen M-T, Bittner HB, Klein S, von Salisch S, Mittag A, Tárnok Dhein AS, Mohr FW, Barten MJ. Assay validation of phosphorylated S6 ribosomal protein for a pharmacodynamic monitoring of mTOR-inhibitors in peripheral human blood. Cytometry B Clin Cytom. 2012;82:151–7.

57. Dillinger S, Straub T, Németh A. Nucleolus association of chromosomal domains is largely maintained in cellular senescence despite massive nuclear reorganisation. PLoS One. 2017;12:e0178821.

58. Dixon J, Selvaraj S, Yue F, Kim A, Li Y, Shen Y, Hu M, Liu J, Ren B. Topological domains in mammalian genomes identified by analysis of chromatin interactions. Nature. 2012;485:376–80.

59. Drygin D, Lin A, Bliesath J, Ho CB, O'Brien SE, Proffitt C, Omori M, Haddach M, Schwaebe MK, Siddiqui-Jain A, Streiner N, Quin JE, Sanij E, Bywater MJ, Hannan RD, Ryckman D, Anderes K, Rice WG. Targeting RNA polymerase I with an oral small molecule CX-5461 inhibits ribosomal RNA synthesis and solid tumor growth. Cancer Res. 2011;71:1418–1430.

60. Dundr M, Olson MO. Partially processed pre-rRNA is preserved in association with processing components in nucleolus-derived foci during mitosis. Mol Biol Cell. 1998;9:2407–2422.

61. Dzau VJ, Inouye SK, Rowe JW, Finkelman E, Yamada T. Enabling Healthful Aging for All - The National Academy of Medicine Grand Challenge in Healthy Longevity. Engl J Med. 2019;381:1699-1701,

62. Eitan E, Hutchison ER, Mattson MP. Telomere shortening in neurological disorders: an abundance of unanswered questions. Trends Neurosci. 2014;37(5): 256–63,

63. Endoh M, Endo TA, Endoh T, Isono K, Sharif J, Ohara O, Toyoda T, Ito T, Eskeland R, Bickmore WA, Vidal M, Bernstein BE, Koseki H. Histone H2A Mono-Ubiquitination Is a Crucial Step to Mediate PRC1-Dependent Repression of Developmental Genes to Maintain ES Cell Identity. PLOS Genetics. 2012;8:e1002774.

64. Espada J, Esteller M. DNA methylation and the functional organization of the nuclear compartment. Seminars in Cell & Developmental Biology. 2010;21:238–46.

65. Farias N, Ho N, Butler S, Delaney L, Morrison J, Shahrzad S. The effects of folic acid on global DNA methylation and colonosphere formation in colon cancer cell lines. J. Nutr. Biochem. 2015;26:818–826.

66. Feil R, Fraga MF. Epigenetics and the environment: emerging patterns and implications. Nat. Rev. Genet. 2012;13:97–109.

67. Feng Z, Chen X, Wu X, Zhang M. Formation of biological condensates via phase separation: characteristics, analytical methods, and physiological implications. J Biol Chem. 2019;294: 14823–14835.

68. Feser J, Truong D, Das C, Carson JJ, Kieft J, Harkness T, Tyler JK. Elevated histone expression promotes life span extension. Mol Cell. 2010;39:724–35.

69. Fischle W, Wang Y, Jacobs SA, Kim Y, Allis CD, Khorasanizadeh S. Molecular basis for the discrimination of repressive methyl-lysine marks in histone H3 by Polycomb and HP1 chromodomains. Genes & Development. 2003;17:1870–1881.

70. Fong YW, Cattoglio C, Tjian R. The intertwined roles of transcription and repair proteins. Mol Cell. 2013;52:291–302. 1.

71. Fontana L, Klein S. Aging, adiposity, and calorie restriction. JAMA. 2007;297:986–94.

72. Fontana L, Partridge L, Longo VD. Dietary Restriction, Growth Factors and Aging: from yeast to humans. Science. 2010;328:321–6.

73. Fromont-Racine M, Senger B, Saveanu C, Fasiolo F. Ribosome assembly in eukaryotes. Gene. 2003;313:17–42.

74. Fu Y, Jia G, Pang X, Wang RN, Wang X, Li CJ, SmemoS, Dai Q, Bayley KA, Nobrega MA, Han KL, Cui Q, He C. FTO-mediated formation of N6-hydroxymethyladenosine and N6-formyladenosine in mammalian RNA. Nat Commun. 2013;4:1798.

75. García-Prat L, Martínez-Vicente M, Perdiguero E, Ortet L, Rodríguez-Ubreva J, Rebollo E, Ruiz-Bonilla V, Gutarra S, Ballestar E, Serrano AL, Sandri M, Muñoz-Cánoves P. Autophagy maintains stemness by preventing senescence. Nature. 2016;529:37–42.

76. Ghosh S, Liu B, Wang Y, Hao Q, Zhou Z. Lamin A Is an Endogenous SIRT6 Activator and Promotes SIRT6-Mediated DNA Repair. Cell Reports. 2015;13:1396–406.

77. Gibbons JG, Branco AT, Godinho SA, Yu S, Lemos B. Concerted copy number variation balances ribosomal DNA dosage in human and mouse genomes. Proc Natl Acad Sci USA. 2015;112:2485–2490.

78. Gibbons JG, Branco AT, Yu S, Lemos B. Ribosomal DNA copy number is coupled with gene expression variation and mitochondrial abundance in humans. Nat Commun. 2014;5:4850.

79. Gibson BA, Doolittle LK, Schneider MWG, Jensen LE, Gamarra N, Henry L, Gerlich, D.W., Redding, S., and Rosen, M.K. Organization of Chromatin by Intrinsic and Regulated Phase Separation. Cell. 2019;179:470-484.e21.

80. Giresi PG, Kim J, McDaniell RM, Iyer VR, Lieb JD. FAIRE (Formaldehyde-Assisted Isolation of Regulatory Elements) isolates active regulatory elements from human chromatin. Genome Res. 2007;17:877–85.

81. Gong H, Sun L, Chen B, Han Y, Pang J, Wu W, Qi R, Zhang TM. Evaluation of candidate reference genes for RT-qPCR studies in three metabolism related tissues of mice after caloric restriction. Sci Rep. 2016;6:38513.

82. Goodfellow SJ, Zomerdijk JCBM. Basic mechanisms in RNA polymerase I transcription of the ribosomal RNA genes. Subcell Biochem. 2013;61:211–36.

83. Gorisse L, Pietrement C, Vuiblet V, Schmelzer CE, Köhler M, Duca L, Debelle L, Fornès P, Jaisson S, Gillery P. Protein carbamylation is a hallmark of aging. Proc Natl Acad Sci U S A. 2016;113(5):1191–6.

84. Gruenbaum Y, Margalit A, Goldman RD, Shumaker DK, Wilson KL. The nuclear lamina comes of age. Nat Rev Mol Cell Biol. 2005;6:21–31.

85. Guelen L, Pagie L, Brasset E, Meuleman W, Faza MB, Talhout W, et al. Domain organization of human chromosomes revealed by mapping of nuclear lamina interactions. Nature. 2008;453:948–51.

86. Guetg C, Lienemann P, Sirri V, Grummt I, Hernandez-Verdun D, Hottiger MO, Fussenegger M, Santoro R. The NoRC complex mediates the heterochromatin formation and stability of silent rRNA genes and centromeric repeats. The EMBO Journal. 2010;29:2135–46.

87. Guetg C, Santoro R. Formation of nuclear heterochromatin: the nucleolar point of view. Epigenetics. 2012;7:811–4.

88. Haaf T, Hayman DL, Schmid M. Quantitative determination of rDNA transcription units in vertebrate cells. Exp Cell Res. 1991;193:78–86.

89. Hammadah M, Al Mheid I, Wilmot K, Ramadan R, Abdelhadi N, Alkhoder A, Obideen M, Pimple PM, O Levantsevych O, Kelli HM, Shah A, Sun YV, Pearce B, Kutner M, Long Q, Ward L, Ko Y, Mohammed KH, Lin J, Zhao J, Bremner JD, Kim J, Waller EK, Raggi P, Sheps D,

Quyyumi AA, Vaccarino V. Telomere Shortening, Regenerative Capacity, and Cardiovascular Outcomes. Circ Res. 2017;120:1130–8.

90. Hancock R. A role for macromolecular crowding effects in the assembly and function of compartments in the nucleus. Journal of Structural Biology. 2004;146:281–90.

91. Hansen M, Taubert S, Crawford D, Libina N, Lee S-J, Kenyon C. Lifespan extension by conditions that inhibit translation in Caenorhabditis elegans. Aging Cell. 2007;6:95–110.

92. Hanssen NM, Wouters K, Huijberts MS, Gijbels MJ, Sluimer JC, Scheijen JLJM, Heeneman S, Biessen EAL, Daemen MJAP, Brownlee M, de Kleijn DP, Stehouwer CDA, Pasterkamp G, Schalkwijk CG. Higher levels of advanced glycation endproducts in human carotid atherosclerotic plaques are associated with a rupture-prone phenotype. Eur Heart J. 2014;35(17): 1137–46.

93. Hardie DC, Gregory TR, Hebert PDN. From Pixels to Picograms: A Beginners' Guide to Genome Quantification by Feulgen Image Analysis Densitometry. J Histochem Cytochem. 2002;50:735–49.

94. Henderson AS, Warburton D, Atwood KC. Locatoin of ribosomal DNA in the human chromosome complement. Proc Natl Acad Sci USA. 1972;69:3394–3398.

95. Henras AK, Plisson-Chastang C, O'Donohue M-F, Chakraborty A, Gleizes P-E. An overview of pre-ribosomal RNA processing in eukaryotes. Wiley Interdiscip Rev RNA. 2015;6:225–42.

96. Henras AK, Soudet J, Gérus M, Lebaron S, Caizergues-Ferrer M, Mougin A, et al. The post-transcriptional steps of eukaryotic ribosome biogenesis. Cell Mol Life Sci. 2008;65:2334–59.

97. Hernandez-Segura A, Nehme J, Demaria M. Hallmarks of Cellular Senescence. Trends Cell Biol. 2018;28:436–53.

98. Hipp MS, Kasturi P, Hartl FU. The proteostasis network and its decline in ageing. Nat Rev Mol Cell Biol. 2019;20:421–35.

99. Horby P, Lim WS, Emberson JR, Mafham M, Bell JL, Linsell L, Staplin N, Brightling C, Ustianowski A, Elmahi E, Prudon B, Green C, Felton T, Chadwick D, Rege K, Fegan C, Chappell LC, Faust SN, Jaki T, Jeffery K, Montgomery A, Rowan K, Juszczak E, Baillie JK, Haynes R, Landray MJ. Dexamethasone in Hospitalized Patients with Covid-19. N Engl J Med. 2021;384:693–704.

100. Hsieh EA, Chai CM, Hellerstein MK. Effects of caloric restriction on cell proliferation in several tissues in mice: role of intermittent feeding. Am J Physiol Endocrinol Metab. 2005;288:E965-972.

101. Hyman AA, Weber CA, Jülicher F. Liquid-Liquid Phase Separation in Biology. Annu Rev Cell Dev Biol. 2014;30:39–58.

102. Jacka CV, Cruza C, Hulla RM, Kellerb MA, Ralserb M, Houseleya J. Regulation of ribosomal DNA amplification by the TOR pathway. PNAS. 2015;31: 9674–9679.

103. Jakočiūnas T, Jordö MD, Mebarek MA, Bünner CM, Verhein-Hansen J, Oddershede LB, Ton G. Subnuclear relocalization and silencing of a chromosomal region by an ectopic ribosomal DNA repeat. PNAS. 2013;110:E4465–73.

104. Jessurun CAC, Hulsbergen AFC, Cho LD, Aglio LS, Nandoe Tewarie RDS, Broekman MLD. Evidence-based dexamethasone dosing in malignant brain tumors: what do we really know? J Neurooncol. 2019;144:249–64.

105. Jiang H, Wang S, Huang Y, He X, Cui H, Zhu X, Zheng Y. Phase Transition of Spindle-Associated Protein Regulate Spindle Apparatus Assembly. Cell. 2015;163:108–22.

106. Jobe AH, Milad MA, Peppard T, Jusko WJ. Pharmacokinetics and Pharmacodynamics of Intramuscular and Oral Betamethasone and Dexamethasone in Reproductive Age Women in India. Clin Transl Sci. 2020;13:391–9.

107. Johnson DS, Mortazavi A, Myers RM, Wold B. Genome-wide mapping of in vivo protein-DNA interactions. Science. 2007;316:1497–502.

108. Johnson SC, Rabinovitch PS, Kaeberlein M. mTOR is a key modulator of ageing and age-related disease. Nature. 2013;493:338–45.

109. Joshi D, Srivastav SK, Belemkar S, Dixit VA. Zingiber officinale and 6-gingerol alleviate liver and kidney dysfunctions and oxidative stress induced by mercuric chloride in male rats: A protective approach. Biomed Pharmacother. 2017;91:645–55.

110. Kapuscinski J. DAPI: a DNA-Specific Fluorescent Probe. Biotechnic & Histochemistry. 1995;70:220–33.

111. Kennedy BK, Berger SL, Brunet A, Campisi J, Cuervo AM, Epel ES, Franceschi C, Lithgow GJ, Morimoto RI, Pessin JE, Rando TA,

Richardson A, Schadt EE, Wyss-Coray T, Sierra F. Geroscience: linking aging to chronic disease. Cell. 2014;159:709–13.

112. Kim G-D. Co-operation and communication between the human maintenance and de novo DNA (cytosine-5) methyltransferases. The EMBO Journal. 2002;21:4183–95.

113. Kim KC, Friso S, Choi SW. DNA methylation, an epigenetic mechanism connecting folate to healthy embryonic development and aging. J Nutr Biochem 2009;20:917-26.

114. Kim Y-I, Bandyopadhyay J, Cho I, Lee J, Park DH, Cho JH. Nucleolar GTPase NOG-1 regulates development, fat storage, and longevity through insulin/IGF signaling in C. elegans. Mol Cells. 2014;37:51–7.

115. Kimura M, Moteki H, Ogihara M. Inhibitory effects of dexamethasone on hepatocyte growth factor-induced DNA synthesis and proliferation in primary cultures of adult rat hepatocytes. J Pharmacol Sci. 2011;115:390–8.

116. Kind J, Pagie L, Ortabozkoyun H, Boyle S, de Vries SS, Janssen H, Amendola M, Nolen LD, Bickmore WA, van Steensel B. Single-cell dynamics of genome-nuclear lamina interactions. Cell. 2013;153:178–92.

117. Klein DC, Hainer SJ. Genomic methods in profiling DNA accessibility and factor localization. Chromosome Res. 2020;28:69–85.

118. Klungland A, Robertson AB. Oxidized C5-methyl cytosine bases in DNA: 5-Hydroxymethylcytosine; 5-formylcytosine; and 5-carboxycytosine. Free Radic Biol Med. 2017;107:62–8.

119. Ko A, Han SY, Song J. Dynamics of ARF regulation that control senescence and cancer. BMB Reports. 2016;49:598–606.

120. Kobayashi T. A new role of the rDNA and nucleolus in the nucleus–rDNA instability maintains genome integrity. BioEssays. 2008;30:267–272.

121. Koh J, Enders GH, Dynlacht BD, Harlow E. Tumour-derived p16 alleles encoding proteins defective in cell-cycles inhibition. Nature. 1995;375:506-510.

122. Kooman JP, Stenvinkel P, Shiels PG. Fabry Disease: A New Model of Premature Ageing? Nephron. 2020;144:1–4.

123. Koonin EV, Makarova KS, Wolf YI. Evolutionary Genomics of Defense Systems in Archaea and Bacteria. Annu Rev Microbiol. 2017;71:233–61.

124. Kourmouli N, Jeppesen P, Mahadevhaiah S, Burgoyne P, Wu R, Gilbert DM, Bongiorni S, Prantera G, Fanti L, Pimpinelli S, Shi W, Fundele R, Singh PB. Heterochromatin and tri-methylated lysine 20 of histone H4 in animals. Journal of Cell Science. 2004;117:2491–501.

125. Kouzarides T. Chromatin modifications and their function. Cell. 2007;128:693–705.

126. Kressler D, Roser D, Pertschy B, Hurt E. The AAA ATPase Rix7 powers progression of ribosome biogenesis by stripping Nsa1 from pre-60S particles. Journal of Cell Biology. 2008;181:935–44.

127. Kuilman T, Michaloglou C, Mooi WJ, Peeper DS. The essence of senescence. Genes Dev. 2010;24:2463–79.

128. Kumar Rajendran N, George BP, Chandran R, Tynga IM, Houreld N, Abrahamse H. The Influence of Light on Reactive Oxygen Species and NF-κB in Disease Progression. Antioxidants (Basel). 2019;8:640.

129. Kumari R, Jat P. Mechanisms of Cellular Senescence: Cell Cycle Arrest and Senescence Associated Secretory Phenotype. Front Cell Dev Biol. 2021;9:645593.

130. Kuo T, McQueen A, Chen T-C, Wang J-C. Regulation of Glucose Homeostasis by Glucocorticoids. Adv Exp Med Biol. 2015;872:99–126.

131. Labrie SJ, Samson JE, Moineau S. Bacteriophage resistance mechanisms. Nat Rev Microbiol. 2010;8:317–27.

132. Lafontaine DLJ, Riback JA, Bascetin R, Brangwynne CP. The nucleolus as a multiphase liquid condensate. Nature reviews Molecular cell biology. 2021;22:165–82.

133. Lakadamyali M, Cosma MP. Advanced microscopy methods for visualizing chromatin structure. FEBS Lett. 2015;589 20 Pt A:3023–30.

134. Lanzuolo C, Orlando V. Memories from the Polycomb Group Proteins. Annu Rev Genet. 2012;46:561–89.

135. Latt SA, Stetten G. Spectral studies on 33258 Hoechst and related bisbenzimidazole dyes useful for fluorescent detection of deoxyribonucleic acid synthesis. The journal of histochemistry and cytochemistry : official journal of. 1976;24:24–33.

136. Lee J-H, Kim EW, Croteau DL, Bohr VA. Heterochromatin: an epigenetic point of view in aging. Exp Mol Med. 2020;52:1466–74.

137. Lehnertz B, Ueda Y, Derijck AAHA, Braunschweig U, Perez-Burgos L, Kubicek S, Chen T, Li E, Jenuwein T, Peters AHFM. Suv39h-mediated histone H3 lysine 9 methylation directs DNA methylation to major satellite repeats at pericentric heterochromatin. Curr Biol. 2003;13:1192–200.

138. Lezhava TA, Jokhadze T, Monaselidze J. The Functioning of Aged Heterochromatin. Senescence. 2012;26:631-46.

139. Lezhava TA. Heterochromatinization as a key factor in aging. Mech Ageing Dev. 1984;28:279–87.

140. Li X, Sun Q, Li X, Cai D, Sui S, Jia Y, Song H, Zhao R. Dietary betaine supplementation to gestational sows enhances hippocampal IGF2 expression in newborn piglets with modified DNA methylation of the differentially methylated regions. European Journal of Nutrition. 2015;54: 1201–1210.

141. Li Y, Daniel M, Tollefsbol TO. Epigenetic regulation of caloric restriction in aging. BMC Med. 2011;9:98.

142. Li Y, Tollefsbol TO. p16INK4a Suppression by Glucose Restriction Contributes to Human Cellular Lifespan Extension through SIRT1-Mediated Epigenetic and Genetic Mechanisms. PLoS One. 2011;6:e17421.

143. Lieberman-Aiden E, van Berkum NL, Williams L, Imakaev M, Ragoczy T, Telling A, Amit I, Lajoie BR, Sabo PJ, Dorschner MO, Sandstrom R, Bernstein B, Bender MA, Groudine M, Gnirke A, Stamatoyannopoulos J, Mirny LA, Lander ES, Dekker J. Comprehensive mapping of long-range interactions reveals folding principles of the human genome. Science. 2009;326:289–93.

144. Lin DH, Stuwe T, Schilbach S, Rundlet EJ, Perriches T, Mobbs G, Fan Y, Thierbach K, Huber FM, Collins LN, Davenport AM, Jeon JE, Hoelzt A. Architecture of the symmetric core of the nuclear pore. Science. 2016.

145. Lippincott-Schwartz J, Snapp E, Kenworthy A. Studying protein dynamics in living cells. Nat Rev Mol Cell Biol. 2001;2:444–56.

146. Liu L, Cheung TH, Charville GW, Hurgo BMC, Leavitt T, Shih J, Brunet A, Rando TA. Chromatin modifications as determinants of muscle stem cell quiescence and chronological aging. Cell Rep. 2013;4:189–204.

147. Longo VD, Di Tano M, Mattson MP, Guidi N. Intermittent and periodic fasting, longevity and disease. Nat Aging. 2021;1:47–59.

148. López-Domínguez JA, Khraiwesh H, González-Reyes JA, López-Lluch G, Navas P, Ramsey JJ, de Cabo R, Burón MI, Villalba JM. Dietary fat and aging modulate apoptotic signaling in liver of calorie-restricted mice. J Gerontol A Biol Sci Med Sci. 2015;4:399-409.

149. López-García P, Moreira D. Selective forces for the origin of the eukaryotic nucleus. BioEssays. 2006;28:525–33.

150. López-Otín C, Blasco MA, Partridge L, Serrano M, Kroemer G. The Hallmarks of Aging. Cell. 2013;153:1194–217.

151. Lu Y, Biancotto A, Cheung F, Remmers E, Shah N, McCoy JP, Tsang JS. Systematic Analysis of Cell-to-Cell Expression Variation of T Lymphocytes in a Human Cohort Identifies Aging and Genetic Associations. Immunity. 2016;45:1162–75.

152. Lund EG, Oldenburg AR, Collas P. Enriched Domain Detector: a program for detection of wide genomic enrichment domains robust against local variations. Nucleic Acids Res. 2014;42:e92.

153. Lund EG, Oldenburg AR, Delbarre E, Freberg CT, Duband-Goulet I, Eskeland R, Buendia B, Collas P. Lamin A/C-promoter interactions specify chromatin state-dependent transcription outcomes. Genome Res. 2013;23:1580–9.

154. Luperchio TR, Sauria MEG, Hoskins VE, Wong X, DeBoy E, Gaillard M-C, et al. The repressive genome compartment is established early in the cell cycle before forming the lamina associated domains. bioRxiv 2018.

155. Madrigal P, Krajewski P. Current bioinformatic approaches to identify DNase I hypersensitive sites and genomic footprints from DNase-seq data. Front Genet. 2012;3:230.

156. Maegawa S, Lu Y, Tahara T, Lee JT, Madzo J, Liang S, Jelinek J, Colman RJ, Issa JJ. Caloric restriction delays age-related methylation drift. Nat. Commun. 2017;8:539.

157. Marchetti MC, Di Marco B, Cifone G, Migliorati G, Riccardi C. Dexamethasone-induced apoptosis of thymocytes: role of glucocorticoid receptor–associated Src kinase and caspase-8 activation. Blood. 2003;101:585–93.

158. Matheson TD, Kaufman PD. Grabbing the genome by the NADs. Chromosoma. 2016;125:361–71.

159. Maze I, Noh K-M, Soshnev AA, Allis CD. Every amino acid matters: essential contributions of histone variants to mammalian development and disease. Nat Rev Genet. 2014;15:259–71.

160. McCay CM, Crowell MF, Maynard LA. The effect of retarded growth upon the length of life span and upon the ultimate body size. 1935. Nutrition. 1989;5:155–71; discussion 172.

161. Medema RH, Herrera RE, Lam F, Weinberg RA. Growth suppretion by p16ink4 requires functional retinoblastoma protein. PNAS. 1995;92:6289-6293.

162. Mercken EM, Crosby SD, Lamming DW, JeBailey L, Krzysik-Walker S, Villareal DT, Capri M, Franceschi C, Zhang Y, Becker K. Calorie restriction in humans inhibits the PI3K/AKT pathway and induces a younge transcription profile. Aging Cell. 2013;12:645-651.

163. Messmer UK, Pereda-Fernandez C, Manderscheid M, Pfeilschifter J. Dexamethasone inhibits TNF-α-induced apoptosis and IAP protein downregulation in MCF-7 cells. British Journal of Pharmacology. 2001;133:467–76.

164. Mikula-Pietrasik J, Niklas A, Uruski P, Tykarski A, Książek K. Mechanisms and significance of therapy-induced and spontaneous senescence of cancer cells. Cell Mol Life Sci. 2020;77:213–29.

165. Min J, Zhang Y, Xu R-M. Structural basis for specific binding of Polycomb chromodomain to histone H3 methylated at Lys 27. Genes & Development. 2003;17:1823–1828.

166. Minton AP. Confinement as a determinant of macromolecular structure and reactivity. II. Effects of weakly attractive interactions between confined macrosolutes and confining structures. Biophysical Journal. 1995;68:1311–22.

167. Minton AP. How can biochemical reactions within cells differ from those in test tubes? Journal of Cell Science. 2006;119:2863–9.

168. Minton AP. Molecular crowding: Analysis of effects of high concentrations of inert cosolutes on biochemical equilibria and rates in terms of volume exclusion. In: Methods in Enzymology. Academic Press; 1998;127–49.

169. Mirrett S. Acridine orange stain. Infect Control. 1982;3:250–2.

170. Misteli T. Concepts in nuclear architecture. BioEssays. 2005;27:477–87.

171. Morris BJ, Willcox BJ, Donlon TA. Genetic and epigenetic regulation of human aging and longevity. Biochim Biophys Acta Mol Basis Dis. 2019;1865:1718–44.

172. Moser JJ, Fritzler MJ. Cytoplasmic ribonucleoprotein (RNP) bodies and their relationship to GW/P bodies. Int J Biochem Cell Biol. 2010;42:828–43.

173. Moskalev AA, Aliper AM, Smit-McBride Z, Buzdin A, Zhavoronkov A. Genetics and epigenetics of aging and longevity. Cell Cycle. 2014;13:1063–77.

174. Nakashima KK, Vibhute MA, Spruijt E. Biomolecular Chemistry in Liquid Phase Separated Compartments. Front Mol Biosci. 2019;6:21.

175. Navarro-Yepes J, Zavala-Flores L, Anandhan A, Wang F, Skotak M, Chandra N, Li M, Pappa A, Martinez-Fong D,Del Razo LM, Quintanilla-Vega B, Franco R. Antioxidant gene therapy against neuronal cell death. Pharmacology & therapeutics. 2014;142:206–30.

176. Németh A, Conesa A, Santoyo-Lopez J, Medina I, Montaner D, Péterfia B, Solovei I, Cremer T, Dopazo J, Längst G. Initial Genomics of the Human Nucleolus. PLOS Genetics. 2010;6:e1000889.

177. Németh A, Längst G. Genome organization in and around the nucleolus. Trends in Genetics. 2011;27:149–56.

178. Ni Z, Ebata A, Alipanahiramandi E, Lee SS. Two SET domain containing genes link epigenetic changes and aging in Caenorhabditis elegans. Aging Cell. 2012;11:315–25.

179. Nielsen B, Albregtsen F, Danielsen HE. Automatic segmentation of cell nuclei in Feulgen-stained histological sections of prostate cancer and quantitative evaluation of segmentation results. Cytometry Part A. 2012;81A:588–601.

180. Nieminen AL, Gores GJ, Dawson TL, Herman B, Lemasters JJ. Toxic injury from mercuric chloride in rat hepatocytes. J Biol Chem. 1990;265:2399–408.

181. Nishino Y, Eltsov M, Joti Y, Ito K, Takata H, Takahashi Y, Hihara S, Frangakis AS, Imamoto N, Ishikawa T, Maeshima K. Human mitotic

chromosomes consist predominantly of irregularly folded nucleosome fibres without a 30-nm chromatin structure. EMBO J. 2012;31:1644–53.

182. Nozaki T, Imai R, Tanbo M, Nagashima R, Tamura S, Tani T, Joti Y, Tomita M, Hibino K, Kanemaki MT, Wendt KS, Okada Y, Nagai T, Maeshima K. Dynamic Organization of Chromatin Domains Revealed by Super-Resolution Live-Cell Imaging. Mol Cell. 2017;67:282-293.e7.

183. O'Sullivan JM, Pai DA, Cridge AG, Engelke DR, Ganley ARD. The nucleolus: a raft adrift in the nuclear sea or the keystone in nuclear structure? Biomol Concepts. 2013;4:277–86.

184. Oh H-Y, Namkoong S, Lee S-J, Por E, Kim C-K, Billiar TR, et al. Dexamethasone protects primary cultured hepatocytes from death receptor-mediated apoptosis by upregulation of cFLIP. Cell Death Differ. 2006;13:512–23.

185. Olins AL, Moyer BA, Kim SH, Allison DP. Synthesis of a more stable osmium ammine electron-dense DNA stain. J Histochem Cytochem. 1989;37:395–8.

186. Padeken J, Heun P. Nucleolus and nuclear periphery: velcro for heterochromatin. Curr Opin Cell Biol. 2014;28:54–60.

187. Palmeira CM, Madeira VMC. Mercuric chloride toxicity in rat liver mitochondria and isolated hepatocytes. Environmental Toxicology and Pharmacology. 1997;3:229–35.

188. Papp B, Müller J. Histone trimethylation and the maintenance of transcriptional ONand OFF states by trxG and PcG proteins. Genes Dev. 2006;20:2041–54.

189. Passos JF, Nelson G, Wang C, Richter T, Simillion C, Proctor CJ, Miwa S, Olijslagers S, Hallinan J, Wipat A, Saretzki G, Rudolph KL, Kirkwood TB, von Zglinicki T. Feedback between p21 and reactive oxygen production is necessary for cell senescence. Mol Syst Biol. 2010;6:347.

190. Patterson GH, Lippincott-Schwartz J. A Photoactivatable GFP for Selective Photolabeling of Proteins and Cells. Science. 2002.

191. Peeters JGC, Picavet LW, Coenen SGJM, Mauthe M, Vervoort SJ, Mocholi E, de Heus C, Klumperman J, Vastert SJ, Reggiori F, Coffer PJ, Mokry M, van Loosdregt J. Transcriptional and epigenetic profiling of nutrient-deprived cells to identify novel regulators of autophagy. Autophagy. 2019;15:98–112.

192. Pelletier J, Thomas G, Volarević S. Ribosome biogenesis in cancer: new players and therapeutic avenues. Nat Rev Cancer. 2018;18:51–63.

193. Peric-Hupkes D, Meuleman W, Pagie L, Bruggeman SWM, Solovei I, Brugman W, Graef S, Flicek P, Kerkhoven RM, van Lohuizen M, Reinders M, Wessels L, van Steensel B. Molecular Maps of the Reorganization of Genome-Nuclear Lama Interactions during Differentiation. Molecular Cell. 2010;38:603–13.

194. Peters R (2006). Introduction to nucleocytoplasmic transport: molecules and mechanisms. Methods Mol Biol. 2006, 322. pp. 235–58.

195. Pfaffl MW, Horgan GW, Dempfle L. Relative expression software tool (REST) for group-wise comparison and statistical analysis of relative expression results in real-time PCR. Nucleic Acids Res. 2002;30:e36.

196. Picelli S, Björklund Å, Reinius B, Sagasser S, Winberg G, Sandberg R. Tn5 transposase and tagmentation procedures for massively-scaled sequencing projects. Genome Research. 2014;24.

197. Pikó L, Hougham AJ, Bulpitt KJ. Studies of sequence heterogeneity of mitochondrial DNA from rat and mouse tissues: evidence for an increased frequency of deletions/additions with aging. Mech Ageing Dev. 1988;43:279–93.

198. Piper MDW, Partridge L, Raubenheimer D, Simpson SJ. Dietary Restriction and Aging: A Unifying Perspective. Cell Metabolism. 2011;14:154–60.

199. Poetker DM, Reh DD. A comprehensive review of the adverse effects of systemic corticosteroids. Otolaryngol Clin North Am. 2010;43:753–68.

200. Pogribny IP, Tryndyak VP, Bagnyukova TV, Melnyk S, Montgomery B, Ross SA. Hepatic epigenetic phenotype predetermines individual susceptibility to hepatic steatosis in mice fed a lipogenic methyldeficient diet. J. Hepatol. 2009;51:176–186.

201. Pombo A, Dillon N. Three-dimensional genome architecture: players and mechanisms. Nat Rev Mol Cell Biol. 2015;16:245–57.

202. Portugal J, Waring MJ. Assignment of DNA binding sites for 4′,6-diamidine-2-phenylindole and bisbenzimide (Hoechst 33258). A comparative footprinting study. Biochimica et Biophysica Acta (BBA) - Gene Structure and Expression. 1988;949:158–68.

203. Quinodoz SA, Ollikainen N, Tabak B, Palla A, Schmidt JM, Detmar E, Lai MM, ShishkinAA, Bhat P, Takei Y, Trinh V, Aznauryan E, Russell P, Cheng C, Jovanovic M, Chow A, Cai L, kcDonel P, Guttman M. Higher-Order Inter-chromosomal Hubs Shape 3D Genome Organization in the Nucleus. Cell. 2018;174:744-757.e24.

204. Ragoczy T, Telling A, Scalzo D, Kooperberg C, Groudine M: Functional redundancy in the nuclear compartmentalization of the late-replicating genome. Nucleus 2014;5, 626–635.

205. Rajendran P, Alzahrani AM, Hanieh HN, Kumar SA, Ben Ammar R, Rengarajan T, Alhoot MA. Autophagy and senescence: A new insight in selected human diseases. J Cell Physiol. 2019;234:21485–92.

206. Rao SSP, Huntley MH, Durand NC, Stamenova EK, Bochkov ID, Robinson JT, Sanborn AL, Machol I, Omer AD, Lander ES, Lieberman Aiden E. A 3D map of the human genome at kilobase resolution reveals principles of chromatin looping. Cell. 2014;159:1665–80.

207. Rehkopf DH, Needham BL, Lin J, Blackburn EH, Zota AR, Wojcicki JM, Epel ES. Leukocyte Telomere Length in Relation to 17 Biomarkers of Cardiovascular Disease Risk: A Cross-Sectional Study of US Adults. PLoS Med. 2016;13:e1002188.

208. Rhee I, Bachman KE, Park BH, Jair KW, Yen RWC, Schuebel KE, Cui H, Feinberg, Christoph Lengauer AP, Kinzler KK, Baylin SB, Vogelstein B. DNMT1 and DNMT3b cooperate to silence genes in human cancer cells. NATURE. 2002;416:552–6.

209. Rhen T, Cidlowski JA. Antiinflammatory action of glucocorticoids--new mechanisms for old drugs. N Engl J Med. 2005;353:1711–23.

210. Richter K, Nessling M, Lichter P. Experimental evidence for the influence of molecular crowding on nuclear architecture. J Cell Sci. 2007;120 Pt 9:1673–80.

211. Robson MI, Heras JI de las, Czapiewski R, Thành PL, Booth DG, Kelly DA, Webb S, Kerr ARW, Schirmer EC. Tissue-specific gene repositioning by muscle nuclear membrane proteins enhances repression of critical developmental genes during myogenesis. Molecular Cell. 2016;62:834–47.

212. Rønningen T, Shah A, Oldenburg AR, Vekterud K, Delbarre E, Moskaug JØ, Collas P. Prepatterning of differentiation-driven nuclear lamin A/C-associated chromatin domains by GlcNAcylated histone H2B. Genome Res. 2015;25:1825–35.

213. Ruiz-Santana S, López A, Torres S, Rey A, Losada A, Latasa L, Manzano JL, Díaz-Chico BN. Prevention of dexamethasone-induced lymphocytic apoptosis in the intestine and in Peyer patches by enteral nutrition. JPEN J Parenter Enteral Nutr. 2001;25:338–45.

214. Santoro R, Grummt I. Epigenetic mechanism of rRNA gene silencing: temporal order of NoRC-mediated histone modification, chromatin remodeling, and DNA methylation. Mol Cell Biol. 2005;25:2539–46.

215. Santoro R, Li J, Grummt I. The nucleolar remodeling complex NoRC mediates heterochromatin formation and silencing of ribosomal gene transcription. Nat Genet. 2002;32:393–6.

216. Sato H, Shibata M, Shimizu T, Shibata S, Toriumi H, Ebine T, Kuroi T, Iwashita T, Funakubo M, Kayama Y, Akazawa C, Wajima K, Nakagawa T, Okano H, Suzuki N. Differential cellular localization of antioxidant enzymes in the trigeminal ganglion. Neuroscience. 2013;248:345–58.

217. Saxton MJ. Lateral diffusion in an archipelago. Dependence on tracer size. Biophys J. 1993a;64:1053–62.

218. Saxton MJ. Lateral diffusion in an archipelago. Single-particle diffusion.. Biophys J. 1993b;64:1766–17.

219. Sayej WN, Knight Iii PR, Guo WA, Mullan B, Ohtake PJ, Davidson BA, Khan A, Baker RD, Baker SS. Advanced Glycation End Products Induce Obesity and Hepatosteatosis in CD-1 Wild-Type Mice. Biomed Res Int. 2016;2016:7867852.

220. Schmickel RD. Quantitation of human ribosomal DNA: hybridization of human DNA with ribosomal RNA for quantitation and fractionation. Pediatr Res. 1973;7:5–12.

221. Schöfer C, Weipoltshammer K. Nucleolus and chromatin. Histochem Cell Biol. 2018;150:209–25.

222. Schones DE, Cui K, Cuddapah S, Roh T-Y, Barski A, Wang Z, et al. Dynamic Regulation of Nucleosome Positioning in the Human Genome. Cell. 2008;132:887–98.

223. Schosserer M, Minois N, Angerer TB, Amring M, Dellago H, Harreither E, Calle-Perez A, Pircher A, Gerstl MP, Pfeifenberger S, Brandl C, Sonntagbauer M, Kriegner A, Linder A, Weinhäusel A, Mohr T, Steiger M, Mattanovich D, Rinnerthaler M, Karl T, Sharma S, Entian KD, Kos M, Breitenbach M, Wilson IB, Polacek N, Grillari-Voglauer R, Breitenbach-Koller L, Grillari J. Methylation of ribosomal RNA by

NSUN5 is a conserved mechanism modulating organismal lifespan. Nat Commun. 2015;6:6158.

224. Schotta G, Sengupta R, Kubicek S, Malin S, Kauer M, Callén E, Arkady Celeste A, Pagani M, Opravil S, De La Rosa-Velazquez IA, Espejo A, Bedford MT, Nussenzweig A, Busslinger M, Jenuwein T. A chromatin-wide transition to H4K20 monomethylation impairs genome integrity and programmed DNA rearrangements in the mouse. Genes and Development. 2008;22:2048–61.

225. Schumacher B, van der Pluijm I, Moorhouse MJ, Kosteas T, Robinson AR, Suh Y, Breit TM, van Steeg H, Niedernhofer LJ, van Ijcken W, Bartke A, Spindler SR, Hoeijmakers JHJ, van der Horst, GTJ, Garinis GA. Delayed and accelerated aging share common longevity assurance mechanisms. PLoS Genet. 2008;4:e1000161.

226. Sedgwick B, Bates PA, Paik J, Jacobs SC, Lindahl T. Repair of alkylated DNA: recent advances. DNA Repair (Amst). 2007;6:429–42.

227. Semba RD, Nicklett EJ, Ferrucci L. Does accumulation of advanced glycation end products contribute to the aging phenotype? J Gerontol A Biol Sci Med Sci. 2010;65(9):963–75.

228. Serrano M, Gomez-Lahoz E, DePinho RA, Beach D, Bar-Sagi D. Inhibition of ras-induced proliferation and cellular transformation by p16INK4. Science. 1995;267:249-252.

229. Sharma S, Acharya J, Banjara MR, Ghimire P, Singh A. Comparison of acridine orange fluorescent microscopy and gram stain light microscopy for the rapid detection of bacteria in cerebrospinal fluid. BMC Res Notes. 2020;13:29.

230. Shaw DJ, Eggleton P, Young P. Joining the dots: production, processing and targeting of U snRNP to nuclear bodies. Biochimica et biophysica acta. 2008;1783:2137-44.

231. Shim AR, Nap RJ, Huang K, Almassalha LM, Matusda H, Backman V, Szleifer I. Dynamic Crowding Regulates Transcription. Biophysical Journal. 2020;118:2117–29.

232. Shin Y, Brangwynne CP. Liquid phase condensation in cell physiology and disease. Science. 2017;357:eaaf4382.

233. Singh BK, Tripathi M, Sandireddy R, Tikno K, Zhou J, Yen PM. Development of an in vitro senescent hepatic cell model for metabolic studies in aging. BioRxiv 2020.

234. Singh I, Contreras A, Cordero J, Rubio K, Dobersch S, Günther S, Jeratsch S, Mehta A, Krüger M, Graumann J, Seeger W, Dobreva G, Braun T, Barreto G. MiCEE is a ncRNA-protein complex that mediates epigenetic silencing and nucleolar organization. Nat Genet. 2018;50:990–1001.

235. Sirri V, Hernandez-Verdun D, Roussel P. Cyclin-dependent kinases govern formation and maintenance of the nucleolus. J Cell Biol. 2002;156:969–81.

236. Sohal RS, Weindruch R. Oxidative stress, caloric restriction, and aging. Science. 1996;273:59-63.

237. Somech R, Shaklai S, Geller O, Amariglio N, Simon AJ, Rechavi G, Gal-Yam EN. The nuclear-envelope protein and transcriptional repressor LAP2beta interacts with HDAC3 at the nuclear periphery, and induces histone H4 deacetylation. J Cell Sci. 2005;118 Pt 17:4017–25.

238. Soong NW, Hinton DR, Cortopassi G, Arnheim N. Mosaicism for a specific somatic mitochondrial DNA mutation in adult human brain. Nat Genet. 1992;2:318–23.

239. Stefanovsky VY, Langlois F, Bazett-Jones D, Pelletier G, Moss T. ERK modulates DNA bending and enhancesome structure by phosphorylating HMG1-boxes 1 and 2 of the RNA polymerase I transcription factor UBF. Biochemistry. 2006;45:3626–34.

240. Stefanovsky VY, Moss T. The splice variants of UBF differentially regulate RNA polymerase I transcription elongation in response to ERK phosphorylation. Nucleic Acids Res. 2008;36:5093–101.

241. Strom AR, Emelyanov AV, Mir M, Fyodorov DV, Darzacq X, Karpen GH. Phase separation drives heterochromatin domain formation. Nature. 2017;547:241–5.

242. Stults DM, Killen MW, Pierce HH, Pierce AJ. Genomic architecture and inheritance of human ribosomal RNA gene clusters. Genome Res. 2008;18:13–18.

243. Su X, A. Ditlev J, Hui E, Xing W, Banjade S, Okrut J, King DS, Taunton J, Rosen MK , Vale RD. Phase separation of signaling molecules promotes T cell receptor signal transduction. Science. 2016;352:595–9.

244. Sullivan GJ, Bridger JM, Cuthbert AP, Newbold RF, Bickmore WA, McStay B. Human acrocentric chromosomes with transcriptionally

silent nucleolar organizer regions associate with nucleoli. EMBO J. 2001;20:2867–74.

245. Sylvester JE, Whiteman DA, Podolsky R, Pozsgay J, Respess J, Schmickel RD. The human ribosomal RNA genes: structure and organization of the complete repeating unit. Hum Genet. 1986;73:193–198.

246. Syntichaki P, Troulinaki K, Tavernarakis N. Protein Synthesis Is a Novel Determinant of Aging in Caenorhabditis elegans. Annals of the New York Academy of Sciences. 2007;1119:289–95.

247. Tanaka Y, Tsuneoka M. Control of Ribosomal RNA Transcription by Nutrients. Intechopen. 2018;71866

248. Taniyama Y, Griendling KK. Reactive Oxygen Species in the Vasculature. Hypertension. 2003;42:1075–81.

249. Theoharides TC, Conti P. Dexamethasone for COVID-19? Not so fast. J Biol Regul Homeost Agents. 2020;34:1241–3.

250. Thorpe SR, Baynes JW. Role of the Maillard reaction in diabetes mellitus and diseases of aging. Drugs Aging. 1996;9(2):69–77.

251. Tiku V, Antebi A. Nucleolar Function in Lifespan Regulation. Trends in Cell Biology. 2018;28(8):662–72.

252. Tiku V, Jain C, Raz Y, Nakamura S, Heestand B, Liu W, Späth M, Suchiman HED, Müller R, Slagboom PE, Partridge L, Antebi A. Small nucleoli are a cellular hallmark of longevity. Nat Commun. 2017;8:16083.

253. Trerè D. AgNOR staining and quantification. Micron. 2000;31:127–31.

254. Trifunovic A, Larsson NG. Mitochondrial dysfunction as a cause of ageing. Journal of Internal Medicine. 2008;263:167–78.

255. Tucker JD. Reflections on the development and application of FISH whole chromosome painting. Mutat Res Rev Mutat Res. 2015;763:2–14.

256. Uversky VN. Protein intrinsic disorder-based liquid-liquid phase transitions in biological systems: Complex coacervates and membrane-less organelles. Adv Colloid Interface Sci. 2017;239:97–114.

257. Uzunhisarcikli M, Aslanturk A, Kalender S, Apaydin FG, Bas H. Mercuric chloride induced hepatotoxic and hematologic changes in rats: The protective effects of sodium selenite and vitamin E. Toxicol Ind Health. 2016;32:1651–62.

258. Van Deursen, M J. The role of senescent cells in ageing. Nature. 2014;509:439–46.

259. van Koningsbruggen S van, Gierlinski M, Schofield P, Martin D, Barton GJ, Ariyurek Y, den Dunnen JT, Lamond AI. High-resolution whole-genome sequencing reveals that specific chromatin domains from most human chromosomes associate with nucleoli. Molecular Biology of the Cell. 2010;21:3735–48.

260. van Sluis M, McStay B. Ribosome biogenesis: Achilles heel of cancer? Genes Cancer. 2014;5:152–153.

261. van Steensel B, Henikoff S. Identification of in vivo DNA targets of chromatin proteins using tethered dam methyltransferase. Nat Biotechnol. 2000;18:424–8.

262. Vardabasso C, Hasson D, Ratnakumar K, Chung C-Y, Duarte LF, Bernstein E. Histone variants: emerging players in cancer biology. Cell Mol Life Sci. 2014;71:379–404.

263. Vecchié A, Batticciotto A, Tangianu F, Bonaventura A, Pennella B, Abenante A, Corso R, Grazioli S, Mumoli N, Para O, Maresca AM, Dalla Gasperina D, Dentali F. High-dose dexamethasone treatment for COVID-19 severe acute respiratory distress syndrome: a retrospective study. Intern Emerg Med. 2021;1–7.

264. Verbrugge FH, Tang WH, Hazen SL. Protein carbamylation and cardiovascular disease. Kidney Int. 2015;88(3):474–8.

265. Vermeij WP, Dollé MET, Reiling E, Jaarsma D, Payan-Gomez C, Bombardieri CR, et al. Restricted diet delays accelerated ageing and genomic stress in DNA-repair-deficient mice. Nature. 2016;537:427–31.

266. Vertii A, Ou J, Yu J, Yan A, Pages H, Liu H, Zhu LJ, Kaufman PD. Two contrasting classes of nucleolus-associated domains in mouse fibroblast heterochromatin. Program in Molecular Medicine Publications. 2019;29. doi:10.1101/gr.247072.118.

267. Vettor R, Di Vincenzo A, Maffei P, Rossato M. Regulation of energy intake and mechanisms of metabolic adaptation or maladaptation after caloric restriction. Rev Endocr Metab Disord. 2020;21:399–409.

268. Villeponteau B. The heterochromatin loss model of aging. Exp Gerontol. 1997;32:383–94.

269. Walter J, Joffe B, Bolzer A, Albiez H, Benedetti PA, Müller S, Speicher MR, Cremer T, Cremer M, Solovei I. Towards many colors in FISH on 3D-preserved interphase nuclei. Cytogenet Genome Res. 2006;114:367–78.

270. Wang L, Gao Y, Zheng X, Liu C, Dong S, Li R, Zhang G, Wei Y, Qu H, Li Y, Allis CD, Li G, Li H, Li P. Histone modifications regulate chromatin compartmentalization by contributing to a phase separation mechanism. Mol. Cell. 2019;76:646–659.

271. Wang M, Lemos B. Ribosomal DNA harbors an evolutionarily conserved clock of biological aging. Genome Res. 2019;29:325–33.

272. Wang Y, Maharana S, Wang MD, Shivashankar GV. Super-resolution microscopy reveals decondensed chromatin structure at transcription sites. Sci Rep. 2014;4:4477.

273. Wang Z, Zang C, Rosenfeld JA, Schones DE, Barski A, Cuddapah S, Cui K, Roh T, Peng W, Zhang MQ, Zhao K. Combinatorial patterns of histone acetylations and methylations in the human genome. Nat Genet. 2008;40:897–903.

274. Waterland RA, Travisano M, Tahiliani KG, Rached MT, Mirza S. Methyl donor supplementation prevents transgenerational amplification of obesity. Int. J. Obes. (Lond.) 2008;32:1373–1379.

275. Weber CM, Henikoff S. Histone variants: dynamic punctuation in transcription. Genes Dev. 2014;28:672–82.

276. Weindruch R, Sohal RS. Caloric Intake and Aging. New England Journal of Medicine. 1997;337:986–94.

277. White RR, Milholland B, de Bruin A, Curran S, Laberge R-M, van Steeg H, Campisi J, Maslov AY, Vijg J. Controlled induction of DNA double-strand breaks in the mouse liver induces features of tissue ageing. Nat Commun. 2015;6:6790.

278. Wiggers GA, Peçanha FM, Briones AM, Pérez-Girón JV, Miguel M, Vassallo DV, Cachofeiro V, Alonso MJ, Salaices M. Low mercury concentrations cause oxidative stress and endothelial dysfunction in

conductance and resistance arteries. Am J Physiol Heart Circ Physiol. 2008;295:H1033–43.

279. Wu C, Bassett A, Travers A. A variable topology for the 30-nm chromatin fibre. EMBO Rep. 2007;8:1129–34.

280. Wu JQ, Kosten TR, Zhang XY. Free radicals, antioxidant defense systems, and schizophrenia. Progress in Neuro-Psychopharmacology and Biological Psychiatry. 2013;46:200–6.

281. Xie W, Ling T, Zhou Y, Feng W, Zhu Q, Stunnenberg HG, Grummt I, Tao W. The chromatin remodeling complex NuRD establishes the poised state of rRNA genes characterized by bivalent histone modifications and altered nucleosome positions. Proc Natl Acad Sci USA. 2012;109:8161–8166.

282. Yang D, Tan X, Lv Z, Liu B, Baiyun R, Lu J, Zhang Z. Regulation of Sirt1/Nrf2/TNF-α signaling pathway by luteolin is critical to attenuate acute mercuric chloride exposure induced hepatotoxicity. Sci Rep. 2016;6:37157.

283. Yang K, Yang J, Yi J. Nucleolar Stress: hallmarks, sensing mechanism and diseases. Cell Stress. 2018;2:125–40.

284. Yu S, Lemos B. The long-range interaction map of ribosomal DNA arrays. PLoS Genet. 2018;14:e1007258.

285. Yue X, Trifari S, Äijö T, Tsagaratou A, Pastor WA, Zepeda-Martínez JA, Lio CWJ, Li X, Huang Y, Vijayanand P, Lähdesmäki H, Rao A. Control of Foxp3 stability through modulation of TET activity. J Exp Med. 2016;213:377–97.

286. Zhang H, Tan X, Yang D, Lu J, Liu B, Baiyun R, Zhang Z. Dietary luteolin attenuates chronic liver injury induced by mercuric chloride via the Nrf2/NF-κB/P53 signaling pathway in rats. Oncotarget. 2017;8:40982–93.

287. Zhang L-F, Huynh KD, Lee JT. Perinucleolar Targeting of the Inactive X during S Phase: Evidence for a Role in the Maintenance of Silencing. Cell. 2007;129:693–706.

288. Zhou H-X, Pang X. Electrostatic Interactions in Protein Structure, Folding, Binding, and Condensation. Chem Rev. 2018;118:1691–741.

289. Zhou Y, Santoro R, Grummt I. The chromatin remodeling complex NoRC targets HDAC1 to the ribosomal gene promoter and represses

RNA polymerase I transcription. EMBO J. 2002;21:4632–40.Martin W, Koonin EV. Introns and the origin of nucleus–cytosol compartmentalization. Nature. 2006;440:41–5.

7. ACKNOWLEDGEMENTS

I would like to especially thank Professor Marco Biggiogera for his scientific support, for believing in me and teaching me positive and enthusiastic approach to scientific research and everyday life.

Thanks to Prof. Maria Grazia Bottone and Prof. Vittorio Bertone for their useful suggestions.

Thanks also to Dr. Gloria Milanesi, Ms Francine Flach and Ms Paola Veneroni for their precious technical support.

I am grateful to my colleagues, Stella, Claudio, Erica, Fabrizio, Beatrice, Chiara to have shared with me laboratory life and for their friendship.

Thanks to the students I met to whom I had the opportunity and the pleasure to share my passion for biology, especially to Matteo, Liliana and Annamaria for their work without which this PhD thesis would be different.

Finally, I would like to thank my family and my friends for their continuous support during this scientific and personal “journey”.

8. LIST OF ORIGINAL MANUSCRIPT

Zannino L, Siciliani S, Biggiogera M. Timing of cytosine methylation on newly synthesized RNA. Methods Mol. Biol. 2020;2175:197-205. https://doi.org/10.1007/978-1-0716-0763-3_14

Zannino L, Casali C, Siciliani S, Biggiogera M. The dynamics of the nuclear environment and their impact on gene function. J. Biochem. 2021;mvaa091. https://doi.org/ 10.1093/jb/mvaa091

Zannino L, Pagano A, Casali C, Saia L, Balestrazzi A, Biggiogera. Mercury Chloride Alters Heterochromatin Domain Organization and Nucleolar Activity in Mouse Liver. Cells. Submitted

Pagano A*, **Zannino L***, Pagano P, Doria E, Dondi D, Macovei A, Biggiogera M, de Sousa Araujo S, Balestrazzi A. Nucleolar processes behind desiccation tolerance in primed and overprimed Medicago truncatula seeds. Plant, Cell & Environment. Submitted (* = Co-first author)

Gianella M, Doria E, Dondi D, Milanese C, Gallotti L, Börner A, **Zannino L**, Macovei A, Pagano A, Guzzon F, Biggiogera M, Balestrazzi A. Physiological and molecular aspects of seed longevity: a case study of a Pisum sativum L. accession with wrinkled seeds. Ann. Bot. Submitted

9. CONGRESS COMMUNICATIONS

Poster communications:

Zannino L, Pagano A, Casali C, Balestrazzi A, Biggiogera M. Dexamethasone remodels some epigenetic features of heterochromatin domains and nucleolar activity in mouse liver. SIBBM, Frontiers in Molecular Biology seminar, web seminar. 7-10 June 2021.

Zannino L, Bertone V, Siciliani S, Saia L, Biggiogera M. Investigating the nucleolar epigenetic code at ultrastructural level. XXVI Wilhelm Bernhard Workshop on the Cell Nucleus, Dijon, France. Biopolym. Cell. 2019; 35(3):243-244.

Oral communications:

Zannino L. The nucleolus epigenetics in a photograph. Life Science, 3rd Joint Annual Symposium of the Departments of Biology and Biotechnology, Molecular Medicine and CNR-Institute of Molecular Genetics, University of Pavia, Italy. 19-21 February 2020.

Abstracts:

Pagano A, **Zannino L**, Pagano P, Doria E, Dondi D, Macovei A, Biggiogera M, de Sousa Araujo S, Balestrazzi A. Nucleolar processes underlying the Medicago truncatula seed resilience to genotoxic injury. EMBO Workshop, Plant genome stability and change, Leiden, Netherlands. 5-8 December 2021.

Pagano A, Pagano P, **Zannino L**, Doria E, Dondi D, Gaonkar SS, Macovei A, Biggiogera M, de Sousa Araujo S, Balestrazzi A. Exploring the stress response induced during the rehydration-dehydration cycle in primed and overprimed Medicago truncatula seeds. 13th ISSS (International Society for Seed Science), web Congress. 9-13 August 2021.

Gianella M, Doria E, Dondi D, Milanese C, Gallotti L, Börner A, **Zannino L**, Macovei A, Pagano A, Guzzon F, Biggiogera M, Balestrazzi A. Exploring physiological and molecular factors involved in seed longevity: the case study of Pisum sativum L. 13th ISSS (International Society for Seed Science), web Congress. 9-13 August 2021.

Casali C, **Zannino L**, Biggiogera M. The nuclear envelope: a toolbooth function for splicing factors. GIC XXXIX, web conference. 14-18 June 2021.

Pagano A, **Zannino L**, Biggiogera M, Galeotti E, Pagano P, Macovei A, de Sousa Araújo S, Balestrazzi A. How do seeds respond to post-priming desiccation? Exploring DNA damage response and mapping chromatin accessibility in Medicago truncatula. Plant Genomes in a Changing Environment, web workshop. 12-14 October 2020.

Biggiogera M, Siciliani S, **Zannino L**. The Perichromatin Region: a crossroad of events. XXVI Wilhelm Bernhard Workshop on the Cell Nucleus, Dijon, France. Biopolym. Cell. 2019; 35(3):203-204.

Siciliani S, Masiello I, **Zannino L**, Basiricò F, Casali C, King E, Lacavalla A, Saia L, Scaltritti M, Biggiogera M. High resolution study of epigenetic processes: new insights into methylation and demethylation. XXVI Wilhelm Bernhard Workshop on the Cell Nucleus, Dijon, France. Biopolym. Cell. 2019; 35(3):178-178.